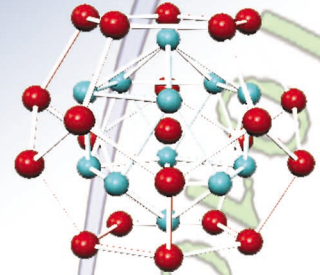
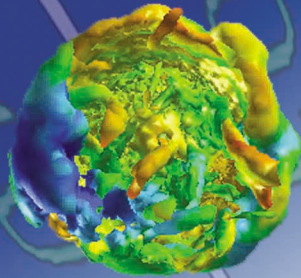


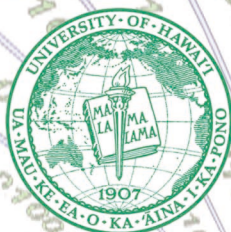
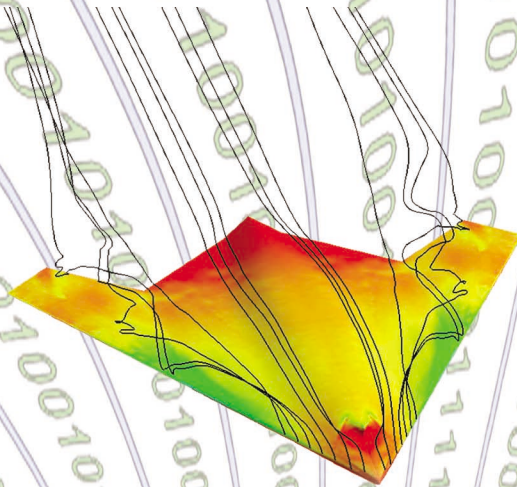
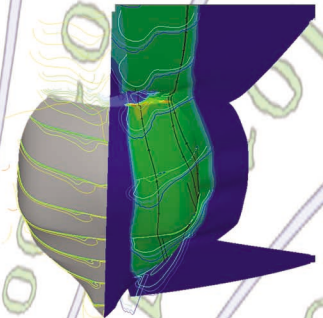
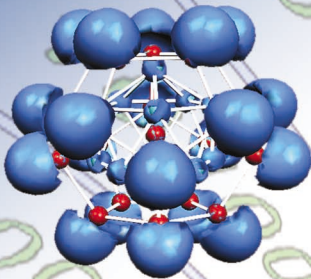


# MAUI HIGH PERFORMANCE COMPUTING CENTER

An Air Force Research Laboratory Center  
Managed by the University of Hawaii

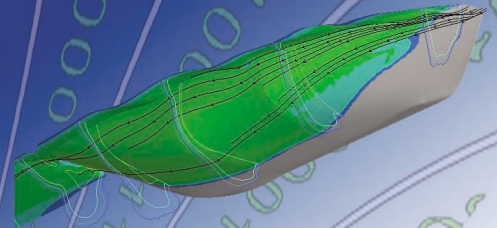
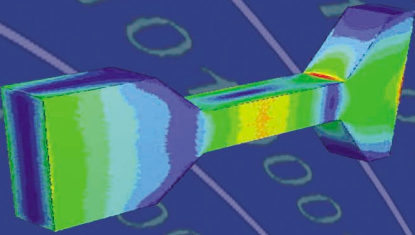
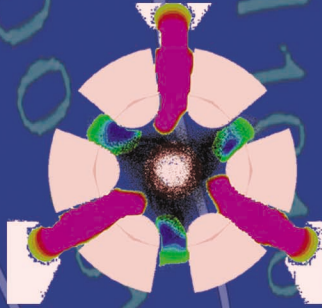
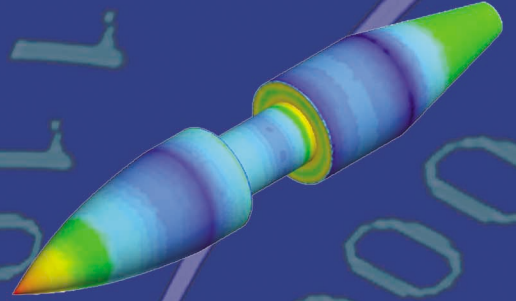
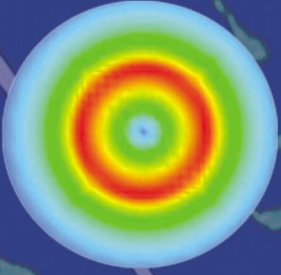
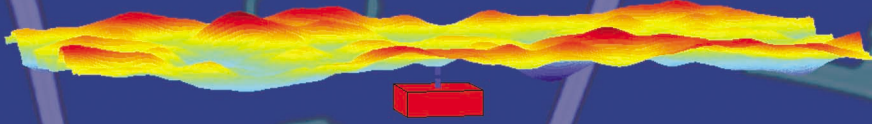


## APPLICATION BRIEFS 2003



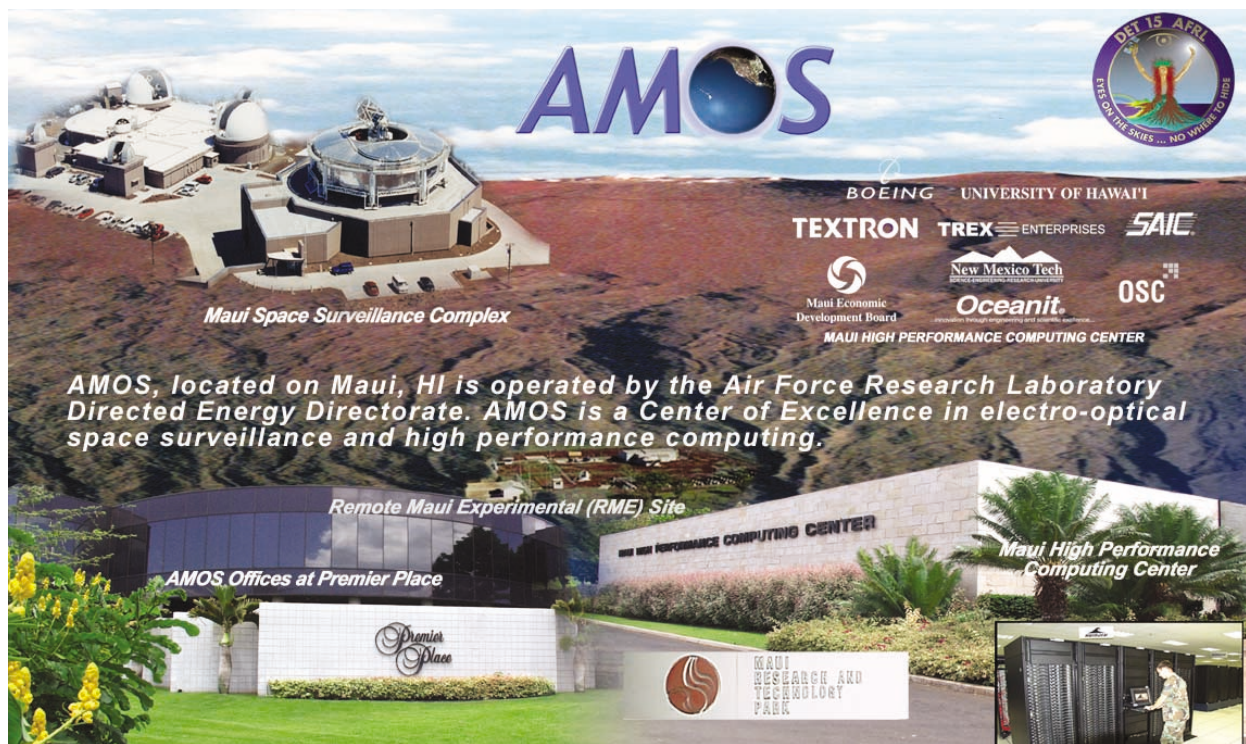
# AMOS

AIR FORCE MAUI OPTICAL & SUPERCOMPUTING SITE



550 Lipoa Parkway, Kihei, Hawaii 96753  
Phone: (808) 879-5077, Fax: (808) 879-5018  
Email: [info@mhpcc.hpc.mil](mailto:info@mhpcc.hpc.mil)  
<http://www.mhpcc.hpc.mil>

## APPLICATION BRIEFS 2003



### Air Force Maui Optical & Supercomputing Site (AMOS)

The views and conclusions contained in this document are those of the authors and should not be interpreted as necessarily representing the official policies or endorsements, either expressed or implied, of the Air Force Research Laboratory, the U.S. Government, the University of Hawaii, or the Maui High Performance Computing Center.

**MAUI HIGH PERFORMANCE  
COMPUTING CENTER**

550 Lipoa Parkway, Kihei-Maui, HI 96753  
 (808) 879-5077 • Fax: (808) 879-5018  
 E-mail: [info@mhpcc.hpc.mil](mailto:info@mhpcc.hpc.mil)  
 URL: [www.mhpcc.hpc.mil](http://www.mhpcc.hpc.mil)

*An Air Force Research Laboratory Center Managed by the University of Hawaii.*

# WELCOME

This is the ninth annual edition of Maui High Performance Computing Center's (MHPCC) *Application Briefs* — which highlights some of the successes our customers have achieved this year.

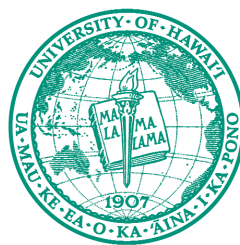
MHPCC, established in September 1993, is an Air Force Research Laboratory (AFRL) Center managed by the University of Hawaii. A leader in scalable parallel computing technologies, MHPCC is primarily chartered to support the Department of Defense (DoD) and other government organizations.

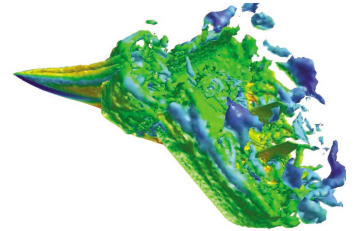
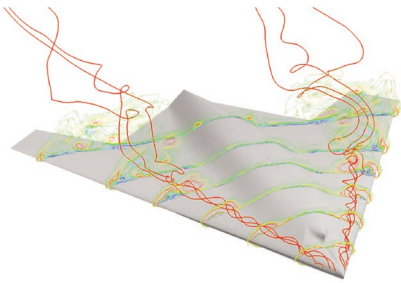
MHPCC offers an innovative environment for High Performance Computing (HPC) applications. This includes:

- **Computational Resources:** Stable and secure parallel computing platforms for prototyping, benchmarking, and testing applications. MHPCC is ranked as one of the top HPC centers in the world in terms of computational capabilities.
- **High-Speed Communications Infrastructure:** OC12 connections (Hawaii), offering 620 megabit per second (Mbps) capacity, provide direct access to MHPCC resources — over the Defense Research and Engineering Network (DREN) and the Hawaii Intranet Consortium (HIC).
- **Support Services:** An expert staff provides MHPCC users with systems, network, and applications support in addition to assistance with code porting, optimization, and application development.

MHPCC is a well-established member of the High Performance Computing community, participating in collaborations and partnerships that extend its basic capabilities. MHPCC represents AFRL as a:

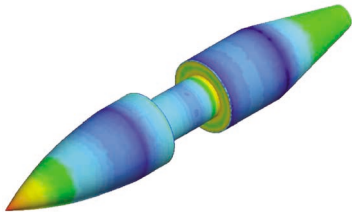
- Center within the Air Force Research Laboratory. MHPCC works closely with DoD and other government researchers to support Research, Development, Testing, and Evaluation (RDT&E) efforts.
- Distributed Center within the DoD High Performance Computing Modernization Program (HPCMP). MHPCC provides resources to the DoD research community, as well as Pacific Region DoD organizations, including the Air Force's Maui Space Surveillance Complex.
- Air Force Research Laboratory resource for the Air Force Maui Optical & Supercomputing Site (AMOS).
- Member of Hawaii's growing science and technology community.



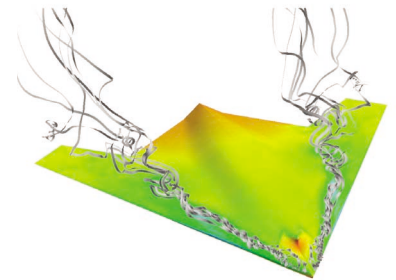


## APPLICATION BRIEFS

The user application briefs in this publication represent selected research efforts that have taken place at MHPCC during 2003. Each application brief was written by an individual researcher or research team, and reflects their first-hand experiences using MHPCC resources. These articles reflect the diverse nature of our users and projects.



The Application Briefs in this document are the result of the efforts of more than 80 authors representing 30 organizations. We acknowledge the contributions of each of these individuals and are grateful for their work. We welcome back those authors who have become regular and frequent contributors. Joel T. Johnson is especially recognized for his ninth consecutive year of contributions to this publication. We also welcome those making their MHPCC Application Briefs debut this year.



The shaded box at the top of each brief's first page is a short summary of the article. Author and/or organizational contact information can be found in the shaded box at the end of each brief. The notation at the bottom of each page indicates each project's primary functional area (DoD, Government, or Academic).

And finally, feedback regarding this publication is solicited. Please direct any communications to: [editor@mhpcc.hpc.mil](mailto:editor@mhpcc.hpc.mil).

*Thank you for your support.*

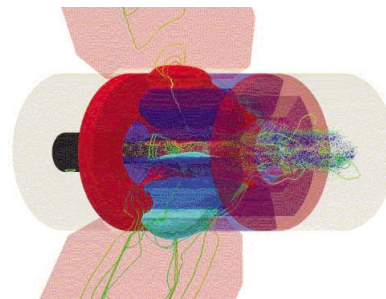
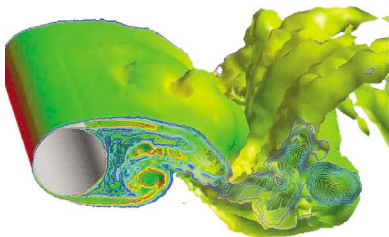


# TABLE OF CONTENTS

<b>Numerical Computation of Scattering From a Penetrable Target Below a Rough Surface</b> .....	1
Joel T. Johnson	
<b>Improving the Performance of Finite Element Computations through Parallel Processing</b> .....	2
S. D. Rajan, D. T. Nguyen, So Hui Yu, David Lau, James St. Ville	
<b>Numerical Studies of Fiber Optical Signal Attenuation from Compression and External Fields</b> ....	4
Garry Rodrigue, Jennifer Mariana, Joseph Koning	
<b>Monte Carlo Simulations of Liquid-Crystalline Elastomers</b> .....	6
Jonathan V. Selinger and B. R. Ratna	
<b>Synthesizing Reference Star Data for Object Amplitude Correction</b> .....	8
Kathy Schulze	
<b>Panoramic Survey Telescopes and Rapid Response System (Pan-STARRS)</b> .....	10
Bruce Duncan, Mark A. Skinner, Brian Banks, Robert Borchers, Paul Bundschuh D. J. Fabozzi, George Gusciora, Maria Hancock, Carl Holmberg, Bobby Hunt, Mitch Murphy, Michael Berning, Kyle Cooper, William DeMeo, Cynthia Giebink	
<b>Endmember Selection and Demixing in Hyperspectral Imagery</b> .....	12
David Gillis, Jeffrey Bowles, Michael Bettenhausen, Michael Winter	
<b>Electronic Structure of Icosahedral As@Ni<sub>12</sub>@As<sub>20</sub> Cluster</b> .....	14
Mark R. Pederson and Tunna Baruah	
<b>Full-Scale Simulations of Bubbly Flows Around the Research Vessel Roger Revelle</b> .....	16
Francisco J. Moraga, Donald D. Drew, Richard T. Lahey, Jr.	
<b>Simulation and Redesign of the Compact A6 Magnetron</b> .....	18
Peter J. Mardahl, Keith L. Cartwright, Lester A. Bowers, Michael D. Haworth, John W. Luginsland, Tony Murphy	
<b>Simulations of Stormtime Ring Current Magnetic Field</b> .....	20
Margaret W. Chen	
<b>Multidisciplinary Applications of Detached-Eddy Simulation to Separated Flows at High Reynolds Numbers (Challenge 92)</b> .....	22
Scott A. Morton, James R. Forsythe, Matthew B. Steenman, Russell M. Cummings, Kenneth E. Wurtzler, Shawn H. Woodson, Kyle D. Squires, Philippe R. Spalart	
<b>High Performance Computing &amp; Visualization Support for Project DE/TOSS</b> .....	25
Brent Swartz, Paul Kominsky, Brian Kruse	
<b>Airborne Laser Atmospheric Characterization/Atmospheric Decision Aide (ADA)</b> .....	26
Randy J. Lefevre, Frank H. Ruggiero, Kevin Roe	
<b>High-Resolution Forecasts to Support AMOS Using MM5</b> .....	28
Kevin Roe and Duane Stevens	

# TABLE OF CONTENTS

<b>High Performance Computing and Web Support for Project Albert: Analysis of Entity-Based Simulations of Combat Operations and Operations Other Than War</b> .....	30
Bob Swanson, Brent Swartz, Maria Murphy, Ron Vilorio, D. J. Fabozzi, Bruce Duncan	
<b>Quantum Lattice Gas and Lattice Boltzmann Simulations of MHD Turbulence</b> .....	32
Linda Vahala, George Vahala, Angus Macnab, Jeffrey Yezep	
<b>Towards a High-Resolution Global Coupled Navy Prediction System: Ocean and Ocean/Ice Components</b> .....	34
Julie McClean, Mathew Maltrud, Detelina Ivanova, Prasad Thoppil, Elizabeth Hunke	
<b>Theater Undersea Warfare (TUSW)</b> .....	36
Bob Dant, Lance Terada, Carl Holmberg, Marie Greene, Thomas Meyer, Mark Radleigh	
<b>Novel Active Optics with <math>10^{23}</math> Photomechanical Actuators</b> .....	38
Joe Ritter, Jim Brozik, Luke Emmert, Mike Fallbach, Rodney Bradford, Don Leo, Ken Meissner	
<b>Novel Combined Cis-Trans/Twisted Intermolecular Charge Transfer (CCT-TICT) Actuated Adaptive Optics</b> .....	40
Joe Ritter and Jim Brozik	
<b>Environment for Design of Advanced Marine Vehicles and Operations Research (ENDEAVOR)</b> .....	42
Robert Dant, D. J. Fabozzi, Carl Holmberg, Scott Splean	
<b>A Highly Parallel Physically Constrained Iterative Blind Deconvolution Algorithm: PCID</b> .....	44
Kathy Schulze, Stuart Jefferies, Charles L. Matson	
<b>Low-Energy Elastic Electron-Magnesium Scattering</b> .....	45
Igor Bray	
<b>INDEX OF AUTHORS</b> .....	Index-1
<b>INDEX OF ORGANIZATIONS</b> .....	Index-2



# Numerical Computation of Scattering from a Penetrable Target Below a Rough Interface

Joel T. Johnson

**G**round penetrating radar is an important technology for the detection of sub-surface objects (such as landmines). These sensors measure scattered electromagnetic fields from both the rough ground surface and any sub-surface objects; separating the two contributions is critical for developing an effective sensor. Simple models can be made to describe these effects analytically, but in many cases the inherent approximations break down. Use of efficient algorithms and parallel computing resources now makes numerical solution of coupled 3-D target/surface geometries possible so that the scattering physics can be studied without approximation.

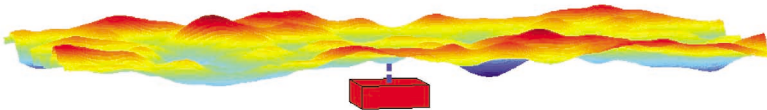
**M**ethodology: The studies of this project involve predicting scattered fields from a target below a statistically described rough surface. A Monte Carlo simulation is used to capture scattered field statistics, and a standard numerical method, the method of moments, is used for scattering calculations. To improve computational efficiency, an iterative rather than direct matrix solver is used. In addition, the "canonical grid" and "discrete dipole" methods are used to compute surface to surface and target to target point couplings

respectively in order  $(N \log N)$ . The studies of interest involve frequency swept calculations; since single frequency results are obtained from the algorithm, parallel computing resources are applied by running separate frequency calculations on individual nodes. Time domain responses can then be synthesized from multiple frequency data in a post-processing step. Because surface roughness effects are stochastic, a parallel Monte Carlo simulation is also used to capture scattered field statistics.

**Results:** A Monte Carlo simulation has been completed for a simple penetrable (plastic-like) object below a moderately rough soil surface, intended to model a non-metallic landmine below rough ground. The Monte Carlo simulation used forty surfaces which were realizations of a Gaussian random process with an isotropic Gaussian correlation function described by rms height 1 cm and correlation length 3.58 cm. Figure 1 illustrates the geometry considered while Figure 2 plots time domain backscattered field statistics at normal incidence (direct surface backscattering is removed) obtained from 2 to 5 GHz data. Results show that average (coherent) fields in the presence of surface roughness can be significantly different from those with a flat surface, and that the standard deviation of time domain fields (incoherent) can also be significant (in this case, comparable to average field values).

Backscattering computed at 16 frequencies from 2-5 GHz for normal and 45 degree incidence

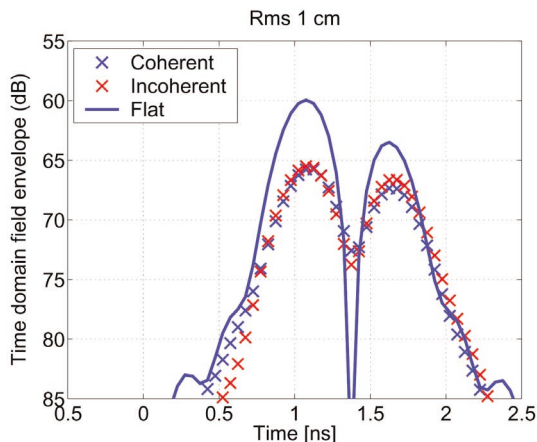
Surface size is  
1.28 x 1.28 m  
 $\epsilon = 5 + i1.25$



Isotropic Gaussian  
correlation function  
Cor. len. 3.58 cm  
Rms ht 3.58 mm or  
1 cm

Box is 7.62 x 7.62 x 2.54 cm,  $\epsilon = 3 + i0.03$   
Center is 8.89 cm below mean surface plane

**Figure 1.** Geometry of target below surface problem considered.



**Significance:** The results of this project can be applied to assess and to extend radar signal processing algorithms for the detection and identification of sub-surface objects. Detailed studies of numerical results can also suggest means for developing improved analytical models of the surface-target scattering process.

**Figure 2.** Time domain object backscattered field statistics for normal incidence. Average (coherent) fields in the presence of surface roughness are significantly different from those with a flat surface, and field standard deviations (incoherent) are also significant.

Author and Contact: Joel T. Johnson  
Organization: Ohio State University, 205 Dreese Laboratories, 2015 Neil Ave., Columbus, OH, 43210  
URL: <http://eewww.eng.ohio-state.edu>  
Resources: IBM Netfinity Linux Supercluster at MHPCC  
Sponsorship: Department of Defense

# Improving the Performance of Finite Element Computations through Parallel Processing

S. D. Rajan, D. T. Nguyen, So Hui Yu, David Lau, James St. Ville

High performance computations (HPC) in the context of this work imply software where a large amount of time is spent in computations involving small and large arrays and floating-point operations. One of the areas where such computations are routinely carried out involves the solution of partial differential equations (PDEs). Of the several approaches to solving PDEs, finite element method (FEM) is the most popular method. FEM has become the defacto industry standard for solving multi-disciplinary engineering problems. The usage of the methodology cuts across several industries (civil, aerospace, automotive, mechanical, biomedical, electronic, hydraulics, environmental, geotechnical, chemical) by virtue of the applications – solid mechanics, fluid mechanics, heat transfer, acoustics, electromagnetics and many more. In this work, the performance of the finite element computations is improved using domain-decomposition (DD) approach coupled with sparse storage scheme and direct and preconditioned iterative solvers. Two examples are presented to illustrate the performance of the developed software system.

**Introduction:** FEM has been used to solve problems involving a small number of unknowns (a few hundred) to extremely large numbers of unknowns (hundred million).<sup>1</sup> However, the bulk of the work is still performed on uniprocessor machines. For the first time ever, two PC-based clusters were able to gain a top 10 spot in the top 500 fastest computer systems in the world. At the fifth position is a cluster at Lawrence Livermore National Laboratory built by Linux NetworX and Quadrics. At eighth position is a cluster at the Forecast Systems Laboratory at NOAA built by HPTi with a Myrinet interconnect.<sup>2</sup> It is a matter of time before commodity PCs are used routinely in areas that require high performance computations either as a standalone unit or in a cluster, in lieu of supercomputer-like machines. In any case, the lines separating the categories of computing platforms are now blurred.

**Research Objectives:** A software system (DESIGN3D) has been developed to implement the FE methodology along with the well-known domain decomposition technique where the original FE model is split into a number of smaller subdomains. Direct sparse solver is used at the subdomain level and preconditioned conjugate gradient (PCG) is used at the interface system level. The finite element equations are then generated and assembled at the individual domain level in parallel. Matrix and vector operations involving sparse matrices form the bulk of the computations in this step. Once these equations are assembled, the condensed system level equations are formed. These condensed system level equations are usually much smaller (but denser) than the original system equations, and hence can be computationally expensive. DESIGN3D is developed using object-oriented concepts in C++ and uses MPI for message passing. The objective then was to study the performance of DESIGN3D on MHPCC's Linux supercluster in solving large FE models that cannot be solved in-core on a 32-bit single processor machine.

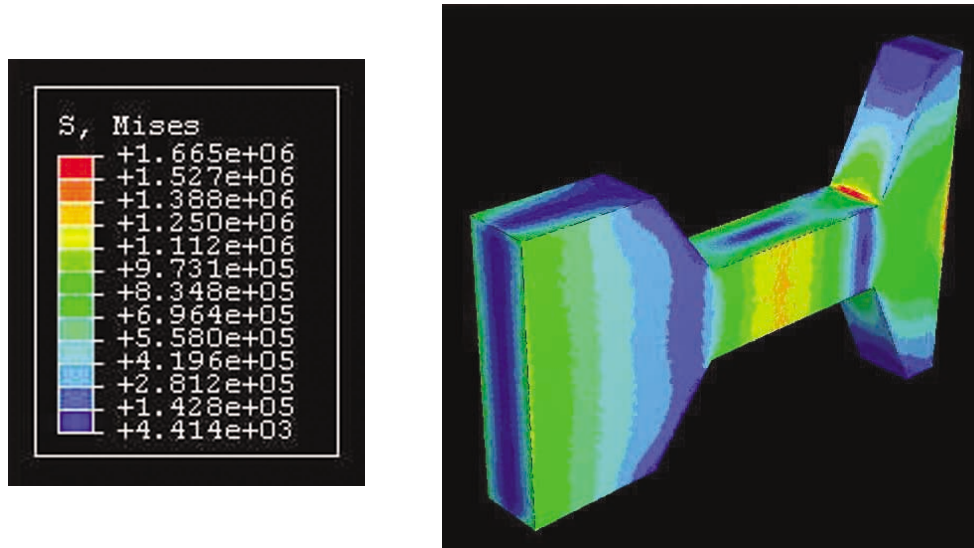


Figure 1. Von Mises stresses in the support platform.

**Results:** Two examples are presented. Both of these examples cannot be solved on a single processor 32-bit OS unless out-of-core equation solvers are used. Figure 1 shows the larger of the two models. It represents a thick support platform fixed at both ends and loaded uniformly at the center. Displacements, strains, and stresses throughout the model are solved. Tables 1 and 2 show the performance gains obtained when the problems are solved on the *Huinalu* cluster (a typical node is a dual-processor Pentium III-933 MHz with 1 GB RAM).

# of Processors	Wall Clock Time (sec.)
8	1911
16	1042
32	588
64	463

**Table 1.** Performance Study for the Support Bracket FE Problem (334,068 unknowns or displacements).

# of Processors	Wall Clock Time (sec.)
8	2878
16	1348
32	828
64	629

**Table 2.** Performance Study for the Support Platform FE Problem (507,429 unknowns or displacements).

**Future Work:** The overall objective of the HPC software system under development is to find the optimal design and manufacturing steps given the performance requirements for an engineering component or system using finite elements, design optimization, and other numerical techniques.

**References:**

- 1) Earth Simulator Center, <http://www.es.jamstec.go.jp>, Japan.
- 2) Top 500 Supercomputing sites, <http://www.top500.org>, 2002.

Author and Contact: S. D. Rajan  
 Organization: Department of Civil Engineering, Arizona State University, Tempe, AZ, 85287  
 Author: D. T. Nguyen  
 Organization: Department of Civil Engineering, Old Dominion University, Norfolk, VA, 23529  
 Authors: So Hui Yu, David Lau, James St. Ville  
 Organization: Hawthorne & York International, Ltd., 3908 E. Broadway, Suite 110, Phoenix, AZ, 85040  
 Resources: IBM Linux Supercluster, *Huinalu*, at MHPCC  
 Sponsorship: U. S. Army Aviation ManTech at Redstone Arsenal

# Numerical Studies of Fiber Optical Signal Attenuation from Compression and External Fields

Garry Rodrigue, Jennifer Mariani, Joseph Koning

**D**igital signal attenuation, disruption and losses in fiber optic communication systems can occur from torsion or compression of the fiber as well as incident external fields on the fiber. Examples include signal losses from optical fiber distortions such as bending or twisting or subjecting the fiber to intense external electromagnetic fields. We have developed a highly efficient numerical simulation to study electro-optical wave propagation in complicated 3-dimensional geometries with the goal of understanding and possibly preventing signal losses from this phenomenon. The fundamental numerical spatial building block is the vector finite element. The time domain is approximated to second order accuracy and uses fully consistent mass matrices.

**M**ethodology: The studies of this project involve modeling optical wave propagation in a cylindrical waveguide that is distorted by bending and subjected to intense external electromagnetic fields and then determining the signal loss. We model the optical wave propagation with the full three-dimensional Maxwell's equations and solve the equations using the vector finite element method. This allows us to represent complicated geometries by unstructured hexahedral grids and to preserve tangential continuity of the electric fields. The Galerkin approach is used to approximate Maxwell's equations by a system of second order ordinary differential equations which are

then solved by the leap-frog time differencing method.<sup>1</sup> The dimension of the mass and stiffness matrices in the ordinary differential equation is the number of edges in the hexahedral mesh approximating the geometry and could be on the order of  $10^9$  because of the grid resolution required by the shortness of the wavelength of light. In addition, stability constraints induced by the speed of light force the leap-frog method to take time steps on the order of  $10^{-14}$ . Since we use consistent mass matrices, a matrix inversion must be performed at each time step on a matrix that is large, sparse, and unstructured.

**Results:** We are currently performing two independent studies. The first is to model the propagation of an optical wave in a bent optical fiber and the second is to model the propagation of an optical wave in a straight optical fiber that has an external microwave incident to it.

**Bent Fiber:** The indices of refraction in a straight step-indexed optical fiber govern the type of light waves that will be guided. However, if the fiber is bent, the guidance properties of the fiber no longer hold and the optical wave may leak out of the fiber core into the cladding resulting in premature wave attenuation. Figure 1(a) illustrates the 1.8 million element approximation of a 52.8 micron length of a bent fiber with 55.13 micron bend radius. 5.66 million unknowns are required to be numerically determined. The computation requires 72 hours on 38 processors of the MHPCC *Huinalu* Linux based supercomputer and 22 hours on 38 processors of the LLNL MCR Linux based supercomputer. The Gaussian pulse of the  $TE_{01}$  mode can be seen in Figure 1(b) where the core is purple and the cladding green. A close up of the pulse interacting with core-cladding interface is shown in Figure 1(c) where the core is again purple and the cladding is blue.

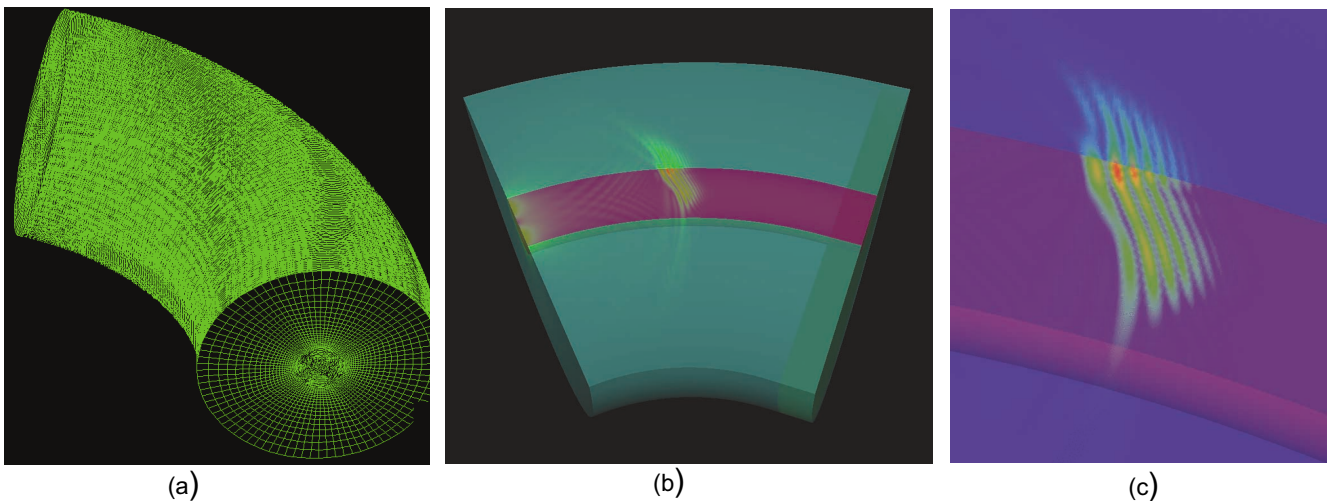


**Figure 1.** (a) Numerical grid of bent fiber, (b) Leakage of transverse Gaussian pulse, and (c) Close up of leakage.

**Microwave Interference:** External electromagnetic fields can affect the propagation properties of a fiber optic waveguide. In particular, the refractive indices of the fiber optic core and cladding can be altered in a nonlinear manner by highly intense external microwaves so as to cause optical signal loss. We study the effects of an incident plane microwave on the propagation of a transverse optical wave ( $TE_{01}$ ) in a step-indexed optical fiber. We track the electric field magnitude and the electric field vectors as the simulation progresses in time. The electric field vectors allow us to visually determine the polarity of the wave and monitor its behavior as it interacts with microwave. Figure 2(a) shows the electric field magnitude distribution of the optical wave at the beginning of the simulation ( $t=0$ ). Here, the impinging microwave has not been introduced and consequently the signal remains intact. The optical wave is shown at a later time of 30 sec. in Figure 2(b). Note that the electric field vectors indicate that the optical wave is linearly polarized and still intact in the core. The outer edge of the cladding is represented by a black circle. Next, the microwave interference is introduced at about 40 sec. and the simulation is allowed to 380 sec. Figure 2(c) shows the interaction of the microwave with the optical wave at 358 sec. The optical wave in this case is no longer confined to the core with some interaction happening within the cladding. The simulation took 5 hours using a single processor of the MHPCC *Huinalu* supercomputer. The computational grid is composed of 301,000 elements.

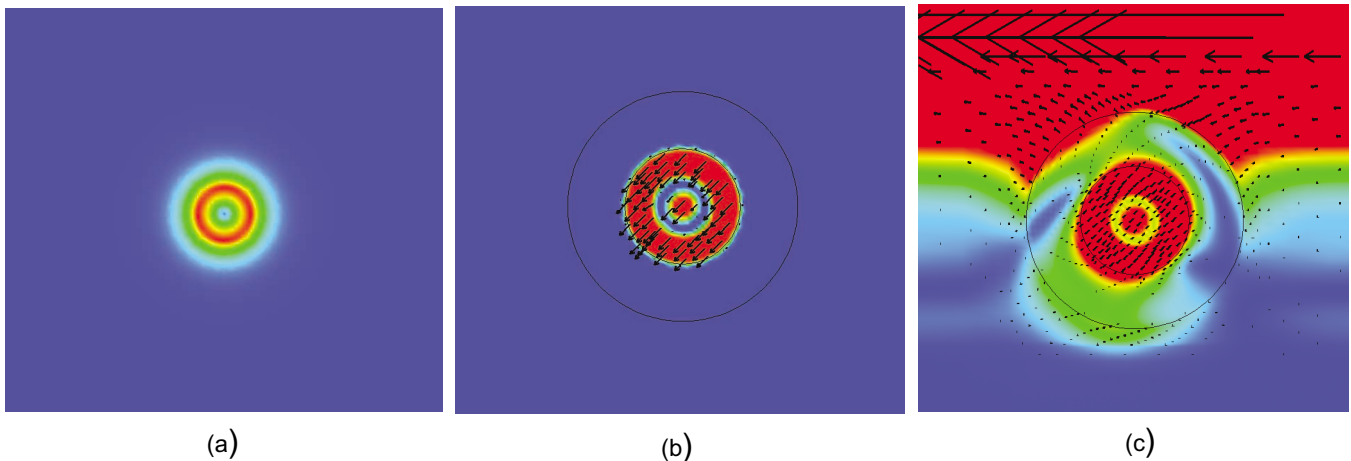


**Figure 2.** (a) Initial state of optical wave, (b) State of optical wave at 30 sec., and (c) State of optical wave at 358 sec., with plane wave microwave interference.

**References:**

- 1) G. Rodrigue and D. White, "A Vector Finite Element Time Domain Method for Solving Maxwell's Equations on Unstructured Hexahedral Grids," *SIAM J. Sci. Comp.*, 23(3) (2001): 683-706.

Author and Contact: Garry Rodrigue  
 Authors: Jennifer Mariani and Joseph Koning  
 Organization: University of California at Davis, Department of Applied Science, Davis, CA, 95616  
 Resources: *Huinalu* Supercluster at MHPCC and MCR at Lawrence Livermore National Laboratory (LLNL)  
 Sponsorship: Air Force Office of Scientific Research and the Department of Energy

# Monte Carlo Simulations of Liquid-Crystalline Elastomers

Jonathan V. Selinger and B. R. Ratna

In liquid-crystalline elastomers, the orientational order and the elastic strain vary smoothly across the isotropic-nematic phase transition, without the expected first-order discontinuity. This broadening of the phase transition is an important issue for applications of liquid-crystalline elastomers as actuators or artificial muscles. To understand this behavior, we have performed Monte Carlo simulations of a lattice model for liquid-crystalline elastomers with quenched disorder. These simulations show a broadening of the phase transition consistent with the experiments and show the heterogeneity that must be controlled to enhance the sharpness of the transition.

**Research Background:** Liquid-crystalline elastomers are unusual materials that combine the elastic properties of rubbers with the anisotropy of liquid crystals. They consist of crosslinked networks of polymers with long, rigid, liquid-crystalline units. Because of this structure, any stress on the polymer network influences the orientational order of the liquid crystal, and conversely, any change in the orientational order affects the shape of the elastomer. These materials are being actively studied for both basic research and applications, including use as actuators or artificial muscles. For this application, the temperature is varied around the transition point

between the nematic phase (with long-range orientational order in the liquid-crystalline units) and the isotropic phase (with no long-range orientational order). Near that transition, a small change in temperature induces a large change in the orientational order, which causes the elastomer to extend or contract.

Our group has been investigating the physical properties of the isotropic-nematic transition in liquid-crystalline elastomers. In conventional liquid crystals, this is a first-order transition, with a discontinuity in the magnitude of the orientational order as a function of temperature. By contrast, experiments on liquid-crystalline elastomers show that both the orientational order parameter and the elastomer strain change smoothly at this transition, with no first-order discontinuity. Surprisingly, this is neither a first- nor a second-order transition, but rather a rapid nonsingular crossover from the isotropic to the nematic phase. Thus, a key question is how to explain this difference between conventional liquid crystals and liquid-crystalline elastomers. That question is important for basic research, because it shows how liquid-crystalline ordering is affected by coupling to a crosslinked polymer network. That question is also important for applications, because it shows how to optimize these materials for artificial muscles, which should have the greatest possible length change for a fixed temperature change.

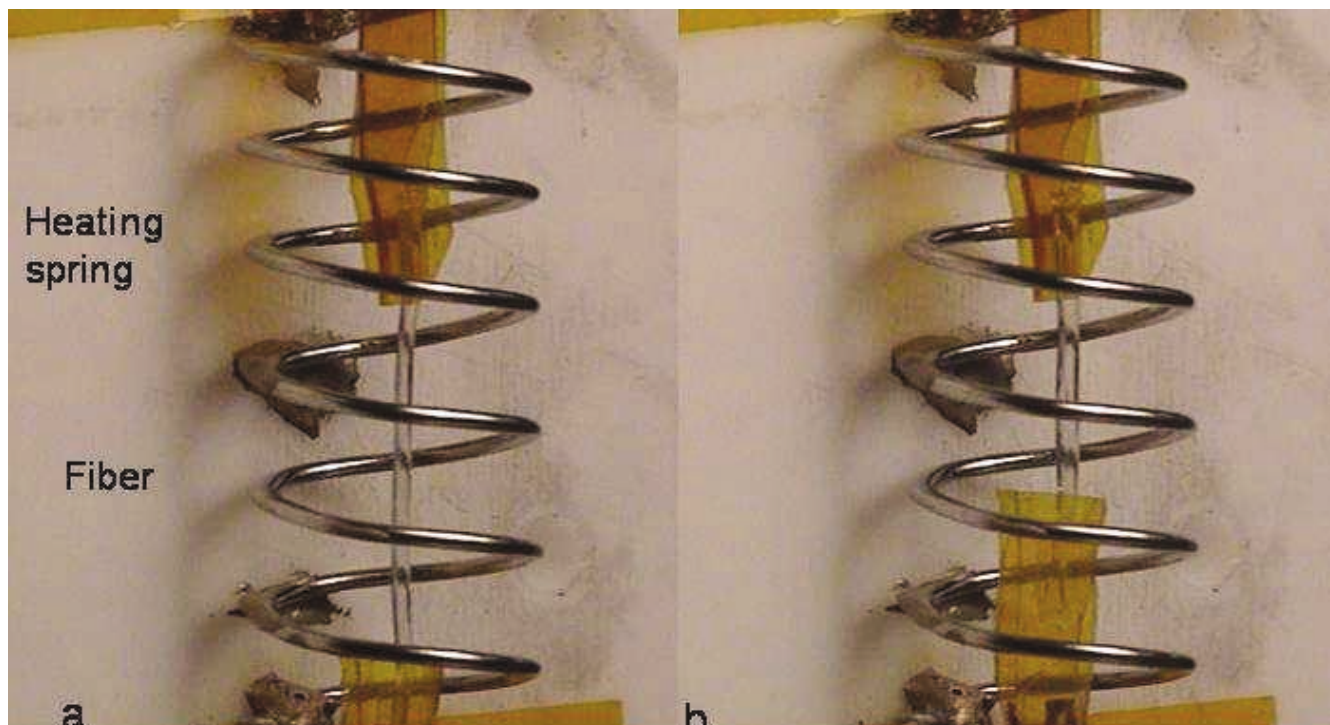


**Figure 1.** Reversible extension and contraction of a liquid-crystalline elastomer fiber, which is heated by an electrical current through a coil. (a) Extended state in the low-temperature nematic phase. (b) Contracted state in the high-temperature isotropic phase.

In a recent experimental study, our group found that the broadening of the isotropic-nematic transition is related to quenched disorder that is fixed into elastomers at the time of crosslinking [J. V. Selinger, H. G. Jeon, and B. R. Ratna, "Isotropic-Nematic Transition in Liquid-Crystalline Elastomers," *Phys. Rev. Lett.* 89, 225701 (2002)]. This result leads to two important theoretical issues. First, how can we model a transition in a heterogeneous material that develops an overall elastic strain? Second, what type of heterogeneity has the greatest effect on the material? This could be a heterogeneity in the chemical composition, leading to a variation in the local isotropic-nematic transition temperature, or a heterogeneity in the local random stress acting on the liquid-crystalline order.

To address these questions, we have developed a lattice model of liquid-crystalline elastomers. In this model, we consider a three-dimensional cubic lattice with a liquid-crystalline director on each site. These directors are coupled to their neighbors through an interaction that favors orientational order. In addition, each director is coupled to a global strain variable that represents the overall elastic distortion of the material. We can introduce quenched disorder into this model in two different ways. Chemical heterogeneity can be represented by a variation in the local bond strength between neighboring directors, while heterogeneous local stresses can be represented by a random local field coupling to the directors.

We have performed Monte Carlo simulations of this lattice model on the *Huinalu* Linux Supercluster at MHPCC. For a homogeneous elastomer, these simulations show the expected behavior: The system has a first-order transition between the isotropic and nematic phases, as indicated by discontinuous jumps in the orientational order and the elastic strain as functions of temperature. However, the behavior changes radically when quenched disorder is introduced. With either type of quenched disorder – chemical heterogeneity or heterogeneous local stresses – the first-order transition can broaden into a smooth crossover between the isotropic and nematic phases, consistent with the experiment.

Our simulation effort has already provided a model for the unusual physical properties of the isotropic-nematic transition that is observed in liquid-crystalline elastomers. In further numerical studies, we are trying to distinguish between these two types of quenched disorder by detailed studies of the distribution of the orientational order parameter. This continuing work will help to improve our understanding of the heterogeneous structure that must be controlled for applications of liquid-crystalline elastomers.

Author and Contact: Jonathan V. Selinger

Author: B. R. Ratna

Organization: Center for Bio/Molecular Science and Engineering, Naval Research Laboratory, Code 6900, Washington, DC, 20375

Resources: *Huinalu* Linux Supercluster at MHPCC

Sponsorship: Department of Defense

# Synthesizing Reference Star Data for Object Amplitude Correction

Kathy Schulze

Satellite data collected using the Maui Space Surveillance System (MSSS) GEMINI sensor is distorted by the earth's atmosphere. Removing the distortions can be accomplished using image recovery algorithms like bispectrum. The bispectrum algorithm, in use at MSSS for over 10 years, estimates the Fourier data of the object separately and requires an additional calibration measurement called a reference star. To be effective, reference star data must be collected under the same seeing conditions as the object. Due to atmospheric variations, this is not always possible resulting in lower quality bispectrum recoveries.

This paper discusses the effect of using incorrect reference star data on bispectrum recoveries and shows results obtained using synthetic reference star data. Also, the use of metrics to determine when the seeing conditions between the object data and the synthesized reference star data are in agreement resulting in optimal recoveries is briefly discussed.

Synthesizing reference star measurements decreases the amount of data collected and reduced, increasing the time available for satellite observations. Research indicates synthesizing this data increases the quality of the recoveries by eliminating the seeing conditions mismatch between object and reference star data.

**Background:** Image recovery algorithms reduce multiple short exposures into one picture or recovery. Linear algorithms, like bispectrum, solve for the Fourier phase and amplitude separately then combine these components to form the recovery. The bispectrum algorithm estimates the Fourier phase of the object (a satellite in this case) from the bispectrum<sup>1</sup> and estimates the Fourier amplitude of the object using Labeyrie's technique.<sup>2</sup> Labeyrie's technique requires a separate collection of calibration data called a reference star. The reference star data is used to estimate the point spread function of the atmosphere causing the distortion in the collected object data. Using reference star data collected under different seeing conditions than the object has a negative impact on the quality of the bispectrum data products.

Sophisticated software to simulate data collected using the MSSS telescopes is used to study effects like this and improve image recovery algorithms. Figure 1 shows a 16 frame bispectrum recovery on the right with a single raw data frame for comparison on the left. In this bispectrum recovery, both the object data and the reference star data used to correct the object amplitude were simulated. For the purpose of this paper, object data was simulated at 15 cm and reference star data was simulated at 5, 10, 15, 20, and 25 cm  $r_0$ . The Fried parameter,<sup>3</sup>  $r_0$ , is a measure of the seeing conditions. The recoveries shown in all other sections were obtained using the corrected ensemble average power spectrum from 16 short exposure frames and the truth phase. Using the truth phase allows direct comparison of the recoveries and the effect of the various amplitude corrections employed.



Figure 1. Raw data with bispectrum recovery.

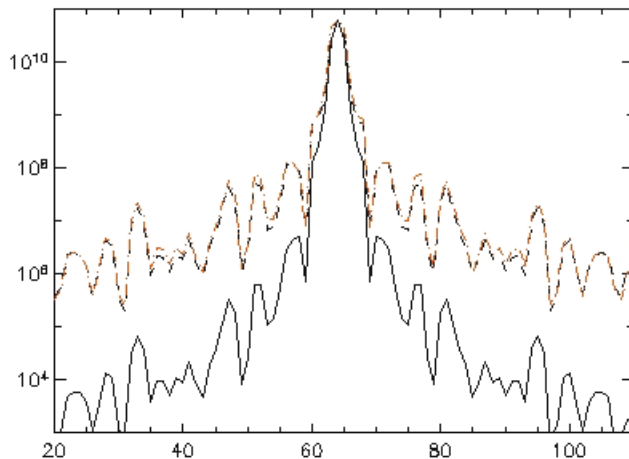


Figure 2. Effect of amplitude correction on recovery.

**The Effect of Amplitude Correction:** Correctly or incorrectly collecting and reducing reference star calibration data affects the object recovery contrast. The procedure is to form the ensemble average power spectrum from the sequence of short exposure frames of the object and separately of the reference star. The reference star ensemble average is normalized and deconvolved from the ensemble average object power spectrum. Consider the 16 frame recoveries shown in Figure 2. The recovery on the left uses no reference star amplitude correction and is only marginally better than the raw data shown in Figure 1. The two recoveries in the center use 'reference star' data that was obtained under different seeing conditions than the object data. These recoveries suffer from 'dishing' where there are areas in the recovery that are missing, or 'clouding' where the recovery is surrounded by a halo effect. The final recovery on the right shows amplitude correction using matching object and reference star data.

The plotted data in Figure 3 are slices through the power spectrum and show very good agreement between the optimally corrected object power spectrum and the truth power spectrum and a good deal of improvement over the uncorrected data. Please keep in mind that our simulated data is noise free.

**Matching  $r_0$  Between Synthetic Reference Star and Object Data:** To optimally correct the object amplitude we must match the seeing conditions ( $r_0$ ) between the synthetic reference star data and the object data. A recovery from the uncorrected amplitude and recoveries from the various synthetic star corrected object amplitude data can be compared using metrics designed to make the match. A threshold metric is used to determine the amount of change in the amplitude of the recovery with the various reference star datasets. A signal to noise metric is used to determine residual noise in the recovery. In the test cases, using both metrics together allows automatic selection of the optimal reference star data for amplitude correction. This automatic selection results in the best fit to the data and gives the best recovery result as shown in Figure 4. The matching reference star and object data (by seeing conditions,  $r_0$ ) is shown along the diagonal from top left to bottom right. These simulated data included both Gaussian and Poisson noise for a realistic test of our matching criteria.



**Figure 3.** Legend: Black solid line—Uncorrected object power spectrum, Orange dashed line—Optimally corrected power spectrum and Black dashed line—Truth power spectrum.

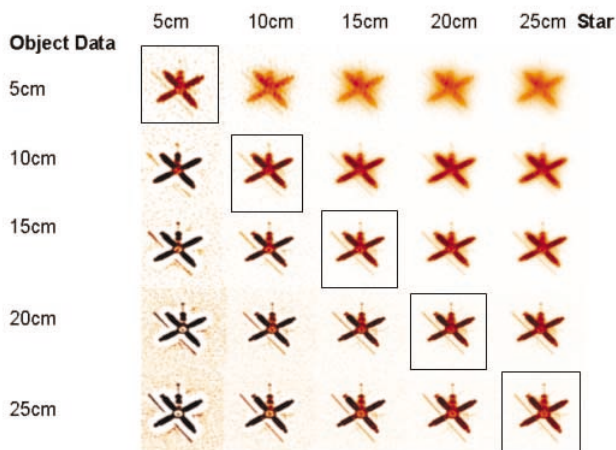


**Figure 4.** Recoveries obtained by cross matching object data with reference star data. True seeing match data is along the diagonal from top left to bottom right.

**Summary:** Although further refinement will be obtained in optimizing these synthetic reference star results, these preliminary results are very promising. Synthesizing the reference star data eliminates the need for the additional calibration data collection tasks and gives optimal amplitude correction to all recoveries within a pass. This technique also opens up a variety of other uses for data reduction using bispectrum that were previously not available. Uses can include support for missile launches, where no reference star data is available.

Successful integration of this research into the GEMINI operational system will eliminate the collection and reduction of reference star data.

**References:**

- 1) T. Matsuoka and T. J. Ulrych, "Phase Estimation Using the Bispectrum," Proc IEEE 72 (1984): 1403-1411.
- 2) A. Labeyrie, "Attainment of Diffraction Limited Resolution in Large Telescopes by Fourier Analyzing Speckle Patterns in Star Images," *Astronomy & Astrophysics*, Vol. 6 (1970): 85.
- 3) D. L. Fried, "Optical Resolution Through a Randomly Inhomogeneous Medium for Very Long and Very Short Exposures," *J. Opt. Soc. Am.*, Vol. 56 (1966): 1372-1379.

Author and Contact: Kathy Schulze  
 Organization: KJS Consulting, P.O. Box 591, Georgetown, DE, 19947  
 Resources: *Tempest* system, interactive and batch and Interactive Display Language (IDL), Fortran and C compilers, and Message Passing Interface (MPI) at MHPCC  
 Sponsorship: Air Force Office of Scientific Research  
 Acknowledgement: The author gratefully acknowledges Major William Hillbun, Program Manager, and Dr. David Tyler, Principal Investigator, for their support.

## Panoramic Survey Telescopes and Rapid Response System (Pan-STARRS)

Bruce Duncan, Mark A. Skinner, Brian Banks, Robert Borchers, Paul Bundschuh, D. J. Fabozzi, George Gusciora, Maria Hancock, Carl Holmberg, Bobby Hunt, Mitch Murphy, Michael Berning, Kyle Cooper, William DeMeo, Cynthia Giebink

**P**an-STARRS is an Air Force Research Laboratory (AFRL) Directed Energy (DE) Directorate program that fuses astronomy, information technology, data processing, and data management. This system will provide unprecedented capabilities for advanced research into deep-space astrometry, photometry, and planetary defense. It is currently estimated that Pan-STARRS will provide a 5 Terabytes (TB) per night data stream and a 100 TB cumulative image database. The 'Core' system will generate a static sky atlas and a difference-image stream for detection of transients and fast-moving objects. The University of Hawaii's (UH) Institute for Astronomy (IfA) has been awarded a grant by AFRL for the overall prime Pan-STARRS system development responsibility, and the design and development of the telescopes, optics, detectors, and related facility infrastructure.

**B**ackground: Pan-STARRS is an Air Force Research Laboratory Directed Energy Directorate program that fuses astronomy, information technology, data processing, and data management. This panoramic optical imaging system is being developed to provide advanced research into deep-space astrometry, photometry, and planetary defense (Figure 1). The Pan-STARRS telescope system will include a dedicated very wide field-of-view (WFOV) array of four small telescopes with extremely large Charge Coupled Device (CCD) cameras with 1 billion pixels each that are capable of taking images of space approximately every 30 seconds (Figure 2). The system will also be comprised of a state-of-the-art Data Processing Pipeline System and Data Management system, with an interface to the National Virtual Observatory (NVO) initiative. Pan-STARRS will survey the entire visible sky observable from Hawaii in four nights. It will provide unique time-resolution capability that will

enable asteroid detection (including potential killer asteroids), and detection of supernovae, gamma ray bursts, other transient objects, and perhaps unknown phenomena. The system will also generate a deep-space digital atlas of 70% of the sky, detecting nearly all dangerous objects and provide ultra-deep-space images of selected regions. Pan-STARRS will detect 24th magnitude objects, allowing it to detect 300 meter size asteroids. The system will enable very efficient detection of multiple moving space objects and their orbit determination. It is currently estimated that Pan-STARRS will provide a 5 Terabytes per night data stream and a 100 TB cumulative image database. The 'Core' system will generate a static sky atlas and a difference-image stream for detection of transients and fast-moving objects. The University of Hawaii's Institute for Astronomy has been awarded a grant by AFRL for the overall prime Pan-STARRS system development responsibility, and the design and development of the telescopes, optics, detectors, and related facility infrastructure.

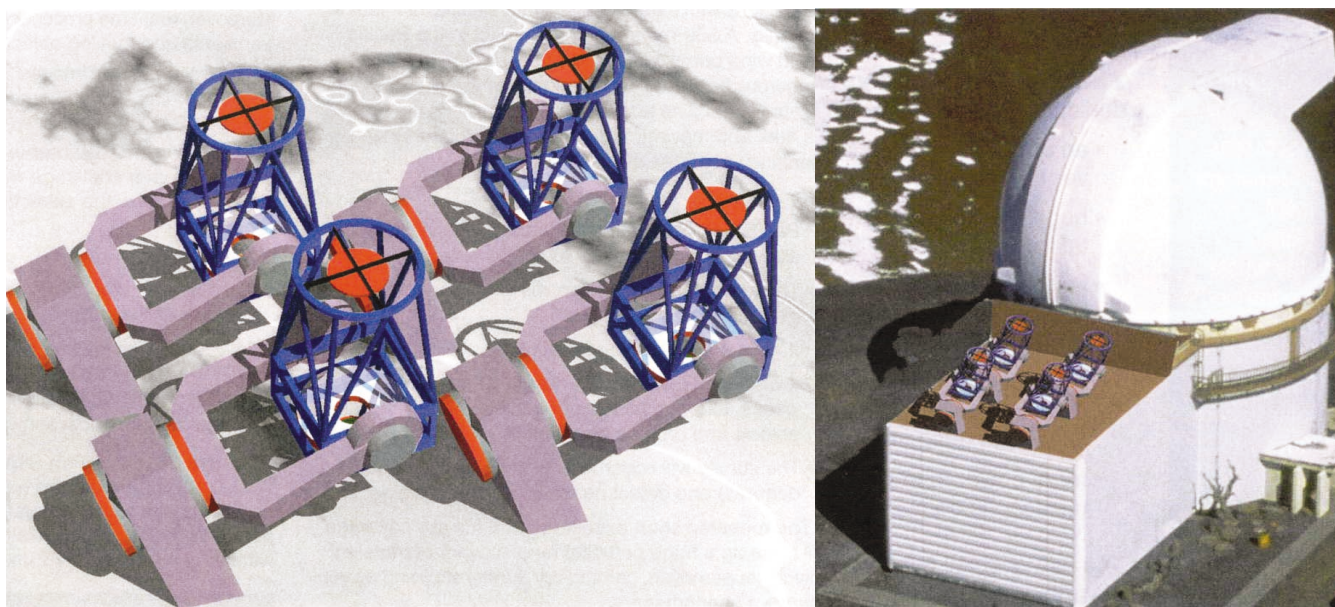
The Maui High Performance Computing Center (MHPCC) will provide the high performance near-real-time parallel processing needed for this system, receiving data from the telescopes over a high-speed fiber optic link. Under an AFRL Task Order contract, MHPCC is an associate contractor for the project and is providing engineering support services and computational support for Pan-STARRS. This work is focusing on system data processing pipeline design and architecture studies, algorithm development, software development and prototyping, data processing system development, data storage and retrieval, and computational and optical research.



Figure 1. A concept drawing of an asteroid impacting Earth.

The MHPCC data processing system is being based on legacy IfA image processing codes. Studies will be conducted to determine if improvements can be made to the baseline codes. This will include identification of potential communication bottlenecks, potential data loss penalties, and requirements to avoid them. Simulations may be developed and utilized by MHPCC to support this activity. Work will also include consideration of alternatives to the currently heavy disk I/O-intensive processes (e.g., storage of calibration images in memory, rather than disk). MHPCC will recommend improvements that emerge from this research. MHPCC plans to implement a prototype parallel computing version of the image data pipeline at MHPCC, after IfA makes the software available to MHPCC. This will include any approved improvements identified in the performance of the pipeline algorithm research/refinement activities. MHPCC will also perform a survey and cost analysis for the data processing pipeline hardware, software, and related infrastructure. MHPCC is designing for image data processing (and planning for operational and maintenance hardware) support for the data reduction pipeline, including flat-fielding, astrometric registration, photometric calibration, accumulation of static sky images, and generation of a difference-image stream along with required catalogs. MHPCC is also planning to provide support for the data processing environment for the astrometry pipeline and dedicated science clients, as well as the data management system, archive, and National Virtual Observatory (NVO) interface.

Finally, MHPCC is conducting research, in coordination with IfA, of diagnostic and "checkpoint" methods to ensure the integrity of the input data and archive-destined data for long-term use and user utility. This includes the application of appropriate loss-less data compression algorithms to minimize the storage requirements of the Pan-STARRS archive. MHPCC is coordinating with IfA to determine specific and general user data mass storage, retrieval, and backup requirements for the image data. MHPCC is also performing a survey and cost/benefit analysis and considering alternatives in planning for Pan-STARRS data storage, retrieval, backup systems, and the needed infrastructure for MHPCC.



**Figure 2.** A concept drawing of a candidate Pan-STARRS telescope system configuration.

Author and Contact: Bruce Duncan

Authors: Mark A. Skinner, Brian Banks, Robert Borchers, Paul Bundschuh, D. J. Fabozzi, George Gusciora, Maria Hancock, Carl Holmberg, Bobby Hunt, Mitch Murphy, Michael Berning

Organization: Maui High Performance Computing Center, 550 Lipoa Parkway, Kihei, HI, 96753

Authors: Kyle Cooper and William DeMeo

Organization: Textron Systems, 535 Lipoa Parkway, Suite 149, Kihei, HI, 96753

Author: Cynthia Giebink

Organization: Maui Scientific Research Center, 590 Lipoa Parkway, Suite 262, Kihei, HI, 96753

Resources: IBM SP3/SP4 *Tempest*, at MHPCC

Sponsorship: Air Force Research Laboratory

# Endmember Selection and Demixing in Hyperspectral Imagery

David Gillis, Jeffrey Bowles, Michael Bettenhausen, Michael Winter

Hyperspectral imagers are remote sensing instruments that are capable of measuring reflectance or thermal energy over hundreds of contiguous spectral channels. A useful technique for processing the large amounts of data generated by hyperspectral imagers is to decompose the scene into a sum of the constituent elements in the scene, known as endmembers. By writing the individual spectra in a scene as a sum of endmembers, the dimensionality of the data can often be reduced by up to an order of magnitude, with little loss of information. This reduction in dimensionality is useful to analysts as both a compression tool and for greatly reducing the amount of calculation needed for post processing applications, such as mineral mapping or target detection.

**Background:** Hyperspectral imagers are a relatively new generation of remote-sensing instruments that record the sensed optical energy in a number of narrow contiguous wavelength channels. They collect image data in hundreds of spectral channels, over wavelength regions that can range from the near ultraviolet through the thermal infrared (depending on the sensor), at resolutions as low as 1 nm. As a consequence of the high spectral resolution, hyperspectral systems produce a massive amount of data in comparison to multispectral or panchromatic systems. Typical images from modern hyperspectral sensors contain over 100 MB of data, with images over 1 GB becoming common.

One technique for dealing with this large amount of data is to decompose the scene into a sum of the constituent elements in the scene. In particular, the linear mixing model (LMM) assumes that each spectrum in the scene may be written as a sum of the dominant spectra in the scene, which are denoted as endmembers. Symbolically, each image spectrum may be represented as an  $n$ -dimensional vector  $v$ , where  $n$  is the number of spectral bands measured by the imager.

The LMM states that  $v$  may be written as the sum

$$v = \sum_{i=1}^k \alpha_i E_i + w$$

where  $E_1, \dots, E_k$  are the endmembers,  $w$  is an  $n$ -dimensional noise vector, and the scalars  $\alpha_1, \dots, \alpha_k$  are the abundance (or mixing) coefficients. Typically, good representation of the data may be found when  $k$  is significantly (up to an order of magnitude) less than  $n$ . Intuitively, the abundance coefficients measure how much of the corresponding endmember is present in a given image spectrum. For physical reasons, the abundance coefficients are usually constrained to be both nonnegative  $\alpha_i \geq 0$  and to sum to one ( $\sum \alpha_i = 1$ ).

**Methodology:** The implementation of the linear mixing model consists of an endmember selection stage, followed by a demixing (abundance coefficient determination) stage. To determine endmembers, we developed parallel versions of two well-known endmember algorithms; the ORASIS algorithm<sup>1</sup> developed by the Naval Research Laboratory, and the N-FINDR algorithm<sup>2</sup> developed by Technical Research Associates. The abundance coefficients were then calculated using a constrained least squares minimization technique.



**Figure 1.** False color hyperspectral image from the NVIS sensor highlighting two similar targets.

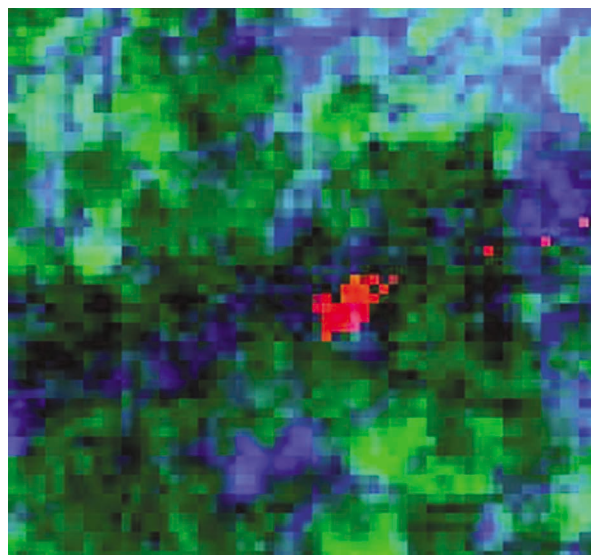


**Figure 2.** Demixed output (using ORASIS endmembers) showing the target from the right hand box of Figure 1 (magnified four times).

**Significance:** The linear mixing model has proven to be a very useful tool in a wide variety of applications that use hyperspectral imagery, including mineral mapping, terrain classification, and anomaly detection. However, the sheer volume of hyperspectral data can be overwhelming. The scalable versions of the algorithms we developed in this project significantly reduce the wall clock times needed to process hyperspectral data. This is especially important in applications that involve large spatial regions (e.g., mapping) or need to be processed in near real time (e.g., target detection).

**References:**

- 1) J. Bowles, D. Gillis, and P. Palmadesso, "New Improvements in the ORASIS Algorithm," Aerospace Conference Proceedings, IEEE, 3 (1999): 18.
- 2) Michael E. Winter, "N-FINDR: An Algorithm for Fast Autonomous Spectral End-Member Determination in Hyperspectral Data," Proc of SPIE Vol 3753, Imaging Spectrometry V (Descour and Shen editors), (1999): 266 -277.

Author and Contact: David Gillis

Authors: Jeffrey Bowles and Michael Bettenhausen

Organization: Naval Research Laboratory, Code 7212, 4555 Overlook Ave. SW, Washington, DC, 20375

Author: Michael E. Winter

Organization: Hawaii Institute of Geophysics and Planetology, 2525 Correa Rd., Honolulu, HI, 96822

Resources: IBM Netfinity Supercluster, *Huinalu*, at MHPCC

Sponsorship: The Common High Performance Computing Software Support Initiative (CHSSI)

# Electronic Structure of Icosahedral As@Ni<sub>12</sub>@As<sub>20</sub> Cluster

Mark R. Pederson and Tunna Baruah

Carbon based fullerenes have been studied extensively in recent years mainly for their potential applications in nanotechnology. At the same time, there have been significant efforts to derive such fullerenes from other elements. Recently, Moses *et al.*<sup>1</sup> have reported synthesis of one such fullerene-like molecule which has an As@Ni<sub>12</sub> cage encapsulated by an As<sub>20</sub> cage. The structure of the molecule was reported to be a near perfect icosahedron. We have carried out an *ab initio* density functional study of its electronic structure, vibrational stability and also its infra-red absorption and Raman scattering spectra. Our calculations show that the isolated molecule has icosahedral symmetry and is vibrationally stable. We also determined the optically active vibrational modes and the corresponding frequencies. Also, we found that there is a repulsive interaction between the nickel and As cages. This is the first *ab initio* study on this molecule and brings out the underlying electronic structure and bonding nature. This study can be useful in further experimental characterization.

**Research Objectives:** A non-carbon fullerene-like molecule was synthesized recently by Moses *et al.*<sup>1</sup> which occurs as [(C<sub>4</sub>H<sub>9</sub>)<sub>4</sub>P<sup>+</sup>]<sub>3</sub>[As@Ni<sub>12</sub>@As<sub>20</sub>]<sup>-3</sup> salt where the [As@Ni<sub>12</sub>@As<sub>20</sub>]<sup>-3</sup> anion (Cf. Fig. 1) is comprised of an icosahedral [As@Ni<sub>12</sub>]<sup>-3</sup> cluster with an arsenic atom core encapsulated by a dodecahedral fullerene-like As<sub>20</sub> cage to give an onion-skin-like [As@Ni<sub>12</sub>@As<sub>20</sub>]<sup>-3</sup> cluster with icosahedral (I<sub>h</sub>) point symmetry. Although As<sub>20</sub> is fullerene-like in structure, it differs electronically from carbon-based fullerenes. The atoms in As<sub>20</sub> are sp<sup>3</sup>-hybridized with three bonding orbitals along the surface of the dodecahedron and a fourth orbital containing a lone pair of electrons pointing outward from the cage. In the carbon-based fullerenes the carbon atoms are sp<sup>2</sup>-hybridized forming a strong covalently-bonded network of σ-bonds surrounded by a sheath of π-electrons in bonding orbitals. We have carried out a density functional theory (DFT) based calculation to investigate the electronic structure and vibrational stability of the isolated neutral molecule.

**Methodology:** Our calculations were performed using the Naval Research Laboratory Molecular Orbital Library (NRLMOL) package.<sup>2</sup> This package employs a Gaussian basis set where the exponentials of the Gaussian basis are optimized for each atom.<sup>3</sup> The basis for the As and Ni atom contains 7s, 6p, and 4d type contracted Gaussians along with a d-type polarization function. Our DFT calculations were performed at the all-electron level with the generalized gradient approximation to describe the exchange-correlation effects. Further, the vibrational modes were calculated by displacing each atom along the Cartesian axes and calculating the forces for the displaced system. These were used to construct the dynamical matrix and the frequencies were obtained by diagonalizing this matrix.<sup>4</sup>

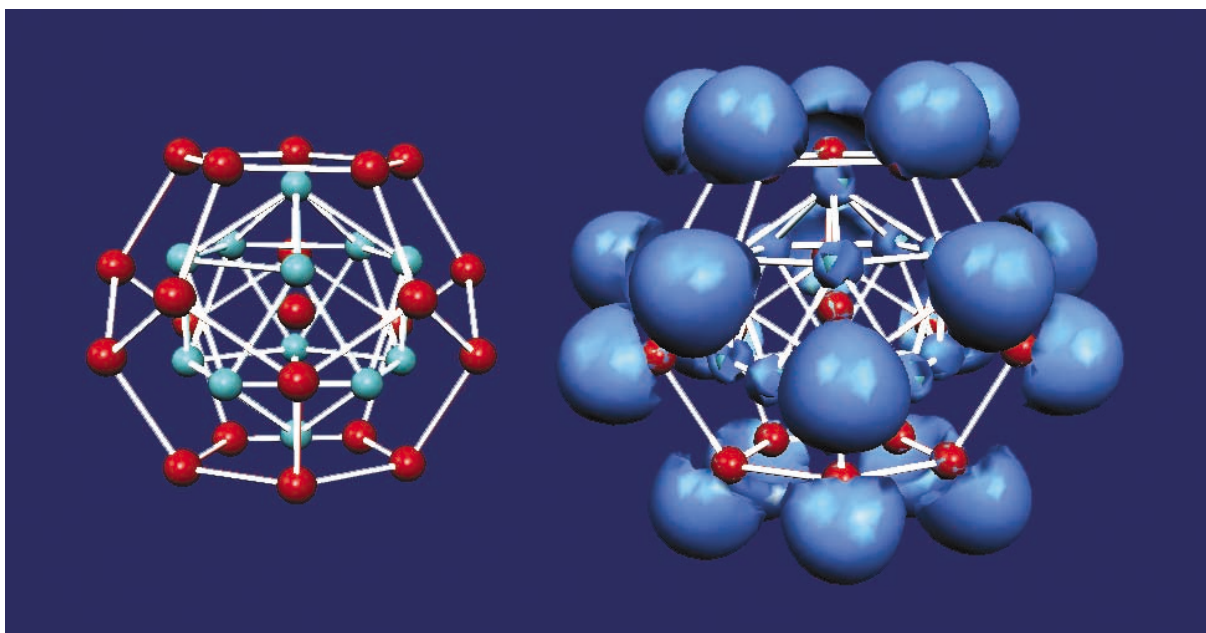


**Figure 1.** The optimized geometry of the As@Ni<sub>12</sub>@As<sub>20</sub> and the isosurface of electron localization function at 0.4 showing delocalized charge on the As cage.

**Results:** The optimized geometry of the isolated  $\text{As@Ni}_{12}\text{@As}_{20}$  displays icosahedral symmetry. Our calculated bond lengths are in good agreement with the experimental values. The molecule has 3-fold degenerate highest occupied and lowest unoccupied molecular orbitals and a gap of 0.115 eV between them which increases to 1.45 eV in its triply charged state. The atomization energy is 3.7 eV showing a stable bound system. Although, the molecule is electronically stable in the triply charged state, in the gas phase it is most stable in the -2 charged state. However, the second electron affinity is low and the electron can be easily detached in experiments using laser beams. Our analysis of the charge transfer between the cages indicates that charge transfer of 1.5 electron occurs from the Ni cage to the outer As cage leading to a relaxation of both the cages due to on-cage Coulomb repulsions which was found to be reinforced strongly by the kinetic energy repulsions between the Ni and As cages. The delocalized charge on the As atoms is shown in Figure 1. The isolated neutral molecule is found to be vibrationally stable. We show that there are in total ten optically active vibrational modes - four infrared active and six Raman active modes. The IR spectrum shows peaks at 84, 163, 212, 265  $\text{cm}^{-1}$  and the Raman spectrum has peaks at 67, 101, 142, 177, 227, and 297  $\text{cm}^{-1}$ . These data can help spectroscopic experiments for characterization of the molecule.<sup>5</sup>

**References:**

- 1) M. J. Moses, J. C. Fettinger, and B. W. Eichhorn, "Science 300," (2003): 778.
- 2) M. R. Pederson and K. A. Jackson, *Phys. Rev. B* 41, (1990): 7453, K. A. Jackson and M. R. Pederson, *Phys. Rev. B.* 42, 3276 (1990); M. R. Pederson and K. A. Jackson, *Phys. Rev. B* 43, (1991): 7312.
- 3) D. V. Porezag and M. R. Pederson, *Phys. Rev. A* 60, (1999): 9566.
- 4) D. V. Porezag and M. R. Pederson, *Phys. Rev. B* 54, (1996): 7830.
- 5) T. Baruah, R. R. Zope, S. L. Richardson, and M. R. Pederson, submitted to *Physical Review Letters*.

Author and Contact: Mark R. Pederson

Organization: Center for Computational Materials Science, Naval Research Laboratory, Washington, DC, 20375

Author: Tunna Baruah

Organization: Department of Physics, Georgetown University, Washington, DC, 20057

Resources: IBM SP at MHPCC and Linux Cluster at Center for Computational Materials Science, Naval Research Laboratory

Acknowledgements: Office of Naval Research Grant No. N000140211046 and the DoD High Performance Computing CHSSI Program

# Full-Scale Simulations of Bubbly Flows Around the Research Vessel Roger Revelle

Francisco J. Moraga, Donald D. Drew, Richard T. Lahey, Jr.

The reliable prediction of the bubbly wake produced by a given ship is necessary to design more efficient and stealth-capable surface ships. A necessary step toward that goal is the simulation of full-scale ship flows. We present the first-ever full-scale simulations (Reynolds number,  $Re=300$  million; Froude number,  $Fr=0.225$ ) of the bubbly flow around the research vessel Roger Revelle operated by the Scripps Institution of Oceanography. Interest in this particular vessel arises from the fact that soon there will be experimental data on its bubbly wake. Thus, we will be able to assess the quality of our two-fluid model, which consists of the ensemble-averaged mass and momentum equations for the liquid and gas phases, in the absence of phase change.

**Background:** Since the pioneering work of Carrica *et al.*, (1999) on CFD of bubbly flow around a surface ship, there has been considerable progress in both CFD applied to ship hydrodynamics and the modeling of bubbly flows. Not only simulations for full scale Reynolds numbers are now possible, but comprehensive validation and verification studies have increased the reliability of CFD of ship flows. In addition, two-fluid models of bubbly flows have benefited from systematic validation using flows of increasing complexity. This methodology makes it possible to isolate the forces on the bubbles that needed to be modeled and excludes, or at least minimizes, the possibility of cancellation of errors between models for the different forces on the bubbles. Turbulence dispersion models for grid

decaying turbulence and mixing layers (Moraga *et al.*, 2002), lift forces (Moraga *et al.*, 2002) and wall forces (Larreteguy *et al.*, 2002) have all been successfully benchmarked.

**Methodology:** The steady-state simulations presented here incorporate all the model improvements described above. The Reynolds number is based in the length,  $L=83$  m, and a traveling speed,  $U=3.6$  m/s, which is the normal cruise speed of the ship. The grid is structured and it has approximately 2.24 million nodes divided in 16 blocks of roughly the same size. The message passing interface library (MPI) is used. By maintaining the same programming strategies with the original single-phase code CFDSIP-IOWA we were able to keep good scalability for multiple processor runs. This particular grid does not include propellers, rudders or bilge keels, although our code can accommodate these features by using overset Chimera grids and the Pegasus code from NASA. Future simulations will include all these features and polydisperse bubble populations. Turbulence in the liquid is simulated with a k-omega model. For further details on the liquid solution see references (Paterson *et al.*, 2002, Stern *et al.*, 2001, Wilson *et al.*, 2000). The bubbles were introduced into the flow at the bow. One purpose of these simulations is to explore the sensitivity of the results to the bubble source position, which is not presently very well known. The bubble diameter,  $D=160$  microns, is representative of the bubble size created by breaking ship waves. These bubbles are small enough to make drag the most dominant force on them. However, they are not small enough to be passive scalars, since they slowly rise under the influence of buoyancy, experience strong lift forces close to the hull, and have a Schmidt number different than unity.

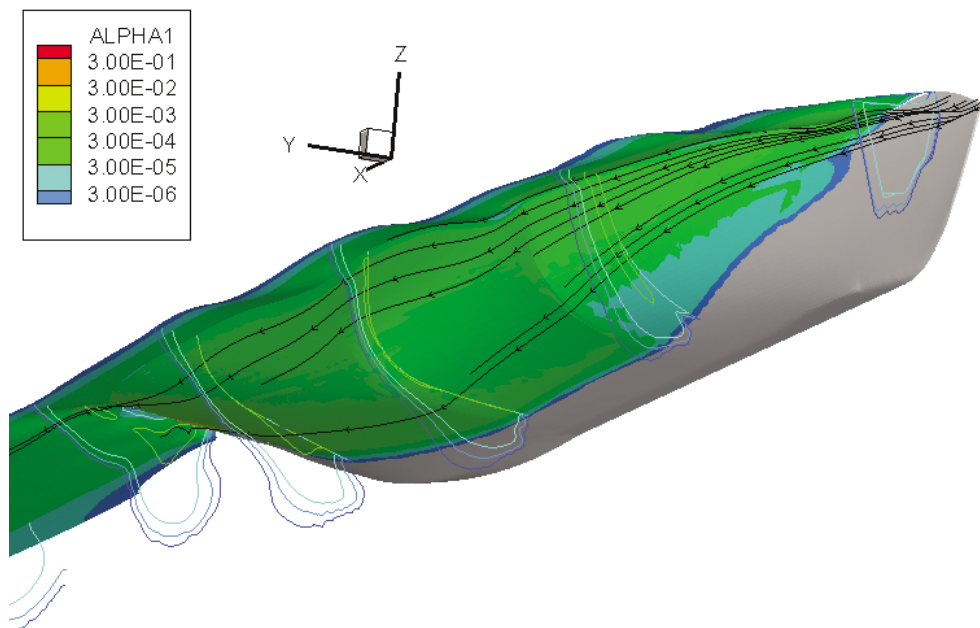


**Figure 1.** Bubble volume fraction at selected vertical planes (color lines), a bubble radius forms the hull and at the free surface, and stream traces around the research vessel Roger Revelle.

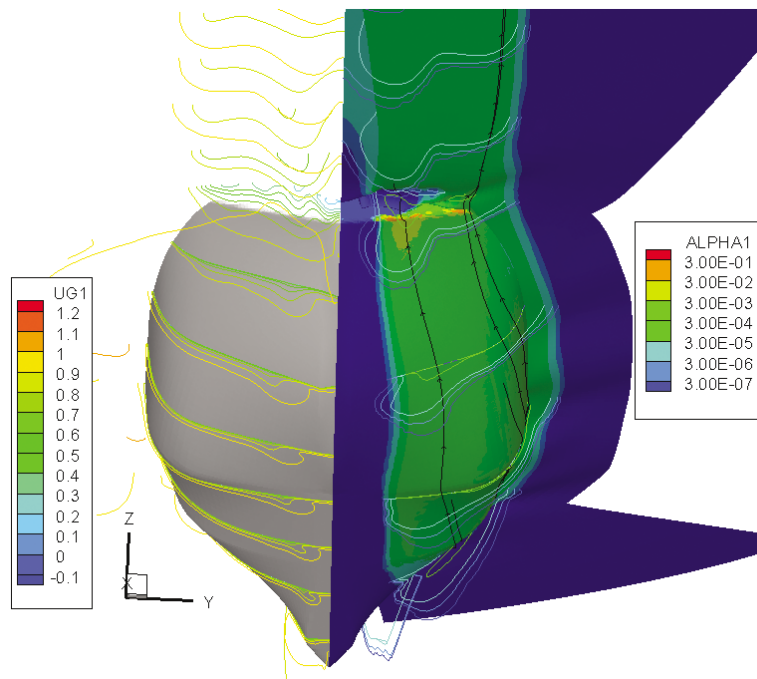


**Figure 2.** Right hand side: as in Figure 1. Left hand side: Hull (gray) and axial bubble velocities at selected vertical planes (color lines).

Figure 1 shows cuts of the void fraction at vertical planes of the form  $x=\text{constant}$  (color lines), a bubble radius from the hull and at the free surface (flooded color). Selected bubble streamlines are also shown. Note the use of an exponential color map, which is necessary to show the spatial distribution of bubbles. The maximum void fraction, alpha approximately 0.22 occurs one bubble radius from the hull at the transom stern as can be seen in the right hand side of Figure 2. This side of Figure 2 contains the same information as Figure 1 in a different view, while the left side shows in gray the hull of the ship and in color contour lines of the axial bubble velocities.

The bulk of the bubble cloud is initially advected downwards by the liquid, which has been deflected by the hull. After passing the first half of the ship, the bulk of the bubble cloud starts to rise very slowly. In agreement with observations at sea, the majority of the bubbles exit the computational domain one ship length into the wake without reaching the free surface. Simultaneously bubbles accumulate very close to the hull. Once in contact with the wall, the bubbles slide along it under the influence of convection and buoyancy. However, these forces are so small that bubbles accumulate at the walls.

#### References:

- 1) P. M. Carrica, D. A. Drew, and R. T. Lahey Jr., "A Polydisperse Model For Bubbly Two-Phase Flow Around a Surface Ship," *Int. J. Multiphase Flow* 25, (1999): 257-305.
- 2) E. G. Paterson, R. V. Wilson, and F. Stern, "General-Purpose Parallel Unsteady RANS Ship Hydrodynamics Code: CFDSHIP-IOWA," IIHR Report No. XXX, (2002) Iowa Institute for Hydraulic Research, The University of Iowa, Iowa.
- 3) R. Wilson, E. Paterson, and F. Stern, "Verification and Validation for RANS Simulation of a Naval Combatant," Gothenburg 2000 Workshop on CFD in Ship Hydrodynamics, Chalmers University of Technology, Gothenburg, Sweden.
- 4) F. J. Moraga, A. E. Larreguy, D. A. Drew, and R. T. Lahey Jr., "Assessment of Turbulent Dispersion Models for Bubbly Flows in the Low Stokes Number Limit," *Int. J. of Multiphase Flow*, Volume 29, Issue 4, (April 2003): 655-673.
- 5) F. J. Moraga, M. Lopez de Bertodano, D. A. Drew, and R. T. Lahey Jr., "The Modeling of Lift and Dispersion Forces in Two-Fluid Model Simulations, Part-I: Jet Flows, and Part II: Boundary Layer Flows," (July 2003) 8th International Symposium On Gas-Liquid Two-Phase Flows, ASME/JSME Joint Fluids Engineering Division Summer Meeting, Honolulu, Hawaii.
- 6) A. E. Larreguy, D. A. Drew, and R. T. Lahey Jr., "A Center-Averaged Two-Fluid Model for Wall-Bounded Bubbly Flows," (2002) Joint US ASME/ European Fluids Engineering Division, Summer Meeting, Montreal, Canada.

Author and Contact: Francisco J. Moraga

Authors: Donald D. Drew and Richard T. Lahey, Jr.

Organization: Rensselaer Polytechnic Institute, 110 8th St., Troy, NY, 12180

Resources: Linux Supercluster, *Huinalu* at MHPCC, Cray T3E, *Yukon* at ARSC, DEC Alpha, and *Opal* at ERDC

Sponsorship: Office of Naval Research

Acknowledgement: We thank the Iowa Institute for Hydraulic Research for providing us with the single-phase code, CFD Ship-Iowa, and Mark Hyman from NSWC Coastal System Division for generating the grid and providing useful input.

## Simulation and Redesign of the Compact A6 Magnetron

Peter J. Mardahl, Keith L. Cartwright, Lester A. Bowers,  
Michael D. Haworth, John W. Luginsland, Tony Murphy

We are using the ICEPIC (Improved Concurrent Electromagnetic Particle-in-cell) simulation code to characterize and design a high power (gigawatt class), compact A6 magnetron. This magnetron may eventually be the basis of a high power microwave weapon which will destroy electronics but not people or buildings, giving U.S. military commanders an important new battlefield option. Our simulations allow designers to test hundreds of proposed designs on a computer before conducting expensive experiments. The result is a better design for less money.

simulations accurately predict RF-production and antenna gain compared with experimental testing. In general, ICEPIC development has been driven by the desire to achieve high power in a compact RF device. This implies that the device is operated at high current and high space charge. Consequently, these devices are highly non-linear. In addition, these devices have complex three-dimensional geometries with small features. ICEPIC may be used both for fine-tuning well-understood devices and for testing new designs.

RF weapons will be designed to work against hostile battlefield electronics. Given the importance of electronics in the modern battlefield, the ability to target these electronics will give the U.S. a distinct advantage against technically advanced adversaries. The effect of RF radiation on the electronics can vary from transient disruption to destruction of hardware, depending on the power and frequency of the radiation. Furthermore, since only electronic equipment is affected, RF radiation can be applied in a non-lethal manner, giving the warfighter a broader range of options for dealing with opponents of varying sophistication and strength. The generation of electromagnetic radiation is critical to the DoD's advanced RF weapon effort.

**Introduction:** ICEPIC predicts the performance of several high power microwave (HPM) devices currently in development for the U.S. Air Force. With an accurate simulation tool, devices such as the relativistic klystron oscillator (RKO), the magnetically insulated line oscillator (MILO), the relativistic magnetron, and high frequency gyrotrons can be improved. ICEPIC simulates the electrodynamics (Maxwell's equations) and charged particle dynamics (relativistic Lorenz's force law) with second-order time and space accuracy in HPM sources. These

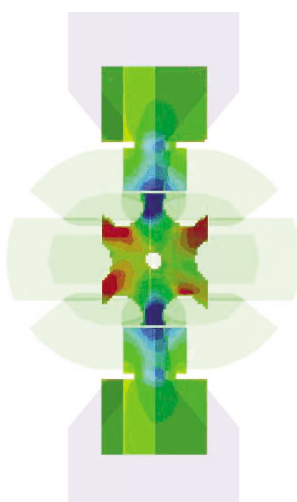


**Figure 1.** Shown is an angled view of an ICEPIC simulation of the Michigan Magnetron. It is a six-cavity magnetron with extraction from the top and bottom cavities. Color indicates the strength of the electric field pointing around the cathode (theta direction). Red indicates high field in one direction, blue high field in the opposite. We see that the fields in the extractors are both blue and are therefore in phase, indicating operation in the  $2\pi/3$  mode, instead of the desired  $\pi$  mode.

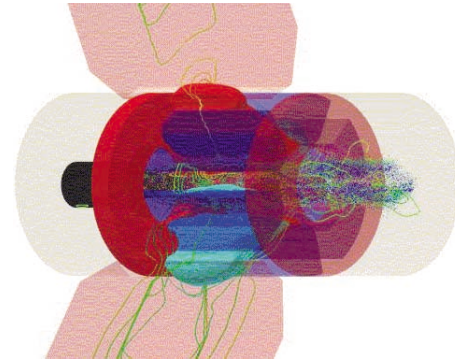


**Figure 2.** This shows the A6 magnetron simulated in ICEPIC. This snap shot shows the electric field and particles 50 ns after the start of the applied voltage. The iso-surfaces in this figure are the electric field pointing around the cathode (theta direction). Red is in the clockwise direction when facing upstream (left in this graphic), green is in the counter clockwise direction. The power extracted from the magnetron into the wave-guides shows a  $\pi$  phase advance between the two cavities. The desired mode has a  $2\pi$  phase advance for the extractors, thus this magnetron is operating in the wrong mode.

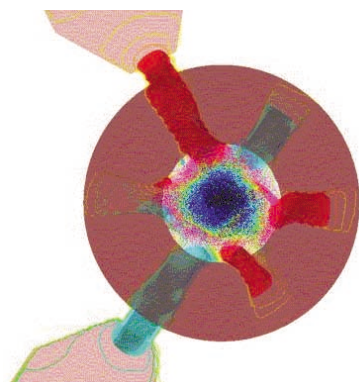


**Figure 3.** This is the A6 magnetron simulated in ICEPIC. Shown are the electric field and particles 50 ns after the start of the applied voltage. The camera is pointing upstream toward the pulse power. The iso-surfaces in this figure are the electric field pointing around the cathode (theta direction). Red is in the clockwise direction when facing upstream, green is in the counter clockwise direction. The power extracted from the magnetron into the wave-guides shows a  $\pi$  phase advance between the two cavities. The desired mode has a  $2\pi$  phase advance for the extractors, thus this magnetron is operating in the wrong mode. The phase advance from cavity to cavity is not constant in this design. The phase advance for the extracting cavities and the cavity between is  $\pi/2$ . The rest of the cavities have a  $3\pi/4$  advance, which makes the average phase advance  $2\pi/3$ .

Our team is tasked to develop compact, gigawatt class microwave sources. The team is now taking the next step in our evolution towards true virtual prototyping; the relativistic magnetron is being simulated before it is built at our lab. The details of the device that will eventually be built, including the geometric structure and the externally generated magnetic field distribution, will be based on our simulations.

Before designing our own tube, the team successfully applied ICEPIC to simulate University of Michigan's relativistic magnetron (Figure 1) by reproducing the RF power level, growth rate, and operating frequency. ICEPIC predicts 300 MW (mega-watt) of total extracted instantaneous power, 150 MW RMS (Root Mean Square), compared with 200 MW RMS measured in the experiment. ICEPIC also predicts the experimental 100 ns delay in the onset of RF after the diode voltage reaches its peak. The operating frequency observed in the ICEPIC results agrees to within a few percent of the 1.03 GHz measured in the experiment. The ICEPIC results also show that the University of Michigan's A6 does not operate in the desired  $\pi$  mode (a  $\pi$  phase shift in the electric field from cavity to cavity). In addition, the ICEPIC results show a large upstream and downstream DC loss current, similar to experimental observation.

In addition to simulating the University of Michigan device, ICEPIC was applied to the A6 magnetron designed for AFRL (Figure 2). The results verify the high power capability of the design, but find severe mode competition that hampers the axial extraction concept needed to meet the compact size goal. The current program provides for an evolutionary step by extracting power radially through two waveguides. However, there is severe mode competition between the  $\pi$  and  $2\pi/3$  modes (Figure 3). The phase advance from cavity to cavity is not constant in this design. The phase advance for the extracting cavities and the cavity between is  $\pi/2$ . The rest of the cavities have a  $3\pi/4$  advance, which makes the average phase advance  $2\pi/3$ . Clearly, the extractors are having a profound effect on the overall electrodynamics of the device. We have found via simulation that using three extractors restores the  $\pi$  mode operation of the device (Figure 4) and greatly increases the power output. This shows the importance of using three dimensional simulation tools and including all the geometry of the source. This issue will not be a problem for the initial proof of principle radial extraction experiments, but limits the output power for our compact axial extraction concepts to about half of the required value. In addition, the peak electric field for these modes is not in the center of the anode block as expected, but downstream of the center (Figure 5). Details of the field and particle structure inside the magnetron is difficult to obtain from experiment because of the high electric field stresses and electron bombardment. Thus, the simulation results provide great insight.

The A6 magnetron design was improved through extensive ICEPIC simulations. The simulations allow studies of the consequences of changing the vane depth and extraction slots to force the tube into the  $\pi$  mode. Using simulation results, the parasitic mode is reduced in amplitude to ten percent of the desired  $\pi$  mode, and cathode end caps are designed to reduce the upstream and downstream loss current. The reduced loss current increases the efficiency of the magnetron. Plans are to build the improved design in late 2003 and to compare the experimental results to simulation results from ICEPIC.

Strict requirements are placed on the performance and size of HPM sources to meet the needs of the warfighter. To obtain optimal performance many design modifications need to be tested and validated. Virtual prototyping can be used to investigate modifications thoroughly and decrease significantly the time and cost involved as compared to an experimental effort only. As demonstrated here, ICEPIC has proven that it is capable of predicting the performance of proposed HPM source designs.

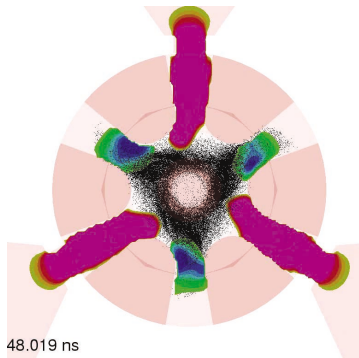


**Figure 4.** The A6 magnetron operates in  $\pi$  mode when power is extracted from three cavities instead of two.

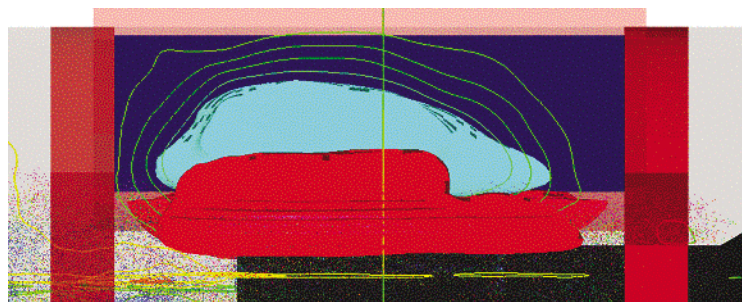


**Figure 5.** This is a side-view of the A6 magnetron simulated in ICEPIC. This snap shot shows the electric field and particles 50 ns after the start of the applied voltage. The peak electric field for these modes is not in the center of the anode block as expected, but downstream (left) of the center (vertical yellow line).

Author and Contact: Peter J. Mardahl

Authors: Keith L. Cartwright, Lester A. Bowers, Michael D. Haworth, Tony Murphy

Organization: Air Force Research Laboratory, 3550 Aberdeen Ave. SE, Kirtland AFB, NM, 87177

Author: John W. Luginsland

Organization: Science Applications International Corporation (SAIC)

Resources: IBM Netfinity at MHPCC, IBM SMP at ARL/ERDC, and SC40 at ERDC

Sponsorship: Department of Defense

# Simulations of Stormtime Ring Current Magnetic Field

Margaret W. Chen

This is a simulation study of ring current ions (energies  $\sim 10 - 200$  keV at 2 to 7 earth radii) under the Assimilative Model of Ionospheric Electrodynamics (AMIE)<sup>1</sup> mapped into a model magnetospheric magnetic field. We compute the guiding-center drifts of ions for magnetic storm events. Using the simulation results we map the stormtime proton phase-space distributions. From the phase-space distributions we compute the radial and azimuthal variations of the pressure, energy density, current density, and magnetic field. Our simulations show the formation of an asymmetric ring current that progressively becomes more symmetric during the storm main phase. Knowledge of realistic flux distributions of ring current particles in the inner magnetosphere is relevant to Air Force and other satellite systems because long-term exposure to such an environment can cause damage to optical coatings and other surface materials.

**Research Objectives:** We simulate the drift and loss of ions under the realistic AMIE electric field in a model magnetic field so as to understand better the formation of the stormtime ring current. Our eventual goal is to develop a self-consistent simulation that calculates particle distributions in a magnetic field that includes the ring current itself.

**Methodology:** We compute the guiding-center drift of ions that conserve their first adiabatic invariant. We follow the drift trajectories of approximately 10,000 representative ions under the time-varying AMIE electric field and a simple magnetic

field consisting of a superposition of a dipolar magnetic field and a uniform southward field parallel to the dipole axis. Using the simulation results, we map proton phase space distributions taking account of loss due to charge exchange with the neutral hydrogen geocorona. We compute distributions of the pressure and current from the phase-space distributions. The ring current magnetic field is computed by applying the Biot-Savart law.

19 October 1998

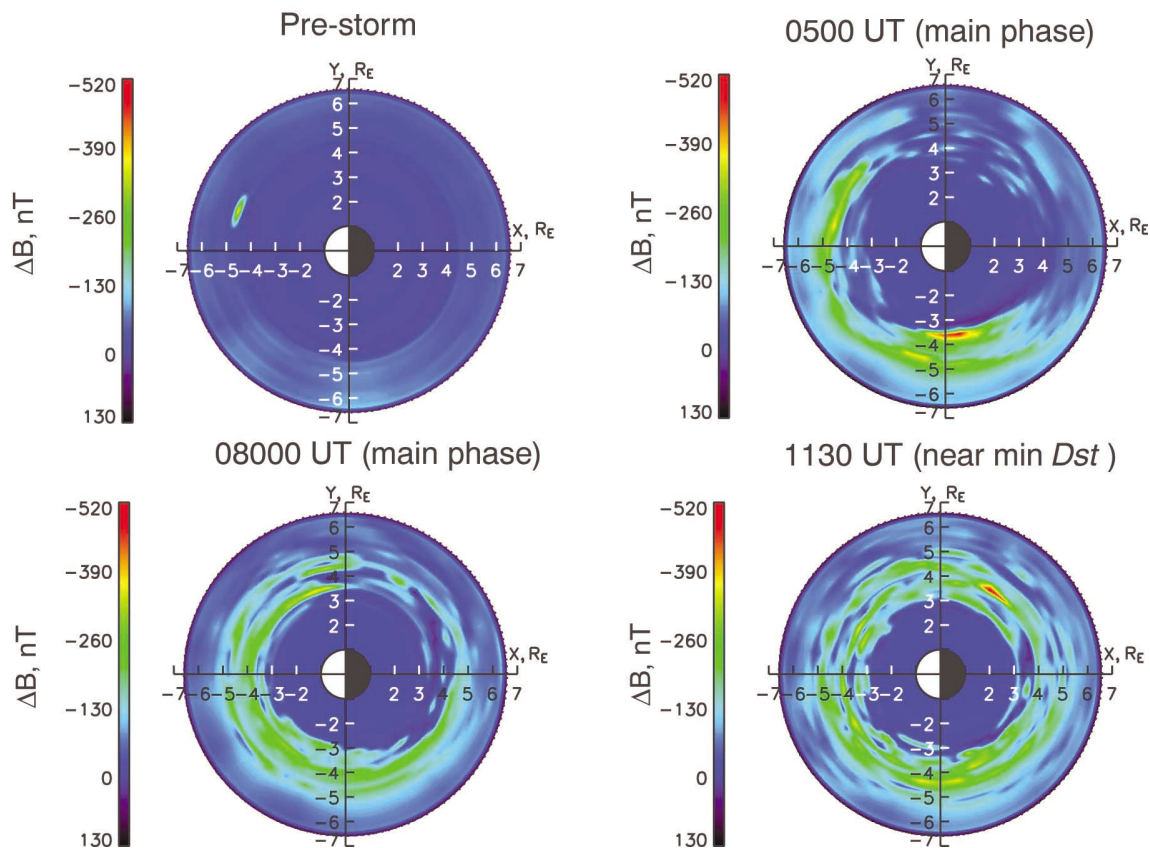


**Figure 1.** The panels show the ring current magnetic field perturbation in the equatorial plane at different times during the main phase of the 19 October 1998 storm. The sun is to the left. During the early storm main phase, a partial ring current is forming. The ring current becomes more azimuthally symmetric as the storm approaches the end of the main phase (minimum value of the Dst index).

**Significance:** The incorporation of realistic electric field models in numerical models of inner magnetospheric dynamics is very important as recent electric field observations<sup>2</sup> show that the storm time near-earth electric field may be much stronger than what is predicted in simplified electric field models that are commonly used. Since the ring current characterizes magnetic storms, it is imperative to understand the temporal development and spatial distribution of the ring current magnetic field. Knowledge of realistic flux distributions of ring current particles in the inner magnetosphere is relevant to Air Force and other satellite systems because long-term exposure to such an environment can cause damage to optical coatings and other surface materials.

#### References

- 1) A. D. Richmond and Y. Kamide, "Mapping Electrodynamic Features of the High-Latitude Ionosphere From Localized Observations: Technique," *J. Geophys. Res.*, 92, (1988): 5471-5759.
- 2) D. E. Rowland and J. R. Wygant, "Dependence of the Large-Scale, Inner Magnetospheric Electric Field on Geomagnetic Activity," *J. Geophys. Res.*, 103, 14, 959-14, 964, (1998).

Author and Contact: Margaret W. Chen  
Organization: Aerospace Corporation, P.O. Box 92957, MS-260, Los Angeles, CA, 90009  
URL: [www.aero.org](http://www.aero.org)  
Resources: IBM SP at MHPCC and the Sun Enterprise 3000 at the Aerospace Corporation  
Sponsorship: Department of Defense and National Science Foundation

## Multidisciplinary Applications of Detached-Eddy Simulation to Separated Flows at High Reynolds Numbers (Challenge 92)

Scott A. Morton, James R. Forsythe, Matthew B. Steenman, Russell M. Cummings, Kenneth E. Wurtzler, Shawn H. Woodson, Kyle D. Squires, Philippe R. Spalart

Numerical simulations are an important tool for predicting aircraft performance, especially in off-design regimes that are difficult to investigate using wind-tunnel or flight testing. While CFD for aerodynamic applications is coming of age at various labs and in universities, e.g., full-airplane computations are now possible. One of the main stumbling blocks to the increased use of CFD for design and analysis has been an inability to accurately predict the unsteady effects of massive flow separations. Recent efforts on predicting massively separated flows around full aircraft at flight Reynolds numbers, however, has shown that Detached-Eddy Simulation (DES) is a viable method for use in this difficult flow regime. The present investigators have predicted the massively separated flow over several aircraft with DES predictions in good agreement with experiments or flight-test data.<sup>1,2</sup> These successful efforts motivate the present research extension of DES to multidisciplinary applications. The two applications considered are flight mechanics and aero-elasticity. The algorithm requirements in extending the current simulation methodology into these areas are similar — principally the use of grid speed terms. The present work focuses on laying the foundation for subsequent grid motion (both deforming and rigid body) calculations. The cases considered are the abrupt wing stall (AWS) of the pre-production F/A-18E and vortex breakdown of the F-18C. This represents both flight mechanics (lateral instability) and aero-elasticity (tail buffet) of full aircraft.

**Abrupt Wing Stall:** During envelope expansion flights of the F/A-18E/F in the Engineering and Manufacturing Development phase, the aircraft encountered uncommanded lateral activity, which was labeled “wing drop.” An extensive resolution process was undertaken by the Navy and its contractors to resolve this issue. A production solution was developed, which included revising the flight control laws and the incorporation of a porous wing fold fairing to eliminate the wing drop tendencies of the pre-production F/A-18E/F. The wing drop events were traced to an abrupt wing stall (AWS) on either the left or right wing panel, causing a sudden and severe roll-off in the direction of the stalled wing. An important distinction between wing drop and AWS is that wing drop is the dynamic response of an aircraft to an aerodynamic vent, while AWS is an aerodynamic event that can trigger a wing drop.<sup>3</sup>

Unsteady measurements on a model of a pre-production F/A-18E were made by Schuster and Byrd<sup>4</sup> motivated by the following statement: “Since AWS and the resulting lateral instabilities are dynamic or, at best highly sensitive quasi-static phenomena, measurement of unsteady wing surface pressures, loads, and accelerations were incorporated into the test procedures to investigate the potential unsteady causes and/or indicators of AWS.” The initial findings from these tests showed highly unsteady surface pressures indicative of shock oscillation.

The baseline case considered here is an 8% model of a pre-production F/A-18E with 10°/10°/5° flaps (leading-edge flaps/trailing-edge flaps/aileron flaps) at Mach 0.9 and no tails. DES calculations are performed on a baseline and adapted grid and compared to unsteady wind tunnel measurements and RANS models.

Time averaged-DES lift coefficients vs. angle of attack are plotted vs. RANS calculations, and experimental values in Figure 1. The DES on the baseline grid follows the lift curve nicely up until 9°, where it drops in lift relative to the experiment. This discrepancy is what prompted the creation of the adapted grid, which matched the experiments better. The adapted grid matches the experiments quite well at all angles of attack, with the largest discrepancies at 12° and 16°. The Spalart-Allmaras RANS results predict the lift at all angles of attack, even at the low angles. Menter’s SST RANS model does a more reasonable job for the low angles of attack, but predicts an early break in the lift curve.

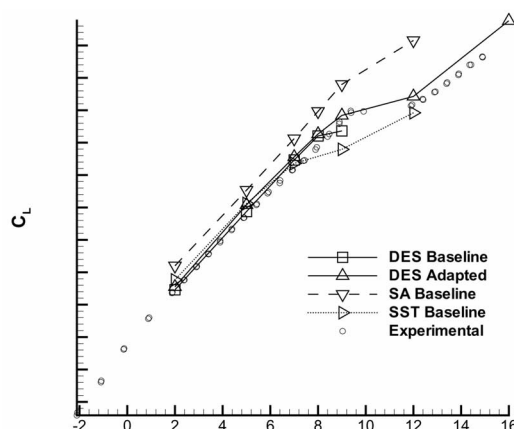


Figure 1. Lift Coefficient vs. alpha for the no tails F/A-18E.

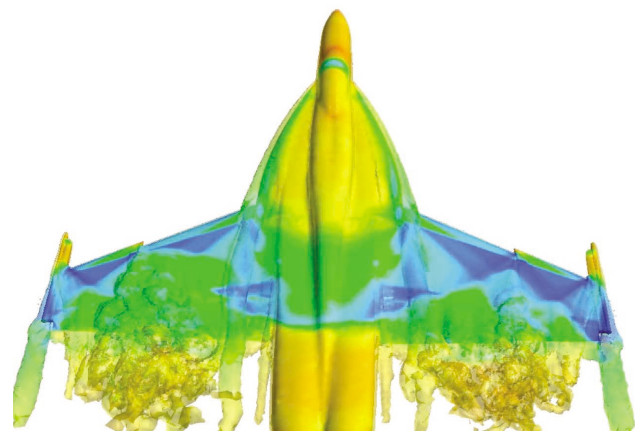


Figure 2. Instantaneous isosurface of vorticity colored by pressure on the F/A-18E at 9° angle of attack.

At  $9^\circ$  angle of attack, the experiments show a smoothly varying pressure distribution from the snag back to about the half chord. Schuster and Byrd<sup>4</sup> showed with unsteady pressure measurements that this pressure distribution occurs due to the time-averaging of an unsteady shock that moves back and forth over the wing. Figure 2 shows an instantaneous flow visualization of a full aircraft calculation at  $9^\circ$  angle of attack. The shocks were seen to travel back and forth over the wing (note the asymmetry in the shock locations in the figure) leading to large magnitude low frequency oscillations in the rolling moment. This unsteady effect, captured in the simulations, highlights unsteady shock oscillation as being a potential trigger event for abrupt wing stall.

**Vortex Breakdown:** The F-18 High Angle of Attack Research Vehicle (HARV; see Figure 3) has proven to be an excellent source of data for researchers working on high angle of attack flowfields.<sup>5,6,7</sup> Extensive flight testing of the HARV has been conducted that provides a rich source of flow visualization, surface pressures, and aero-elastic information. The F-18 utilizes wing leading edge extensions (LEX) to generate vortices which enhance the wing lift, and the twin vertical tails are canted to intercept the strong vortex field and increase maneuverability. At large incidence, the LEX vortices breakdown upstream of the vertical tails, resulting in a loss of yaw control power and severe aero-elastic effects.<sup>8</sup> This tail buffet phenomenon was reduced by using extensive flight tests to design a LEX fence. The ultimate goal of computationally modeling the flowfield shown in Figure 3 would be to accurately simulate the aero-elastic impact of the LEX vortices on the twin vertical tails.



Figure 3. NASA F-18 High Angle of Attack Research Vehicle (HARV).

The specific aim of this work is to test the accuracy and efficiency of DES in predicting vortex breakdown over a full aircraft. This work builds on previous successful work on vortex breakdown over a delta wing.<sup>9</sup> Another goal of the work is to apply adaptive mesh refinement (AMR) to this challenging flow. Computations are made for the F-18C at  $\alpha = 30^\circ$ ,  $M_\infty = 0.2755$ , and  $Re_\infty = 13.9 \times 10^6$  which determine the importance of highly refined grids on the accurate prediction of complex vortical flowfields. Comparisons have been made between steady Reynolds-averaged Navier-Stokes (RANS), unsteady Reynolds-averaged Navier-Stokes (U-RANS), and Spalart-Allmaras DES (SADES), and the resulting predictions were compared with available flight test data for the F-18 HARV.

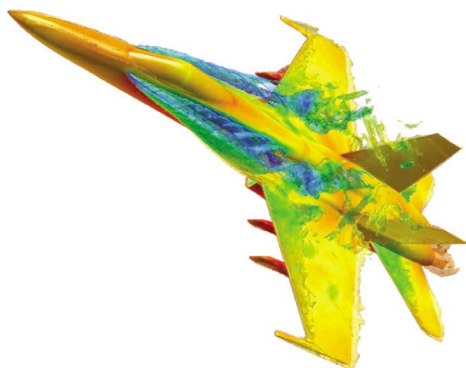


Figure 4. Instantaneous isosurface of vorticity colored by pressure on the F-18C at  $30^\circ$  angle of attack.

Figure 4 shows an instantaneous view of the F-18C with an iso-surface of vorticity colored by pressure for the DES solution on the adapted grid. The solutions are in excellent qualitative agreement with the vortex breakdown observed in Figure 3. The DES solution captures the separation over the wing and horizontal tail. Careful examination of Figure 4 shows that the solution captures small scale structures surrounding the LEX vortex better, consistent with earlier delta wing case. It is clear from the simulation that the tails are in a very unsteady environment contributing to the fatigue issues well documented for the F-18 without the LEX fence. Corresponding RANS simulations failed to predict any significant unsteadiness.

Figure 5 is a well known plot in the literature of the streamwise location of the LEX vortex breakdown as a function of angle-of-attack.<sup>6</sup> For the  $30^\circ$  angle-of-attack of interest in this study, vortex breakdown occurs between 40% and 50%. The location of breakdown observed in Figure 4 for the simulations is at 60%. This discrepancy is not surprising when considering the fact that the diverter slot is covered up on the F-18 HARV. Mitchell *et al*<sup>10</sup> demonstrated that along the core blowing from the surface can move the breakdown position aft. The jet-like behavior of the diverter slot could be acting like a vortex breakdown flow control device, explaining the aft position of vortex breakdown for the F-18C with a diverter slot.

**Summary:** In summary, Detached-Eddy Simulation has been applied to the pre-production F/A-18E with  $10^\circ/10^\circ/5^\circ$  flap set with comparison to steady and unsteady experimental measurements and leading RANS models. Comparisons were made to experimental surface pressures (both time-averaged and steady) and mean force coefficients. Solution based adaptation was used to improve the simulations.

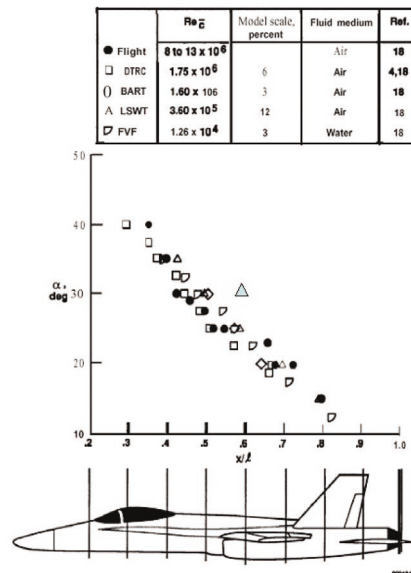


Figure 5. Streamwise LEX Vortex breakdown position as a function of angle of attack extracted from<sup>6</sup> SADES AMR grid solution vortex breakdown location plotted with the flight test and experimental data for comparison.

The mean flow predictions on the adapted grid were seen to be in excellent agreement with the experiments, showing a slight improvement over the SST RANS model, and a larger improvement over the SA RANS model. Low frequency unsteady rolling moments due to shock oscillations give strong support to evidence that unsteady effects can provide a trigger event for abrupt wing stall.

The combined DES and adaptive mesh refinement approach was demonstrated on an F-18C to determine if the unsteady tail loads could be simulated. As was the case in previous delta wing work, the DES solution showed an improvement in capturing small scale features of the LEX vortex as compared to the baseline grid calculations. In all cases the RANS solutions (not shown) proved completely inadequate for computing vortex breakdown for a flight vehicle at high Reynolds number. Flight test data from the NASA HARV program was used to show the solutions were reasonable even though the aircraft configurations were different. Qualitative agreement between the DES solutions and the HARV data was obtained for the lift and the vortex breakdown position. Future research will focus on an F-18C grid that is a closer match to the HARV by moving the leading-edge flap to a -33° position, closing off the diverter slot, and eliminating the under-wing pylons.

## References

- 1) J. R. Forsythe, K. D. Squires, K. E. Wurtzler, and P. R. Spalart, "Detached-Eddy Simulation of Fighter Aircraft at High Alpha," *AIAA 02-0591*, (January 2002).
- 2) K. D. Squires, J. R. Forsythe, S. A. Morton, W. Z. Strang, K. E. Wurtzler, R. F. Tomaro, M. J. Grismer, and P. R. Spalart, "Progress on Detached-Eddy Simulation of Massively Separated Flows," *AIAA 02-1021*, (January 2002).
- 3) R. Hall and S. Woodson, "Introduction to the Abrupt Wing Stall (AWS) Program," *AIAA 03-0589*, (January 2003).
- 4) D. Schuster and J. Byrd, "Transonic Unsteady Aerodynamics of the F/A-18E at Conditions Promoting Abrupt Wing Stall," *AIAA 03-0593*, (January 2003).
- 5) B. H. K. Lee, "Vertical Tail Buffeting of Fighter Aircraft," *Progress in Aerospace Sciences* 36, (2000):193-279.
- 6) D. Fisher, J. H. Del Frate, and F. A. Zuniga, "Summary of In-Flight Flow Visualization Obtained From the NASA High Alpha Research Vehicle," NASA TM-101734, (January 1991).
- 7) Ames Research Center Dryden Flight Research Facility, "High Alpha Research Vehicle Phase II Flight Report, Flight 197-199," HA94-70-660, (February 1994).
- 8) S. M. Murman, Y. M. Rizk, R. M. Cummings, and L. B. Schiff, "Computational Investigation of Slot Blowing for Fuselage Forebody Flow Control," *Aircraft Design*, 2, (1999): 45-63.
- 9) S. A. Morton, J. R. Forsythe, A. M. Mitchell, and D. Hajek, "Detached-Eddy Simulations and Reynolds-Averaged Navier-Stokes Simulations of Delta Wing Vortical Flowfields," *Journal of Fluids Engineering*, 124, No. 4, (2002): 924-932.
- 10) A. M. Mitchell, P. Molton, D. Barberis, and J. Détery, "Oscillation of Vortex Breakdown Location and Control of the Time-Averaged Location by Blowing," *AIAA Journal*, 38, No. 5, (May 2000): 793-803.

Author and Contact: Scott A. Morton

Authors: Matthew B. Steenman and Russell M. Cummings

Organization: United States Air Force Academy, Department of Aeronautics

Authors: Kenneth E. Wurtzler and James R. Forsythe

Organization: Cobalt Solutions, LLC

Author: Shawn H. Woodson

Organization: Naval Air Systems Command

Author: Kyle D. Squires

Organization: Arizona State University, Department of Mechanical and Aerospace Engineering

Author: Philippe R. Spalart

Organization: Boeing Commercial Airplanes

Resources: IBM SPs at MHPCC

Sponsorship: Department of Defense High Performance Computing Modernization Program

# High Performance Computing & Visualization Support for Project DE/TOSS

Brent Swartz, Paul Kominsky, Brian Kruse

The Air Force Research Lab's (AFRL) Directed Energy (DE)/Tactical Operations System Simulation (TOSS) Project involves establishing a Virtual Concept Design Center (VCDC) to provide a Government capability for concept development and performance assessment, to support advocacy for promising concepts, and to identify and establish goals for enabling technologies. This task will support the VCDC through infrastructure revitalization by modernizing legacy codes and acquiring new codes that will be accessible through the Maui High Performance Computing Center (MHPCC). The DE/TOSS Team includes the MHPCC Contractor Team, Science Applications International Corporation (SAIC), and New Mexico Tech (NMT).

**Research Objectives:** The objective of this task is to provide modeling and simulation support for new DE weapon system concepts by reconstituting and modernizing legacy physics codes, by acquiring and porting industry modeling/simulation codes to the MHPCC, and by conducting studies and analysis of DE systems.

**Methodology:** The MHPCC Contractor Team has worked in concert with the supporting contractors to develop methodologies and tools needed for the large-scale analysis of DE weapon system concepts. This development includes the porting of legacy simulation codes to MHPCC computing systems, the performance optimization of these codes for these systems, as well as tools for analysts to visualize and

comprehend the phenomenology of the simulations. Specifically, in support of AFRL/DE's weapon system concept modeling methodology, MHPCC staff has ported the Atmospheric Compensation Simulation (ACS) and Laser Lethality Assessment by Mesh-Free Algorithms (LLAMA) codes to the IBM SP parallel supercomputer. Staff also performed single CPU performance optimization on these codes, and then altered them to run in parallel on the IBM SP nodes available at MHPCC. Staff also provided visualization support by producing visualizations of the resultant simulation output. The information generated from this execution of model simulations, along with the associated mechanisms for visualization, will provide analysts with the tools required to assess the performance of many potential concepts.

**Results:** This year's activities have completed the port and optimization of the ACS and LLAMA codes for the MHPCC IBM SP supercomputer. The final ACS code was 37 times faster than the original, when running on the 32 CPU Power4 nodes. The final LLAMA code was 44 times faster than the original. Both of these codes now employ OpenMP directives on loops that consume significant CPU time to achieve parallelism on the IBM SMP nodes.

**Significance:** This initiative has led to a continuing evolution and refinement of a new generation of analytical models and tools. MHPCC will continue to collaborate with the DE/TOSS team to further develop simulation and visualization methodologies that may eventually improve AFRL/DE's ability to evaluate the applicability of these simulations to actual combat doctrine.

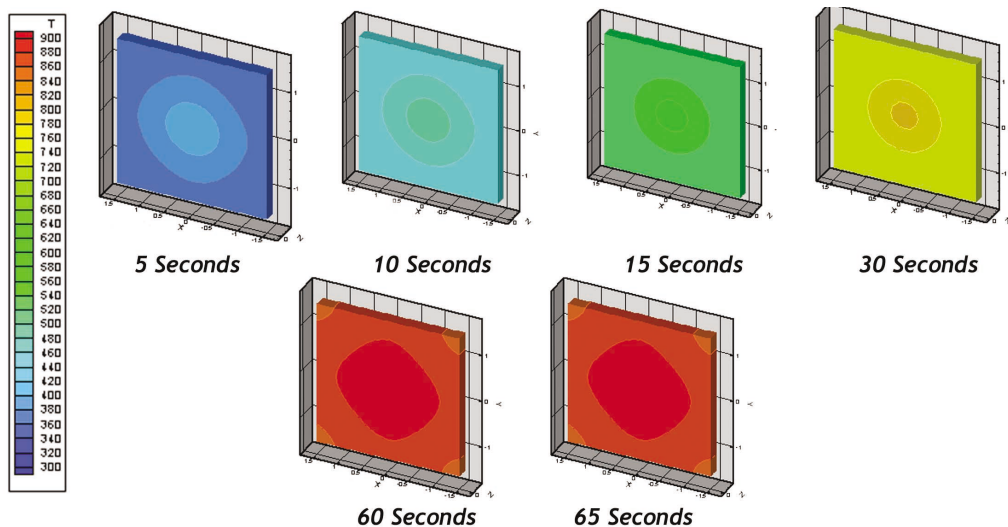


Figure 1. Thermal response of Al-6061 subject to laser heating.

Author and Contact: Brent Swartz  
Authors: Paul Kominsky and Brian Kruse  
Organization: Maui High Performance Computing Center, 550 Lipoa Parkway, Kihei, HI, 96753  
Resources: IBM SPs at MHPCC  
Sponsorship: Air Force Research Laboratory Directed Energy

# Airborne Laser Atmospheric Characterization/Atmospheric Decision Aid (ADA)

Randy J. Lefevre, Frank H. Ruggiero, Kevin Roe

The Airborne Laser (ABL) is being developed as one element of our nation's Ballistic Missile Defense System. The ABL Element Office is developing an Atmospheric Decision Aid (ADA) to diagnose and forecast the location and magnitude of optical turbulence in the upper troposphere and lower stratosphere. Development of the ADA relies on an understanding about the strengths and weaknesses of numerical weather prediction (NWP) models, plus the sensitivity of the optical turbulence algorithms to the NWP spatial and temporal resolution. This case study compared the accuracy and precision of the ADA optical turbulence algorithms to several horizontal and vertical NWP resolutions. Results indicate that for a given vertical resolution using a finer horizontal resolution does not significantly improve the accuracy of the forecast, but for a given horizontal resolution increasing the vertical resolution does improve the forecast accuracy.

**Introduction:** The Airborne Laser, an element of our nation's Ballistic Missile Defense System (BMDS), will detect and destroy boosting ballistic missiles. The ABL Element Office is managing the development of an Atmospheric Decision Aid to diagnose and forecast the location and magnitude of optical turbulence in the upper troposphere and lower stratosphere. Optical turbulence is the fluctuation of density in the atmosphere and acts to defocus laser beams and thus reduce their effective range. Layers of intense optical turbulence, while possibly stretching hundreds of kilometers in the horizontal, tend to occur on

vertical scales of a centimeter to 100 meters. An objective method of predicting optical turbulence has been developed at the Air Force Research Laboratory (AFRL). This method combines the forecast output of numerical weather prediction (NWP) models with a parameterization of the optical turbulence tailored to the model (Ruggiero and DeBenedictis 2000, 2002). Others have also used this approach in support of astronomy operations (e.g., Businger *et al.*, 2002). Ruggiero and DeBenedictis (2002) presented validation results that reveal the optical turbulence parameterization method is capable of representing coarse guidance on optical turbulence intensity. However the results also indicated that the predictive skill of the optical turbulence parameterization is limited by the ability of the NWP model to depict atmospheric features at a small spatial resolution.

The ABL's ADA is designed to use this objective optical turbulence prediction method. In practice the ADA will access real-time mesoscale NWP model forecast data from the Air Force Weather Agency (AFWA). Given the ABL's need for small-scale vertical depiction of atmospheric phenomena and the operational constraints of the AFWA, it is important to determine the optimal configuration in terms of grid spacing of the mesoscale model. The Maui High Performance Computing Center (MHPCC) is the perfect testbed to determine this configuration.

**Significance:** This work will determine what is the best mesoscale model spatial resolution, both in the vertical and horizontal, for predicting optical turbulence with the Dewan *et al.*, model (1993). It will aid in the eventual operations of the Airborne Laser being able to know the potential atmospheric effects on the lasers' propagation. This will allow mission planners to optimally locate the ABL's orbit to protect the asset while maximizing the lethality capability.



Figure 1. Artistic impression of ABL program.

## References:

- 1) J. H. Brown, R. E. Good, P. M. Bench, and G. Faucher, "Sonde Measurement for Comparative Measurements of Optical Turbulence," Air Force Geophysics Laboratory Technical Report, AFGL-TR-82-0079, ADA, (1982), 118740.
- 2) S. Businger, R. McLaren, R. Ogasawara, D. Simons, and R. J. Wainscoat, "Starcasting," *Bull. Amer. Meteor. Soc.*, 83, (2002): 858-871.
- 3) E. M. Dewan, R. E. Good, B. Beland, and J. Brown, "A Model for  $C_n^2$  (Optical Turbulence) Profiles using Radiosonde Data," Phillips Laboratory Technical Report, PL-TR-93-2043, (1993), ADA 279399.
- 4) G. A. Grell, J. Duhia, and D. R. Stauffer, "A Description of the Fifth Generation Penn State/NCAR Mesoscale Model (MM5)," NCAR Tech. Note T/N-398 + STR, (1995); 122 pp, [Available from NCAR Information Services, P.O. Box 3000, Boulder, CO 80307] (<http://www.mmm.ucar.edu/mm5/documents/mm5-desc-doc.html>)
- 5) G. Y. Jumper and R. R. Beland, "Progress in the Understanding and Modeling of Atmospheric Optical Turbulence," 31st AIAA Plasma Dynamics and Laser Conf., 19-22 June 2000, Denver, CO.
- 6) J. Michalakes, "The Same-Source Parallel MM5, Sci. Programming," 8, (2000): 5-12. (<http://www.mcs.anl.gov/~michalakes/JOSP-michalakes.ps>)
- 7) F. H. Ruggiero and D. A. DeBenedictis, "Forecasting Optical Turbulence from Mesoscale Numerical Weather Prediction Models," Preprints, 2002 DoD High Performance Modernization Program Users Group Conference, 10-14 Austin, TX. ([http://www.hpcmo.hpc.mil/Htdocs/UGC/UGC02/paper/frank\\_ruggiero1\\_paper.pdf](http://www.hpcmo.hpc.mil/Htdocs/UGC/UGC02/paper/frank_ruggiero1_paper.pdf))
- 8) F. H. Ruggiero and D. A. DeBenedictis, "Three-Dimensional Modeling of Optical Turbulence," Preprints, 2000 DoD High Performance Modernization Program Users Group Conference, 5-8 June, Albuquerque, NM. ([http://www.hpcmo.hpc.mil/Htdocs/UGC/UGC00/paper/frank\\_ruggiero\\_paper.pdf](http://www.hpcmo.hpc.mil/Htdocs/UGC/UGC00/paper/frank_ruggiero_paper.pdf))
- 9) V. I. Tatarski, 1961, "Wave Propagation in a Turbulent Medium," McGraw-Hill.



**Figure 2.** Airborne Laser being refueled during early flight tests.

Author and Contact: Lt. Col. Randy Lefevre, USAF  
Organization: Airborne Laser (ABL) Element Office, Kirtland AFB, NM  
Author: Frank H. Ruggiero  
Organization: AFRL, Space Vehicles Directorate, Hanscom AFB, MA  
Author: Kevin Roe  
Organization: Maui High Performance Computing Center, 550 Lipoa Parkway, Kihei, Hi, 96753  
Resources: IBM SP3/SP4 at MHPCC  
Sponsorship: Air Force Research Laboratory

## High-Resolution Forecasts to Support AMOS Using MM5

Kevin Roe and Duane Stevens

The Hawaiian Islands contain a variety of microclimates in a very small region. Some islands have rainforests within a few miles of deserts; some have 10,000 foot summits only a few miles away from the coastline. Because of this, weather models must be run at a much finer resolution to accurately predict in these regions. NCAR's Mesoscale Model Version 5 (MM5) is run from a coarse 27 km resolution (surrounding an area of approximately 5000 by 5000 km) nested down to a 1 km resolution daily. Since the computational requirements are high to accomplish this in a reasonable time frame (as to still be a forecast) MM5 is run in parallel on MHPCC's IBM SP3s and SP4s. Utilizing 32 processors the MM5 model is run daily over the above conditions in approximately seven hours. These forecasts have been in place for over two years now and are being utilized by operators at the telescope on Haleakala, Maui.

**Research Objectives:** The telescope operations on Haleakala are highly dependent on weather conditions on the Hawaiian Island of Maui. If the wind speed is too high then the telescope cannot be utilized. Problems also exist if there are clouds overhead. Rainfall and relative humidity are also a factor in determining the capabilities of the telescopes. In order to effectively schedule telescope operations, an accurate weather prediction is extremely valuable. Current forecasts that are available from the National Weather Service (NWS) give good indications of approaching storm fronts but only at the coarse level (30-50 km resolution). Because of this and the location of the telescope on Maui this can be insufficient for their needs.

The additional benefit of the telescope operators having access to an accurate forecast (even for only a day in advance) is that they can still perform some scheduling. If a storm is predicted they can plan maintenance for this time period. This allows them to function more effectively by giving them the capability to schedule downtime. This in turn saves time, improves operating efficiency, and potentially saves money.

**Daily Operations:** Every night at Midnight Hawaiian Standard Time (HST), a PERL script is run to handle all the operations necessary to produce a forecast, prepare the data, and post it to the MHPCC web page (<http://weather.mhpcc.edu/mm5>). The procedures the script executes are:

- 1) Determine and download the latest global analysis files from NCEP for a 48-hour simulation,
- 2) Begin processing by sending these files through MM5's REGRID program,
- 3) Take the output data files from REGRID and input into INTERPF,
- 4) Prepare the MM5 model for the current simulation,
- 5) Submit the MM5 run to MHPCC's IBM SP3 (Tempest) for execution (daily reservation starting at 1:00 A.M.),
- 6) Average daily run requires between 7 - 7.5 hours for completion on 32 processors (2 nodes),
- 7) Data is output in 1-hour increments,
- 8) Data is processed in parallel to create useful images for meteorological examination,
- 9) Convert images to a web viewable format,
- 10) Create the web pages for these images, and
- 11) Post web pages and images to MHPCC's web site.



Figure 1. Maui Space Surveillance Site located atop Mt. Haleakala.

**Web Output:** Now that the above processes have created images, they must be made available for the telescope operators. This is accomplished by posting the images to the MHPCC web page; specifically, <http://weather.mhpcc.edu/mm5>. This title page gives the user the option of what area and resolution they would like to examine. From the title page, the user can select the all island area at a 27 or 9 km resolution, one of the 4 counties (Hawaii, Maui, Oahu, and Kauai) at a 3 km resolution, or the summit of Haleakala at a 1 km resolution. Once one of the above has been selected, the user is transported to a web page that initially includes an image of the temperature in the selected area. On the regional web page, the viewer can select to see the previous or next image through the use of a small JavaScript. If the viewer prefers, an animation of the images (in 1 hour increments) can be started and stopped. Finally, the user can select any of the images from a pull down menu. If the viewer would like to change the field being examined, a pull down menu on the left side of the page will transport the user back to the main menu or allow them to choose a different field. Lastly, if the JavaScript becomes a problem for the viewer's browser, they have the option of being switched to a non-JavaScript equivalent version web page.

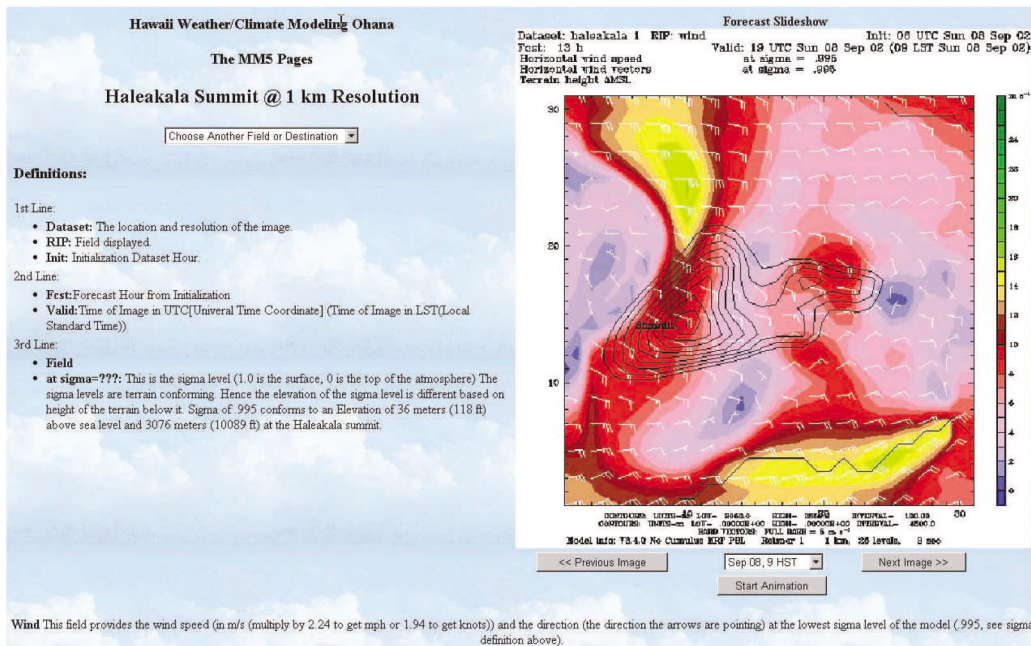


**Figure 2.** Website screen capture of weather modeling of the Haleakala Summit.

## References:

- 1) J. Michalakes, "The Same-Source Parallel MM5," *Journal of Scientific Programming*, 8, (2000): 5-12.
- 2) J. Michalakes, S. Chen, J. Dudhia, L. Hart, J. Klemp, J. Middlecoff, and W. Skamarock, "Development of a Next Generation Regional Weather Research and Forecast Model," *Developments in Teracomputing, Proceedings of the Ninth ECMWF Workshop on the Use of High Performance Computing in Meteorology*, Eds., Walter Zwiefelhofer and Norbert Kreitz, World Scientific, Singapore, (2000): 269-276.
- 3) J. Dudhia, "A Nonhydrostatic Version of the Penn State/NCAR Mesoscale Model, Validation Test and Simulation of an Atlantic Cyclone and Cold Front," *Mon. Wea. Rev.*, 121, (1993): 1493-1513.
- 4) Yi-Leng Chen and J. Feng, "Numerical Simulation of Airflow and Cloud Distributions over the Windward Side of the Island of Hawaii, Part I: The Effects of Trade Wind Inversion," *American Meteorological Society*, (May 2001): 1117-1134.
- 5) Yi-Leng Chen and J. Feng, "Numerical Simulation of Airflow and Cloud Distributions over the Windward Side of the Island of Hawaii, Part II, Nocturnal Flow Regime," *American Meteorological Society*, (May 2001): 1135-1147.
- 6) K. P. Roe and D. Stevens, "High Resolution Weather Modeling in the State of Hawaii," *The 11th PSU/NCAR Mesoscale Model Users' Workshop*, Boulder, CO, 2001.
- 7) K. P. Roe and D. Stevens, "High-Resolution Weather Modeling to aid AMOS," *DoD HPCMP User Group Conference*, Bellevue, WA, 2003.

Author and Contact: Kevin Roe

Organization: Maui High Performance Computing Center, 550 Lipoa Parkway, Kihei, Maui, HI, 96753

Author: Duane Stevens

Organization: Department of Meteorology, University of Hawaii at Manoa, 2525 Correa Road, HIG 350, Honolulu, HI, 96822

URL: <http://weather.mhpcc.edu/mm5>

Resources: IBM SP3/SP4 at MHPCC

Sponsorship: Air Force Research Laboratory

# High Performance Computing and Web Support for Project Albert: Analysis of Entity-Based Simulations of Combat Operations and Operations Other Than War

Bob Swanson, Brent Swartz, Maria Murphy, Ron Vilorio, D. J. Fabozzi, Bruce Duncan

The Marine Corps Warfighting Laboratory's (MCWL) Project Albert involves research to assess the general applicability of the "New Sciences" to combat operations and operations other than war. While simulations based on these New Sciences (or complexity theory, which models behavior and interaction at the entity level) are considered part of an infant science, they do provide insight into evolving patterns of macroscopic behavior that result from collective interactions of individual agents. Simulations based on entity-level interactions represent a significantly different approach from the traditional attrition estimation techniques based on Lanchester equations, which assert that the loss rate of forces on one side of a battle is proportional to the number of forces on the other side. MCWL Project Albert is an effort to investigate how complexity theory may be applied to combat in a manner to augment and, perhaps in some cases, replace Lanchester modeling in the future.

**Research Objectives:** MCWL is continuing the development of a complex systems analyst's toolbox for exploiting emergent, collective patterns of behavior on the battlefield, and is using several multiagent-based simulations of notional combat. Current models that are being employed include Irreducible Semi-Autonomous Adaptive Combat (ISAAC), MANA, Socrates, and Pythagoras. These models simulate the interaction between two or more variable size forces of agents. The action of each agent is determined by parameters, such as the agent's ability to sense its surroundings and to communicate with other agents. Besides the common physical parameters measured by the model (such as range of fire and probability of kill), more abstract concepts are also modeled. Such concepts can include an agent's attraction

to friendly and opposing forces and the influence of behaviors based on determinable thresholds, such as the tendency of an agent to follow orders. The magnitude and granularity of these independent variables provide the analyst with great flexibility in simulating various hypotheses. This same flexibility, coupled with the stochastic nature of the simulations, requires a significant computational capability to determine likely outcomes with any statistical significance for each single hypothesis. This requirement becomes even greater for the analyst who wants to study hypotheses over multiple varying independent parameters, a requirement that easily overtaxes the capability of a single personal computer.

**Methodology:** The Maui High Performance Computing Center (MHPCC) Project Albert contractor team has performed computer systems engineering services in concert with military analysts from MCWL and other supporting contractors, to develop methodologies and tools needed for the large-scale analysis of agent-based distillation models. This development includes processing and data reduction required for statistical analysis of such simulations and the tools for analysts to visualize and comprehend the phenomenology of the simulations. Specifically, in support of MCWL's data farming methodology, MHPCC has ported the core engine of the ISAAC, Socrates, and Pythagoras models to its IBM SP parallel supercomputer, a cluster of Windows workstations, and its Linux Supercluster to provide high performance computing support for the project. The resultant codes can execute and statistically reduce multiple combat hypotheses. The output of the multiple simulation runs is a set of statistically calculated fitness values that are used as measures of battlefield effectiveness. The Visualization Toolkit provides analysts the ability to assess the combined results of the model outputs and to simultaneously conduct a comparative analysis of multiple playbacks (time/space representations of battlefield agents). The information generated from this exhaustive execution of model simulations, along with the associated mechanisms for visualization, will provide analysts with the tools required to investigate multiple hypotheses with statistical significance.

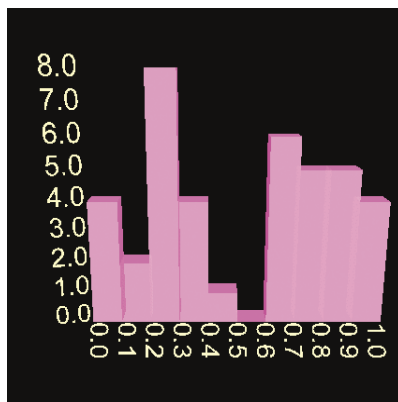


**Figure 1.** An initial basic prototype of the new Distribution Plot is shown here.

**Results:** The MHPCC contractor team has continued to provide further refinements to the system and more tools to aid the analytical process. It has updated the Web-based submission system that it previously developed. The Web site is controlled by MCWL and is located at <http://www.mcwl.quantico.usmc.mil/divisions/albert/index.asp>. The updated system allows analysts to submit large scenario runs over the Web, thereby allowing analysts to easily explore a given scenario in many ways. MHPCC added an enumeration capability, which allows the user to data farm over user supplied sub-trees of the input XML file, so that virtually any subsection of the input file can be data farmed. MHPCC also modified the Web system to dynamically display parameters in the input XML file, so that any design modifications to the input file are automatically recognized by the Web system. The team has also developed and tested a software download capability to the Web site, and deployed relational databases that provide storage and retrieval capability to the growing scenario archive. MHPCC has also coupled the scenario databases to the job submittal system to inform users of relevant recent scenarios. The Web site has been modified to allow MOE output data to be converted to various output formats, including database (.mdb), comma-separated value (CSV), HDF5, and XML format. This allows the MOE output data to be processed by many existing statisti-

cal and visualization tools. MHPCC has also continued enhancements to the Parallel Execution System (PES), a set of portable Java programs, which allow multiple models (currently ISAAC, Socrates, MANA, and Pythagoras) to be executed in parallel on the many platforms available at MHPCC.

Release revisions of Socrates, MANA, and Pythagoras models were migrated to MHPCC several times during this past year, with each new MANA model being fully integrated with existing PES code and the MHPCC Condor IBM PC cluster. The PES supports all of the platforms at MHPCC, including the IBM SP, the Condor PC cluster, and the Linux Supercluster. The PES is designed to improve the overall portability, performance, and scalability required to produce model output files. It is also designed to more easily integrate future models into the PES. This will allow these models to be run in parallel on the various MHPCC platforms, while simultaneously allowing the Visualization Toolkit to be used on the resulting output. SMP parallelism is achieved by simultaneously executing as many model runs as will fit the number of CPUs available on a computational node. MHPCC has recently modified the PES to allow the number of excursions that can be practically executed to increase by a factor of ten, allowing a hundred million model executions to be performed with a single scenario submission. An XML file is used to completely describe each user-defined scenario. This file is created by user interaction with the Web-based submission system, then passed to the PES for model execution, and finally used in the Visualization Toolkit for the display of the results. As designed, the original PES allowed for full combinatorial executions of the parameter space. In support of efforts by partners in the Project Albert team, MHPCC modified the Web site and PES to allow different algorithms, including genetic algorithms, to be used in the parameter space search. These alternative algorithms may allow optimal solutions to be found with a significantly reduced computational resource requirement. As part of the ongoing code re-engineering effort, the PES code (written in Java) was updated to generalize the XML interfaces and to enable Document Object Model (DOM4J) XML Open Source Framework and to simplify the upgrade path to future Java releases, including the latest version, Java 1.4. Other various PES job interactive enhancements, designs, and other model work have also been performed, including an update to the job submittal script and tool. MHPCC also added a metadata database capability to the Web site, so that a user can search previously executed scenarios for scenarios that match their search criteria. The MHPCC Project Albert team also added a new, advanced 3U Blade computing cluster that provides dedicated support to the program for normal operations research and during more intensive data farming working sessions. Additional Web site and PES enhancements are also planned to provide more functionality and user empowerment.

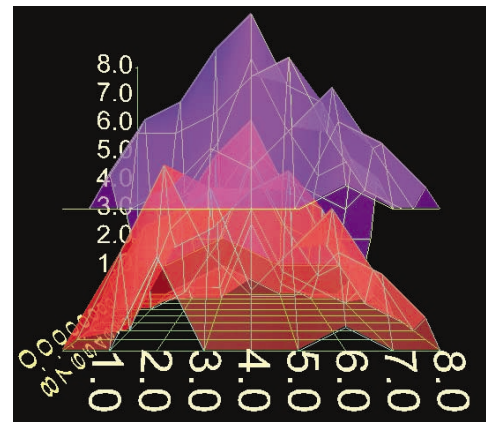


**Figure 2.** An initial basic prototype of the new Landscape Tool is shown here. Analysts can click on the red mountain to turn MOE spheres on and off. Once the spheres are activated, users can click on them to move them. The spheres are prototyped to reduce the amount of text that needs to be sent. Transparency animation "blinking" of the mountains and spheres could also be provided as an option.

This year's roadmap for technical work has also included Visualization planning and the beginning of the design and development of next-generation Landscape and Playback tools, including new MOE and playback file designs. As part of this work area, code was modified to use the latest version HDF5 Java Application Program Interface (API). Successful prototyping of 2-D and 3-D requests and retrieval has also been completed. The MHPCC Project Albert contractor team has also performed Extensible 3-D (X3D) technology investigations and conducted initial evaluations of this technology. Preliminary VRML files were created to demonstrate what the future landscape tool might look like. In this implementation, XSLT translators convert VRML97 compliant files to and from X3D compliant files. The team has also examined various Java Applets for 3-D with a minimum of client-side requirements and has explored new Graphical User Interfaces (GUI), including views, controls, linking, and other functions and objects. The work performed thus far in this area has initially resulted in the development of a basic new VRML Distribution Plot prototype, and a new Landscape Tool prototype as shown in Figures 1 and 2.

MCWL has successfully applied these tools to reinforce intuitive conclusions. Comparison of these results with several historical battles has further validated the various models' applicability. MCWL has also used Project Albert and the associated products as a springboard for other collaborative research and analysis activities. Such activities include significantly increased participation of analysts from a wide variety of U.S. Department of Defense and Department of Energy organizations, and friendly nations, at various conferences and working sessions over the past year where the participants research analytical methods and a new generation of modeling tools to address additional issues including homeland defense, urban military operations, force protection, and unmanned vehicles.

**Significance:** This initiative has led to a continuing evolution and refinement of the new generation of analytical models and tools. It is anticipated that MCWL will continue to require further development of simulation, visualization, and statistical methodologies that may enhance MCWL's ability to evaluate the applicability of these simulations to actual combat doctrine. These efforts will expand the existing infrastructure to incorporate new technologies.

Author and Contact: Bob Swanson  
 Authors: Brent Swartz, Maria Murphy, Ron Vioria, D. J. Fabozzi, Bruce Duncan  
 Organization: Maui High Performance Computing Center, 550 Lipoa Parkway, Kihei, Maui, HI, 96753  
 Resources: IBM SP3/SP4 and IBM Linux Supercluster at MHPCC  
 Sponsorship: Marine Corps Warfighting Laboratory (MCWL)

# Quantum Lattice Gas and Lattice Boltzmann Simulations of MHD Turbulence

Linda Vahala, George Vahala, Angus Macnab, Jeffrey Yezpez

Since MHD turbulence involves complex spatiotemporal intermittency involving coherent structures, it is prudent to first investigate simpler systems that are more amenable to detailed analysis yet contain some of the basic properties of the full problem. It is precisely this philosophy that has led to the development of the Burger's equation as a model for Navier-Stokes turbulence. We are developing models to simulate the 1D MHD equations: Lattice Boltzmann methods (for both uniform and multi-grid meshes) as well as a quantum lattice gas algorithm that uses 2 qubits/spatial mesh. The simulations show that in early times, there can be strong transfer of kinetic to magnetic energy, during which time there is no decay in the total energy in the system. Eventually, the magnetic energy can undergo stronger decay than the kinetic velocity – even though the resistivity is less than the viscosity. The energy spectra strongly follow the  $k^{-2}$  law.

the grid points in regions of high spatial gradients. We have also developed a quantum lattice gas algorithm<sup>1</sup> that utilizes unitary collision and streaming operators to entangle qubits and spread that entanglement across the lattice. We use 2 qubits/scalar field at each lattice point. It is the quantum entanglement of qubits that yields the exponential speed-up of quantum computers over classical computers.

**Project:** The 1D MHD model, like Burger's equation, drops the pressure gradient term but still retains a self-consistent magnetic back-pressure which permits energy exchange between the velocity and magnetic fields. The compressible equations are:

$$\frac{\partial u}{\partial t} + u \frac{\partial u}{\partial x} = - \frac{\partial}{\partial x} \left( \frac{\mathbf{B}^2}{2} \right) + \nu \frac{\partial^2 u}{\partial x^2}$$

$$\frac{\partial \mathbf{B}}{\partial t} + \frac{\partial}{\partial x} (u\mathbf{B}) = \eta \frac{\partial^2 \mathbf{B}}{\partial x^2} \quad \text{and}$$

where  $\mathbf{u} = u(x,t)\hat{\mathbf{x}}$  and  $\mathbf{B}(x,t) = B_y(x,t)\hat{\mathbf{y}} + B_z(x,t)\hat{\mathbf{z}}$  with  $\nabla \cdot \mathbf{B} = 0$ .

We have developed Lattice Boltzmann algorithms based on the simple BGK collision operators using a distribution function for the velocity field and a vector distribution function for the magnetic field using both a 4-bit (streaming in  $\pm 1, \pm 2$  on a uniform mesh) and a 3-bit (streaming in  $0, \pm 1$ ) – both for a uniform spatial mesh<sup>1</sup> as well as a multigrid mesh<sup>2</sup> which concentrates

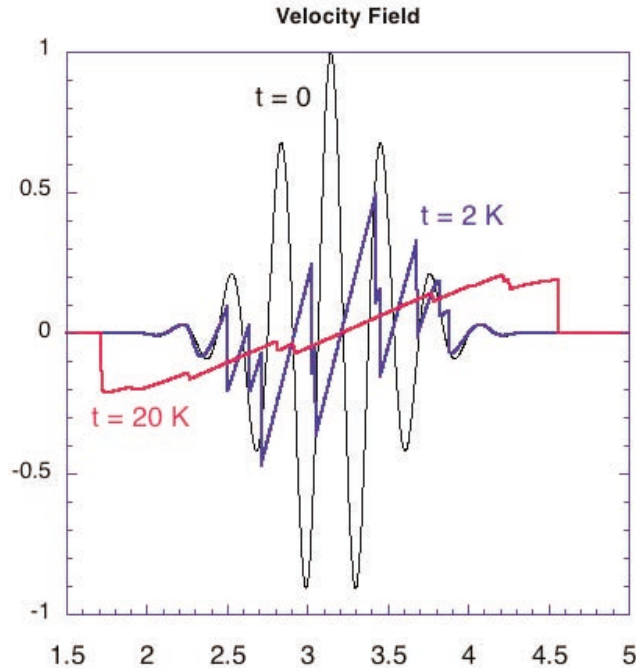


**Figure 1. VELOCITY FIELD .** The evolution of the velocity wave packet. Shocks form at  $t = 2K$  and then coalesce for later times ( $t = 20K$ ).

For the simulations (performed on *Tempest*, MHPCC as well as on *Chilkoot*, ARSC) we consider Gaussian wave packet fields for the velocity and magnetic field. Figure 1 shows the evolution of the velocity wave packet: evolution of shocks ( $t = 2K$  iteration) which then coalesce ( $t = 20K$ ). During the formation of the shocks, there is a marked energy exchange from the velocity to the magnetic fields, Figure 2. In the early stage of the dissipative evolution,  $t < 230$ ,  $E_{TOT} \approx const.$  to within 0.1%, while the magnetic energy nearly doubles. At later times ( $t > 10K$ ) the total energy as well as the kinetic and magnetic energy undergo power law decay (at different rates).

In Figure 3 we plot the evolution of the kinetic energy spectrum,  $E_K(k,t)$ , where  $E_K(t) = 2 \int_0^\infty dk E_K(k,t)$  for several times. At  $t = 40$  K iterations the energy spectrum decays as  $k^{-2}$ .

These simulations were performed on a uniform 32000 spatial mesh. While easily achieved in 1D, this fine mesh would be prohibitive in moving to 3D or even 2D. A multigrid approach can significantly reduce this without loss of accuracy.<sup>2</sup> A quantum lattice gas multigrid algorithm is under consideration.

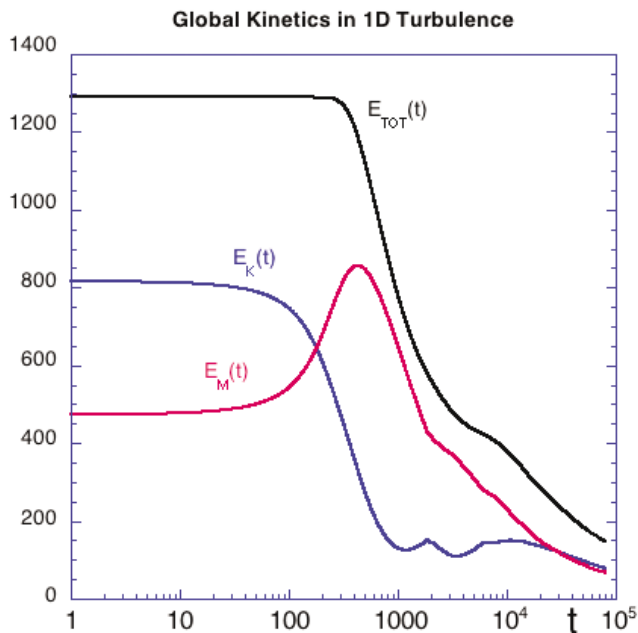


**Figure 2. GLOBAL KINETICS IN 1D TURBULENCE.** The time evolution of the global kinetic and magnetic energies. For  $t < 300$ , there is negligible decay in the total energy in the dissipative MHD equations. At early times there is a strong transfer of energy from velocity to the magnetic field.

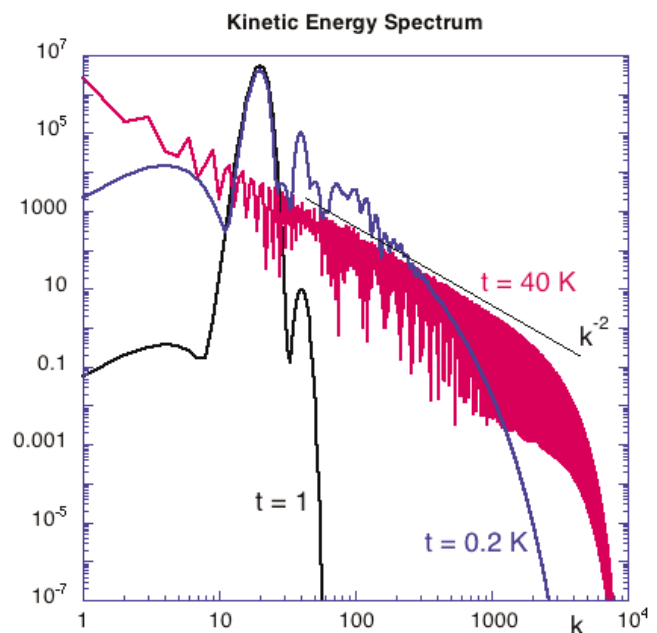


**Figure 3. KINETIC ENERGY SPECTRUM.** The evolution of the turbulent kinetic energy spectrum.

**References:**

- 1) L. Vahala, G. Vahala, and J. Yepez, "Lattice Boltzmann and Quantum Lattice Gas Representations of One-Dimensional Magnetohydrodynamic Turbulence," *Phys. Lett. A306*, (2003): 227-234.
- 2) A. Macnab, G. Vahala, and L. Vahala, "Nonuniform Grids in the Lattice Boltzmann Representation of 1D MHD Turbulence," to be published; also A. Macnab, Ph. D Thesis, William & Mary (2003).

Author and Contact: Linda Vahala  
 Organization: Department of Electrical & Computer Engineering, Old Dominion University, Norfolk, VA  
 Authors: George Vahala and Angus Macnab  
 Organization: Department of Physics, William & Mary College, Williamsburg, VA, 23187  
 Author: Jeffrey Yepez  
 Organization: Air Force Research Laboratory, Hanscom AFB, MA, 02137  
 Resources: *Tempest* at MHPCC and *Chilkoot* at ARSC  
 Sponsorship: Air Force Office of Scientific Research, Computational Mathematics Branch

# Towards a High-Resolution Global Coupled Navy Prediction System: Ocean and Ocean/Ice Components

Julie McClean, Mathew Maltrud, Detelina Ivanova, Prasad Thoppil, Elizabeth Hunke

In the future, short-term (up to 5 days) environmental forecasts for the U.S. Navy will be provided by a high-resolution global coupled air/ocean/ice prediction system with very high-resolution regional air/ocean models nested into the global system at strategic locations. Realistic ocean and coupled ocean/ice components are currently being developed, tested, and run over several decades to understand the integrity of the resulting solution prior to coupling with the atmospheric predictive model and the inclusion of the forecasting scheme in the ocean model. These model components will also be used in a future coupled climate prediction system and to better understand ocean and ice dynamics.

**Research Objectives:** Towards the realization of a high-resolution global coupled air/sea/ice Navy prediction system, we are continuing the development, testing, and integration of realistic high-resolution ocean and coupled ocean/ice components.

**Methodology:** The first step in the development of a synoptic ocean prediction system is to determine if the underlying ocean model is statistically consistent with observations at the relevant space and time scales. Here the scales are 10-1000 km and days to several months, respectively. A feasibility study (McClean *et al.*, 2002) was conducted using a North Atlantic high-resolution (0.1°, 40-level) configuration of the Los Alamos National Laboratory Parallel Ocean Program (POP). The study showed that the ocean model produced

realistic current strengths, eddy energy levels, and intrinsic scales. Subsequently, a 0.1-degree, 40-level global POP simulation forced with realistic surface fluxes was integrated for two decades (1979-1999); the last five years of the simulation were completed in 2003 at the Maui High Performance Computing Center (MHPCC). Comparisons of statistical analysis from observations and the model are underway to identify model biases. As well, we tested a 0.4°, 40-level global configuration of POP coupled to the Los Alamos National Laboratory sea ice model (CICE). Lower resolution is used in the first instance while coupling issues are explored. A suite of runs has been completed to understand the importance of the surface forcing and initial conditions.

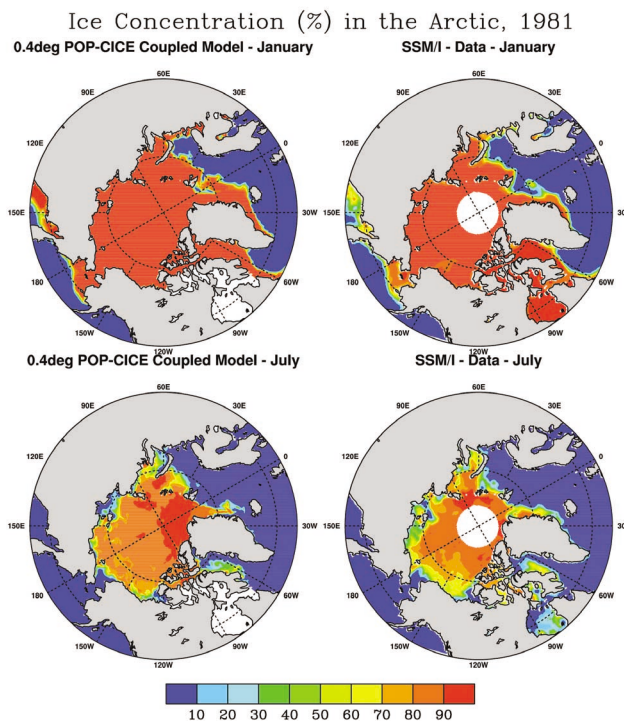


**Figure 1a.** Sea ice concentration (%) in the Arctic from the 0.4°, 40-level global POP/CICE model and passive microwave data in winter and summer of 1981.

**Results:** The high-resolution global ocean simulation was monitored in terms of its ability to reproduce the observed ocean state. Statistical quantities from data sets with global or near-global coverage such as those obtained from satellite altimeters and surface drifting buoys were compared with model quantities. Results indicate that the distribution and strength of the eddy energy agrees well with satellite altimetry in most high-activity areas. Overall, the general circulation is well represented, with acceptable values for overturning mass and heat transports, and good agreement with transport estimates of the major current systems.

Shown here are the results of the coupled POP/CICE simulation initialized from uniform 2 m ice beginning in January 1980. Figures 1a and b show the seasonal ice concentration in the Arctic and Antarctica, respectively, from the coupled model and passive microwave data.

The data, Nimbus-7 and DMSP-F8, and -F11 and Sea Ice Concentrations 1978 through 1995, were obtained from the EOS-DIS NSIDC Distributed Active Archive Center (NSIDC DAAC), University of Colorado at Boulder. In the Arctic, the modeled and observed ice concentration and ice edge location show very good agreement during January, and reasonable agreement during July. In Antarctica, the modeled ice area is too extensive in both seasons. It should be noted that much of this overly extensive ice in the coupled model is very thin, and is therefore subject to the variability of the ocean state.

**Significance:** The high-resolution global integration is one of the highest horizontal and vertical ocean simulations to be performed to date. It affords us the opportunity to study the ocean circulation, particularly mesoscale variability and processes as well as their interactions with the larger scales, in parts of the ocean that hitherto have not been simulated at such fine resolution. The successful coupling of the ocean and ice components will produce more realistic surface fluxes, which in turn, will improve the ocean model's accuracy in representing synoptic processes.

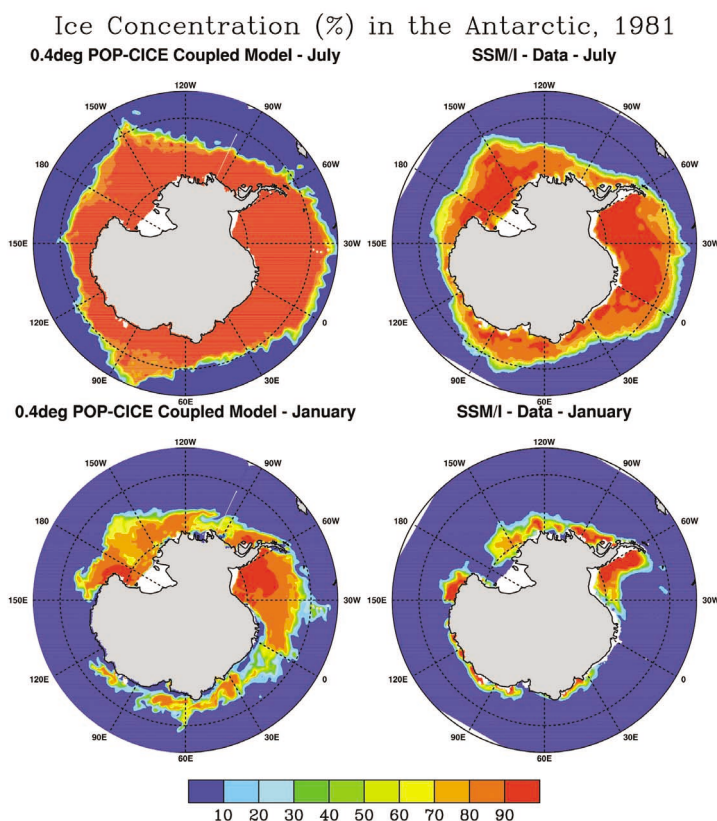


**Figure 1b.** Sea ice concentration (%) in the Antarctic from the 0.4°, 40-level global POP/CICE model and passive microwave data in winter and summer of 1981.

**Reference:**

- 1) J. L. McClean, P. M. Poulain, J. W. Pelton, and M. E. Maltrud, "Eulerian and Lagrangian Statistics from Surface Drifters and a High-Resolution POP Simulation in the North Atlantic," *Journal of Physical Oceanography*, 2, (2002): 2472-2491.

Author and Contact: Julie McClean

Authors: Detelina Ivanova and Prasad Thoppil

Organization: Department of Oceanography (OC/Mn), Naval Postgraduate School, Monterey, CA, 93943

Author: Mathew Maltrud and Elizabeth Hunke

Organization: Los Alamos National Laboratory, Los Alamos, NM, 87545

Resources: IBM SP3 and SP4 at MHPCC, IBM SP3 and SP4 at NAVO, and IBM SP3 at ARSC, and Origin 3000 at ARL

Sponsorship: Office of Naval Research, DoD High Performance Computing Modernization Program, Department of Energy, and National Science Foundation

## Theater UnderSea Warfare (TUSW)

Bob Dant, Lance Terada, Carl Holmberg, Marie Greene, Thomas Meyer, Mark Radleigh

A Linux cluster was purchased and installed at the Air Force Research Laboratory's Maui High Performance Computing Center (AFRL/MHPCC) for dedicated Theater UnderSea Warfare (TUSW) use. This TUSW cluster provides high performance computing resources to TUSW users for computationally intensive undersea warfare (USW) simulations. The cluster was designed to be easily expandable for future modifications and growth of the system. The TUSW cluster initially has 32-nodes (two processors per node), with a Network Attached Storage (NAS) system that can be upgraded to a more robust Storage Area Network (SAN) architecture at some future date. In addition, AFRL/MHPCC purchased and installed a Relational Database Management System (RDBMS) that used IBM Informix software to support the dynamic data files for the Navy's Tactical Environmental Display Server (TEDS) system. The TEDS databases (both dynamic and static data files) were hosted on the TUSW cluster at AFRL/MHPCC and remote processing capabilities were developed. Secure connectivity (via SIPRNet) to Pearl Harbor (Commander Task Force-12, CTF-12) was also established, allowing "remote" access to the MHPCC computing resources for computationally intensive acoustic model research activities.

**Methodology:** Research efforts for the initial TUSW program (Year 1) at AFRL/MHPCC focused on: 1) implementing a database management system (DBMS) on a Linux cluster at MHPCC, 2) porting selected TUSW database applications to the TUSW system, and 3) establishing secure communications between AFRL/MHPCC and CTF-12 (Pearl Harbor), using a message passing protocol.

Potential applications of TUSW technologies were investigated that could support characterization of a "battle space" environment at the Pacific Missile Range Facility (PMRF) on Kauai (Hawaii), to include the potential synergy of simulation software, multi-hypothesis trackers, environmental analysis and display, and high quality visualization of the PMRF "synthetic" range.

**Results:** AFRL/MHPCC purchased and installed a 32-node (64 processor) Linux cluster system for exclusive TUSW use, which included a RAID5 configured Network Attached Storage (NAS) device and GigE interfaces for communications. Five dynamic database (DB) files were installed on the cluster, as well as 11 static DB files that provided operational and environmental data for determining potential undersea conditions and possible targets. The Linux cluster hosted an IBM Informix Dynamic Server (IDS) and associated software. In-house system "tuning" optimized the database accessing routines and the implementation of both the static and dynamic database segments.

AFRL/MHPCC implemented a secure network interface between the Linux cluster operating system and "remote" TUSW users at CTF-12 (Pearl Harbor, HI).

**Research Objectives:** The TUSW program objectives involved: 1) developing and testing of a PC-based advanced USW workstation, 2) enhancing the design and implementation of a USW segment for the Net-Centric Collaboration Toolset, 3) engaging shore-based high performance computing power by porting operational databases and executing computationally intensive acoustic models within the AFRL/MHPCC processing environment, 4) creating TUSW Command Centers with automated knowledge management tools, 5) integrating air reconnaissance assets into the real-time USW net-centric environment, and 6) transitioning these new technologies to the acquisition community for eventual integration into the Navy's operational USW fleet and the Marine Corps warfighting inventory.

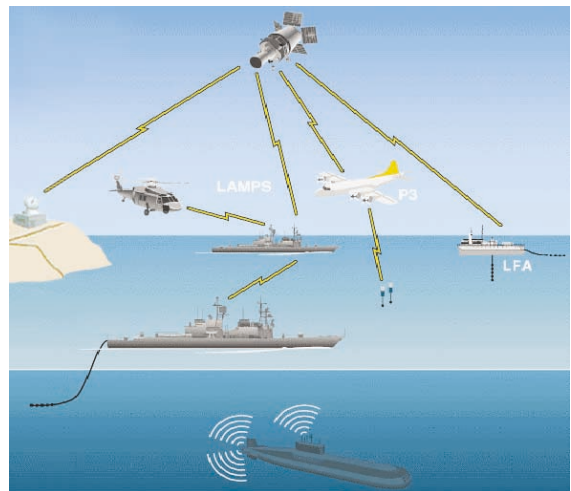


Figure 1. Various naval assets are available to perform USW activities, using a net-centric collaborative environment.

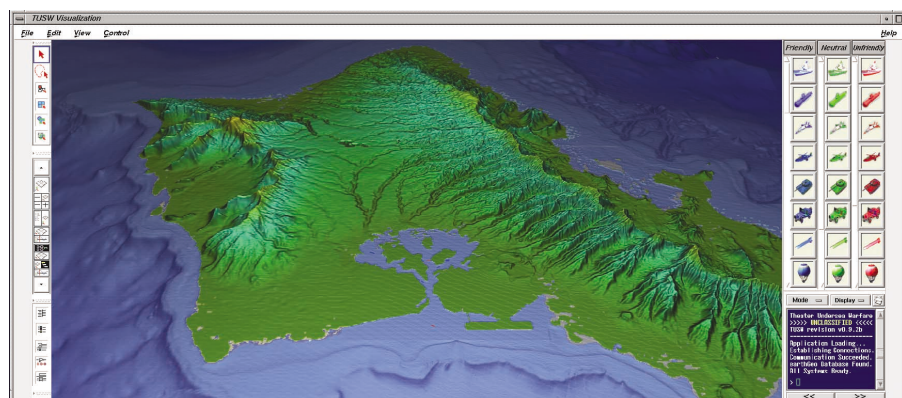
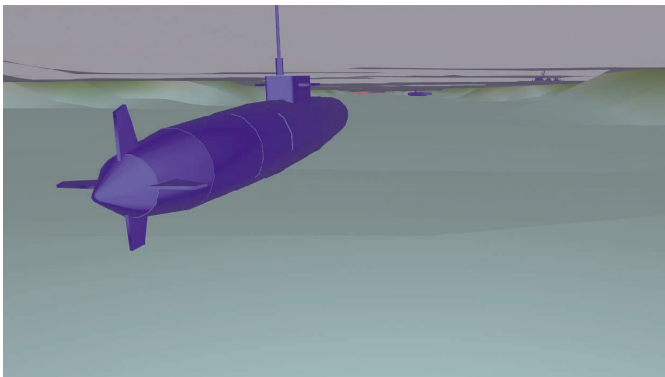


Figure 2. 3D geospatial data environments fused with interactive manipulation of naval assets and warfare scenarios were part of the USW visualization development.

In addition, AFRL/MHPCC participated in TUSW code testing and in developing proof-of-concept demonstrations that highlighted initial TUSW program resources and capabilities.

Visualization efforts included the development of code to integrate and manipulate data from various resources. Actual data from existing TUSW applications were developed and fused with geospatial data to create a conceptual TUSW Synthetic Simulated Environment (SSE). Increased functionality was demonstrated with the addition of interactive 'drag and drop' capabilities of warfare assets, real-time weapons deployment, environmental fly-through, and multiple asset tracking capabilities.

Future efforts will include the design of a TUSW cluster "scheduler/manager" that will provide load balancing for multiple, concurrent TUSW user requests for dynamic data, as well as allow scheduled jobs fast access to static databases, regardless of the location of the users. For visualization activities, future efforts will include the development of a graphics software system with increased interactivity, incorporation of real-world data (asset variables, weather, bathymetry, topography, active sonar effects), integration of existing USW databases, simulation of vulnerabilities, and other areas of interest. A user-friendly application will also be developed for a multi-platform environment.



**Figure 3.** Ongoing USW research activities involved real - world operational databases linked with simulated environmental data, as well as methods to display detection, counter-detection, and other areas of interest.

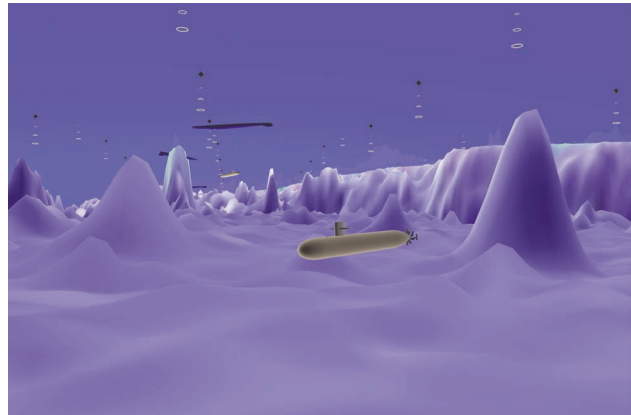


**Figure 4.** Methods involving time-lapse sonar data, vulnerability probabilities, and buoy patterns are part of the ongoing research to augment existing USW graphical software.

**Significance:** The U.S. Navy has encouraged the identification, development, testing, and deployment of technologies that enable undersea warfare decision makers to rapidly exploit the new advances in data fusion, knowledge management, high performance computing, and communications reach-back capabilities. Consequently, the Office of Naval Research (ONR)-Code 35, Greater MIDPAC, has promoted research and development of innovations that will provide technology-based options



**Figure 5.** Future TUSW research will include airborne assets in determining resource allocation and environmental analysis of TUSW activities.

for future U.S. Navy and Marine Corps capabilities. One of these options is the investigation of new technologies for TUSW activities. The need for integrated, net-centric TUSW technologies that capitalize on PC and UNIX-based workstations has been well documented through the Fleet Anti-Submarine Warfare Improvement Program. In addition, the Mission Needs Statement for the Navy's Common Undersea Picture (CUP) program has also formalized this requirement, and the Commander Submarines Pacific has outlined a USW initiative that supports the theater undersea portion of the CUP program. As such, the goal for TUSW is to "Implement a 'leap ahead' command center of the future for knowledge development, resource allocation, and environmental analysis for undersea warfare." CTF-12 has spearheaded these efforts with web-centric communications packages in the USW net-centric domain.

Author and Contact: Bob Dant

Authors: Lance Terada, Carl Holmberg, Marie Greene, Thomas Meyer, Mark Radleigh

Organization: Maui High Performance Computing Center, 550 Lipoa Parkway, Kihei, HI, 96753

Resources: Linux cluster at MHPCC

Sponsorship: Office of Naval Research

## Novel Active Optics with 10<sup>23</sup> Photomechanical Actuators

Joe Ritter, Jim Brozik, Luke Emmert, Mike Fallbach, Rodney Bradford, Don Leo, Ken Meissner

It is now possible to build amazing molecular-scale machines and devices. This new technological thrust is inspired both by biology and by the decreasing dimensions of semiconductor devices, and will ultimately result in novel devices set apart from any others currently used and understood. Work on molecular machines today is as important and fundamental as work on semiconductors was 50 years ago. The development of novel lightweight space qualified optics is of vital importance to national defense. Optical correction devices are an essential component of the tradespace for reducing primary mirror mass. Higher capability active optics would enable lighter primary mirrors, and could provide an order of magnitude reduction in mirror production costs. Inexpensive, optically addressable, lightweight, high pixel density, high control capability active optics will dramatically improve mission capabilities by providing a critical enabling technology.

**Photonic Muscles:** Compounds such as  $\pi-\pi^*$  mixed valence organic laminates, and various Azo-Benzene compounds undergo photoinitiated distortion. Early work by Ritter investigated use of Cis-Trans isomerization to effect figure change in membrane optics. When irradiated by the correct wavelength of light some chromophores (e.g., azo derivatives) undergo a structure change (photoisomerization), which if placed in a matrix (polymer, crystal, or other) can cause movement of the matrix. Materials which incorporate these and related compounds can show a change in bulk dimension with the application of light. This suggests the following uses: compensation for errors in membrane mirrors, inducing controlled deformations to correct wavefront aberrations induced by atmospheric propagation (AO systems), figure control of HEL mirrors, figure control of large space optics, and damping of oscillations caused by telescope repointing and environmental perturbations in a large deformable mirror allowing a robust response to pointing and slewing membrane space optics.

Advances in active optics have been made; however, current efforts are scale limited by the size and control capabilities of substrate technologies. Prototype correctors with a few thousand corrective elements have been produced at very high cost, and these correctors are far from the inexpensive high capability correctors proposed here. The key innovation of this approach is using photoactive materials to produce optically addressable non-contact molecular actuators. Photoinitiated distortion makes these materials ideally suited for integration into active and adaptive optics multiconjugate adaptive telescopes require higher than current pixel density with increased control capability, and significantly larger deformable mirrors, which cannot currently be produced at any price.

**Objective:** Using a completely novel approach we are making active optic correctors in an effort to achieve a 1000-fold improvement in pixel density, and factor of 10 reduction in production cost.  $\pi-\pi^*$  metal stacking lamellar polymers have been synthesized and incorporated into flexible substrates to construct molecular "laser actuators" to make non-contact, optically addressable active optic elements. This development will enable space telescopes and other applications requiring high-precision collection and concentration of electromagnetic radiation (from radio to infrared) while reducing cost and mitigating deployment risk.

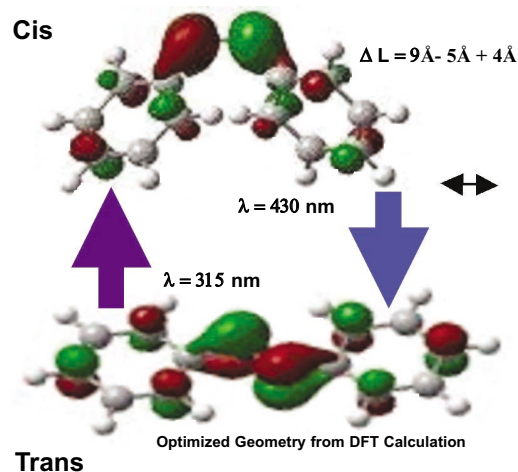


Figure 1. Cis and trans photoisomers of diazobenzene.

**Technical Approach:** In order to achieve high Strehl ratios and megapixel adaptive mirrors, what is required is a way to actively control the shape of substrates without additional wires, electronics, or heavy complex reaction structures. A  $\pi-\pi^*$  transition corresponds to exciting an electron from a bonding  $\pi$  orbital to an antibonding  $\pi^*$  orbital. Photoactive  $\pi-\pi^*$  systems of interest are composed of stacks of monomer units forming elongated structures. Lamellar structures have been built from mixed-valence,  $\pi-\pi^*$  stacking, metal-metal stacking compounds. The materials are incorporated into flexible polymer matrix substrates through covalent bonding or doping.

The goal is to synthesize materials, generate a picture of molecular scale mechanical forces, bulk geometric distortions, and to optimize the systems for active optical elements. After synthesizing appropriate photoactive substances, active substrates were produced and tested to quantify control authority. We have made Azo-gel precursors and used them to synthesize the AZO gel (4,4'-azodibenzoyl cross linked poly N-isopropylacrilamide-co-vinylamine) as well as several other azo compounds.

**Density Functional Theory Calculations:** In both cases the highest occupied molecular orbital (HOMO) is a non-bonding orbital located on the nitrogen atoms and lowest unoccupied molecular orbital (LUMO) is a  $\pi^*$  orbital located on the benzene rings.

The HOMO's and LUMO's don't change much in energy during the cis-to-trans isomerization but the cis isomer has a dipole moment while the trans isomer does not. Because of this, the  $n-\pi^*$  transition is much more allowed for the cis isomer than for the trans isomer. The lowest  $\pi-\pi^*$  transition does change dramatically in going from the trans to cis isomer in which the lowest  $\pi-\pi^*$  transition in the trans isomer is much lower in energy than seen in the cis.

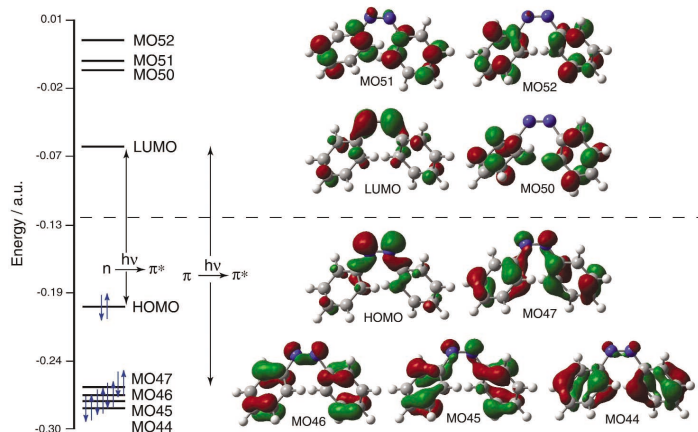


**Figure 2.** Energy levels and orbital structures of cis and trans isomers of azobenzene.

**The Future:** Our team has demonstrated a core technology which will enable ultra-lightweight large aperture primaries, high control authority correctors, and high pixel density multiconjugate adaptive optic systems. It is our team's belief that this novel technology has the potential to revolutionize the fields of Astronomy and Reconnaissance. There is the possibility of an even greater innovation: This technology opens up the possibility of closed loop optical correction of secondary optics which in turn control wavefront phase. This could possibly eliminate the need for large matrix inversion in adaptive optical applications allowing control of active and adaptive optics without a digital computer. This amazing possibility, having potentially enormous correction bandwidth and low cost, is a likely related spin-off of this research effort.

**Acknowledgements:** This paper is dedicated to our friend, colleague, and co-author Rodney Bradford, an invaluable member of our team who died during the writing of this manuscript. The authors are grateful for the support of the National Reconnaissance Office DII program office, the Air Force Office of Scientific Research NM and NL Directorates, the Air Force Research Laboratory Directed Energy Detachment 15, the Maui High Performance Computing Center, the University of Hawaii, the University of New Mexico, Virginia Polytechnic Institute, Science Applications International Corporation, and valuable conversations with Dr. Edmond Ritter and other scientists.

**References:**

- 1) SPIE Conference, San Diego, August, 2003, "Novel Photomechanical Actuators," Innovative Telescope Technologies.
- 2) J. Ritter, "Ultra-High Bandwidth Control of Active Optics Using Chemo-Optical Computation," MHPCC/AFRL Application Briefs, 2002.
- 3) J. Ritter, J. Brozik, J. Newhouse, and D. Keller, "Novel Laser Actuated Optically Addressable Adaptive Optics," MHPCC/AFRL Application Briefs, 2002.
- 4) J. Ritter, J. Newhouse, J. Brozik, and D. Evans, "Novel Ultra-Lightweight Space Telescopes Using Optically Active Polymer Membrane Mirror Shape Control," MHPCC/AFRL Application Briefs, 2001.
- 5) J. Newhouse, D. Evans, and J. Ritter, "Ab Initio Calculations Characterizing an Effective Hamiltonian for Polymeric Photonic "Muscles", " MHPCC/AFRL Application Briefs, 2001.
- 6) Brozik, Evans, Hampton, Keller, and Lopez, "Nanoscale Photonic Muscles: Fundamentals and New Technologies," Proposal to (Department of Defense) Defense University Research Initiative on Nanotechnology,(DURINT), FY2001.
- 7) Joe Ritter *et al.*, "Optically Active Polymer Membrane Mirror Shape Control Using Lasers," NRA 00-055-06, Gossamer Spacecraft Exploratory Research and Technology, December, 2000.

Author and Contact: Joe Ritter  
 Organization: Science Applications International Corporation  
 Author: Jim Brozik, Luke Emmert, Mike Fallbach  
 Organization: University of New Mexico  
 Author: Don Leo and Ken Meissner  
 Organization: Virginia Polytechnic Institute  
 Resources: AMOS Facilities  
 Sponsorship: Air Force Office of Scientific Research and the National Reconnaissance Organization

# Novel Combined Cis-Trans/Twisted Intermolecular Charge Transfer (CCT-TICT) Actuated Adaptive Optics

Joe Ritter and Jim Brozik

The proposed research is to design, synthesize, optimize and test hybrid electrically and optically actuated active substrates which use "Combined Cis-Trans/Twisted Intermolecular Charge Transfer" (CCT-TICT) materials to harness electro-optically induced molecular forces and distortions to create the first hybrid high pixel density dual mode electrically and optically addressable active optic.

**State-of-the-Art:** Active polymers such as diffusion limited ion exchange membranes, gel polymers, electrostrictives, and piezo-electrics have been demonstrated and advances in the production of membrane optics have been made; however, previous thin-film mirror pre-forming efforts and methods of active control are heavy and crude. With the exception of optically active polymers, most of these technologies are unsuitable for the space environment. Cis-Trans (CT) photoisomer based optically actuated mirrors have

been successfully produced by our research team and have demonstrated controllable strain upon photoexcitation. An understanding of the fundamental physics of TICT and CT materials has led our team to invent the new class of hybrid molecular actuators proposed here.

In order to achieve high Strehl ratios and low aerial density goals, what is required is a way to actively control the shape of substrates without heavy complex reaction structures. Electro-photoactive shape controlled optics that correct for low and mid-spatial frequency error by application of light and electricity can meet this challenge. Development of this technology would advance the state-of-the-art by offering a practical, low-cost approach to enable large/precise photon collection areas.

**Technical Approach:** Electrophotomechanical molecular machines that undergo shape change after electrical OR photoexcitation are proposed for use in active optical applications. This effort will involve: synthetic chemistry, spectroscopy, electronic structure studies, *ab-initio*, micromechanical and finite element modeling, optical and contact metrology, and control systems development.

Novel unified hybrid CCT-TICT molecules will be studied and processed into active optics. The goal is to synthesize novel materials, model and generate a picture of molecular scale mechanical forces, bulk geometric distortions, and to optimize the systems for active optical elements. After synthesis, active substrates will be produced. Test apparatus will be used to quantify control authority. Once the chemistry has evolved, a down selection will occur, and new substrates will be fabricated and tested.

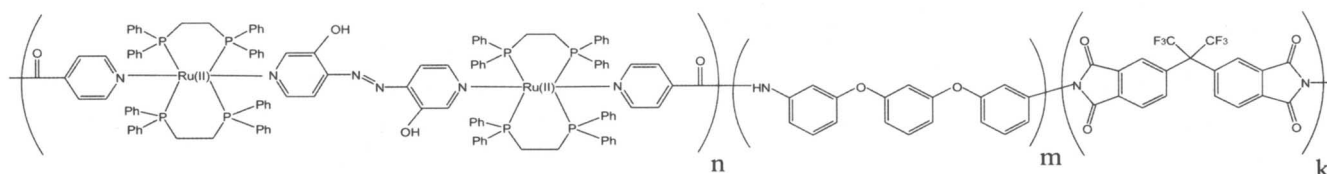


Figure 1. Co-Polymerization of the electrophotomechanical CCT-TICT moiety.

**Combined Cis-Trans/Twisted Intermolecular Charge Transfer (CCT-TICT) Materials:** A novel approach for the design of actuators is to combine the switchability of a CT photo-isomerization with the electrostatic "power stroke" involved in a TICT. In CT isomerization, a molecule, such as diazobenzene, can be reversibly switched back and forth between its two isomeric ground states and thereby reversibly change its shape. The switching is activated by two different colors of light, one corresponding to the cis isomer and the other to the trans. This process occurs when a double bond in the ground state of the molecule is broken in the excited state and the molecule is able to rotate freely between the cis and trans states. As the molecule decays back to the ground state it is trapped as either the C or T isomer.

By using a wavelength of light that corresponds to either the C or T isomer one can selectively switch (control) the material. The drawback to such a scheme is that the isomerization is entirely controlled by the free rotation about the single bond in the excited state and this rotation has to occur within the short (picosecond) lifetime of the excited state. This is an equilibrium condition in solutions but, in constrained polymeric systems steric interactions hinder this free rotation and decrease the maximal photomechanical effect.

Molecules that undergo a twisted intermolecular charge transfer have a "power stroke" associated with their conformation change and can overcome steric interactions. During a charge transfer transition, part of the molecule will act as an electron donor with the second half of the molecule acting as an electron acceptor. In the excited state the molecule can twist about a single bond in order to minimize the transient electrostatic nature of the excited state molecule. In this way the molecule will change its geometry in order to minimize its excited state energy (the "power stroke").

The draw back to a pure TICT material is that as the molecule relaxes back to the ground state so does its geometry.

To overcome the limitations imposed by nature we propose to synthesize a new material that combines a TICT with CT photoisomerization. In the proposed electro-photoactive Ru(II) moiety an electron is promoted from a d-orbital on the metal center into the modified diazo-bipyridine ligand connecting the rutheniums. After the electronic excitation, the charge transfer significantly weakens the double bond connecting the two nitrogens and nearly free rotation can occur. Because the transition is a charge transfer the photoactive moiety will rearrange in order to minimize its electrostatic interactions, this is the "power stroke" step, and as the moiety relaxes back to the ground state the double bond is reformed locking the polymer into a set geometric configuration. The polymer molecule can be switched back by exciting into a  $\pi\pi^*$  transition which will break the nitrogen-nitrogen double bond but not produce a charge transfer. Although many varieties of this invention are envisioned, the molecular structure of one possibility is shown in Figure 1.

This molecule incorporates all of the functional groups necessary for good mechanical properties, processibility, electro-optic control authority and atomic oxygen resistance necessary for the production of active optics suitable for both ground and space-based telescopes.

#### References:

- 1) J. Ritter, J. Brozik, L. Emmert, M. Fallbach, R. Bradford, D. Leo, and K. Meissner, "Novel Active Optics with  $10^{23}$  Photomechanical Actuators," MHPCC/AFRL Application Briefs, 2003.
- 2) SPIE Conference San Diego, August, 2003, "Novel Photomechanical Actuators, Innovative Telescope Technologies."
- 3) J. Ritter, "Ultra-High Bandwidth Control of Active Optics Using Chemo-Optical Computation," MHPCC/AFRL Application Briefs, 2002.
- 4) J. Ritter, J. Brozik, J. Newhouse, and D. Keller, "Novel Laser Actuated Optically Addressable Adaptive Optics," MHPCC/AFRL Application Briefs, 2002.
- 5) J. Ritter, J. Newhouse, J. Brozik, and D. Evans, "Novel Ultra-Lightweight Space Telescopes Using Optically Active Polymer Membrane Mirror Shape Control," MHPCC/AFRL Application Briefs 2001.
- 6) J. Newhouse, D. Evans, and J. Ritter, "Ab Initio Calculations Characterizing an Effective Hamiltonian for Polymeric Photonic "Muscles", " MHPCC/AFRL Application Briefs, 2001.
- 7) Brozik, Evans, Hampton, Keller, and Lopez, "Nanoscale Photonic Muscles: Fundamentals and New Technologies," Proposal to (Department of Defense) Defense University Research Initiative on Nanotechnology (DURINT), FY2001.
- 8) Joe Ritter *et al.*, "Optically Active Polymer Membrane Mirror Shape Control Using Lasers," NRA 00-055-06, Gossamer Spacecraft Exploratory Research and Technology, 2000.

Author and Contact: Joe Ritter

Organization: Science Applications International Corporation

Author: Jim Brozik

Organization: University of New Mexico, Department of Chemistry

Resources: AMOS Facilities

Sponsorship: Air Force Office of Scientific Research and the National Reconnaissance Organization

Acknowledgements: The authors are grateful for the support from the Air Force Office of Scientific Research, the Air Force Directed Energy Detachment 15, and the Maui High Performance Computing Center.

# Environment for Design of Advanced Marine Vehicles and Operations Research (ENDEAVOR)

Bob Dant, D. J. Fabozzi, Carl Holmberg, Scott Splean

As the Nation transforms its military force structure for the 21st Century, there is a pressing need to re-evaluate the nature of naval ships and their design. New advanced hull types can both decrease drag and detectable signature, while increasing both speed and stability providing obvious operational and budgetary pay-offs. The benefits of advanced hull designs also have a commercial spin-off in high-speed transport and ferries. The ENDEAVOR project aims to provide an integrated capability to rapidly create an Advanced Marine Vehicle (AMV) design at the concept level, assess AMV performance, and determine operational characteristics. We are working to design, test, and integrate naval architectural tools and simulation software with oceanographic and marine vessel databases on a high performance computing system. Eventually, this system will be available over the Internet for use by customers from their desktop computers.

**Methodology:** The technologies involved include: 1) PC-based client software with which a user manipulates the parameters for their designs and test conditions via a convenient GUI, 2) a central "web services" infrastructure through which the client's software submits designs to be processed and stored, and 3) material and environmental databases and physics simulation codes hosted on a high performance parallel computing system, where users test their designs.

**Research Objectives:** The main objective of this effort is to integrate a number of existing tools into a single, high-performance design environment. By utilizing a supercomputer back-end, the ENDEAVOR system will greatly shorten the cycle time of an iterative design and test process, enabling designers to quickly optimize complex designs. This capability will give users more freedom to consider trade-offs over a wider range of concepts against the time given to a product's design phase.



Figure 1. Rendering Of Advanced Marine Vehicle Concept.

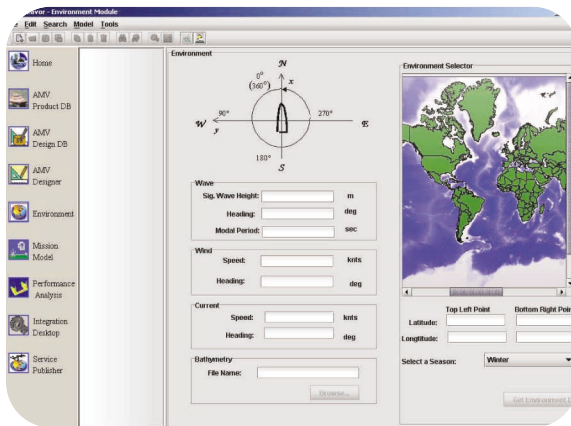


Figure 2. Designer Client Interface.

**Results:** AFRL/MHPCC purchased and installed a commercial off the shelf (COTS), Linux-based, dual processor web services computer with a capacity for considerable mass-storage upgrades. The foundations for user services, including the Apache web server and Tomcat application engine, have been installed. Initial work has begun on implementing the object-oriented design model web service. A separate Geographic Information System (GIS) has been modified to return data to the user for realistic marine environments in which design models may be tested. "Truth" data is being collected from an existing advanced marine vehicle prototype, under development by a commercial partner.



Figure 3. GIS Data Extracted To Test Design Over Realistic Route.

**Significance:** The U.S. Navy is currently entertaining a host of novel concepts, including Arsenal Ship derivatives, Corsair, and Sea Lance, with promises of more to come. The benefits of advanced hull designs also have a commercial spin-off in high-speed transport and ferries. For global transportation, cargos can be transported from one continent to another within days instead of weeks. For regional transportation, people and cargos in offshore islands can have quick and easy access to other islands or to the mainland, of particular interest for the challenging conditions between the Hawaiian Islands. The impact to the global and local economy can potentially be very significant. As the ENDEAVOR system matures, designers can realistically explore the possibilities hidden in unproven concepts.

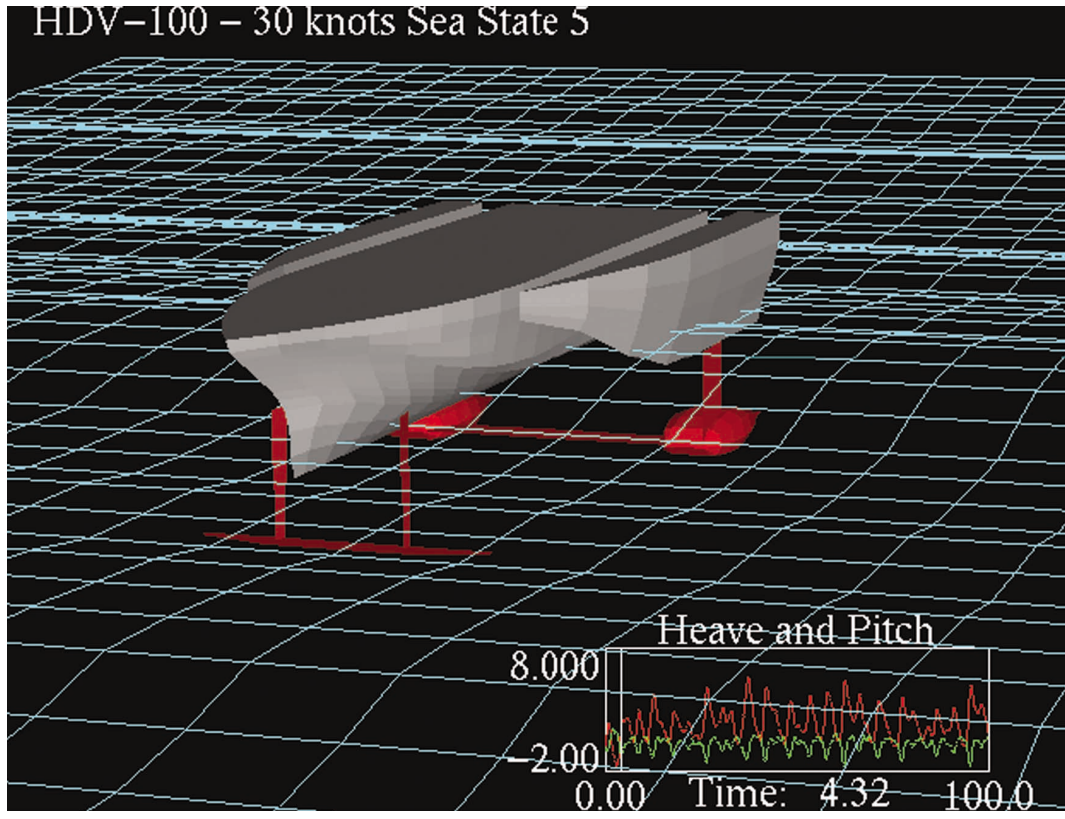


**Figure 4.** Test Environment Visualization.

Author and Contact: Carl Holmberg  
Authors: Bob Dant, D. J. Fabozzi, Scott Splean  
Organization: Maui High Performance Computing Center, 550 Lipoa Parkway, Kihei, HI, 96753  
Resources: IBM SP3 and SP4 and Dell PowerEdge 2650 server at MHPCC  
Sponsorship: Office Of Naval Research and Lockheed Martin-ORINCON

# A Highly Parallel Physically Constrained Iterative Blind Deconvolution Algorithm: PCID

Kathy Schulze, Stuart Jefferies, Charles L. Matson

**Physically constrained iterative deconvolution (PCID)** is a multi-frame blind deconvolution algorithm designed to reduce large numbers of short exposure observatory data frames as a single ensemble. PCID was specifically engineered to use parallel processing allowing hundreds of frames to be reduced together in a timely fashion. Using large ensembles of frames minimizes noise amplification, a common problem with non-linear algorithm data reduction, and improves signal to noise resulting in higher resolution restorations. However, using large numbers of frames increases the memory requirements, processing load and time to obtain a recovery. Using the parallel nodes to process a large frame ensemble reduces the overall memory load and decreases the processing time for the recovery.

**Parallel System Engineering:** PCID uses the multi-program multi-data (MPMD) paradigm. As shown in Figure 1, the master program runs on a single processor and orchestrates the execution of the worker program on each of the rest of the processors. The master program controls all input and output including data and processing parameters, and drives the minimization process. The worker processors respond to the master's commands to either receive or send data, or complete some function on the data and return a result.

Spreading the frames across the worker processors allows the frames in the ensemble to be processed in parallel and reduces the memory requirements for processing the ensemble. As memory requirements are reduced, the execution of the program is more efficient.

**Processing Options:** PCID is able to use all the frames in the ensemble, even truncated frames (where the object being recovered lies partially off the imaging array) and very blurry frames. As each frame has some information of potential use to the recovery process, it is a matter of appropriately using the information. Parallel processing the frames also allows use of other memory intensive operations to improve the algorithms performance. Embedding the data to recover information lost in cropped frames, and block replicating the data to capitalize on tracker jitter, each increase the individual frame size by a factor of 2. Embedding the data and then block replicating the data causes a single frame of data on an original grid size of  $128^2$  to now require  $512^2$ . This factor of 16 times the original data size is propagated through all the required variables and work arrays. However, spreading the frames in the ensemble across many worker processors keeps the required memory to a manageable level.

PCID typically uses Zernike polynomials to model the phase of the wave front blurring the frames of data. While modeling the phase of the wave front gives good results, it has been shown by Jefferies<sup>1</sup> that modeling the amplitude of the wave front can be important. In the very latest version of this algorithm being used to restore shuttle Columbia data, estimation of both the amplitude and phase of the wave front is used.

The many processing options of PCID, including type of PSF estimation, error metric type, noise weighting, number of frames, block replicating, embedding and support constraints, and frame weighting, all combine to make PCID a very powerful observatory data reduction tool. One of the goals of development of PCID is to automate as many processing parameter selections as possible making the algorithm usable by non-imaging experts.

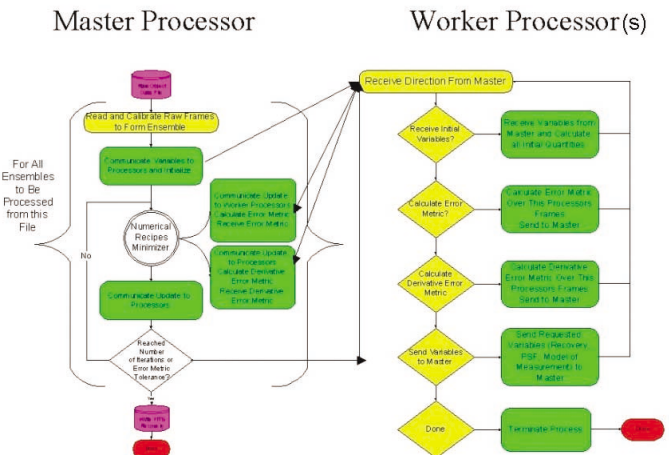


**Figure 1.** PCID uses the multi-program multi-data (MPMD) paradigm.

**Reference:**

- 1) S. M. Jefferies et al., "Sensing Wave-Front Amplitude and Phase with Phase Diversity," *Applied Optics*, Volume 41, No. 11, 2002.

Author and Contact: Kathy Schulze  
 Organization: KJS Consulting, PO Box 591, Georgetown, DE, 19947  
 Author: Stuart Jefferies  
 Organization: Maui Scientific Research Center, 590 Lipoa Parkway, Suite 272, Kihei, HI, 96753  
 Author: Charles L. Matson  
 Organization: Air Force Research Laboratory, Directed Energy Directorate, Kirtland AFB, NM, 87117  
 Resources: *Tempest* system batch nodes and Message Passing Interface (MPI) at MHPCC  
 Sponsorship: Air Force Office of Scientific Research (AFOSR)  
 Acknowledgement: The author gratefully acknowledges the AFOSR for their support and funding on this project.

# Low-Energy Elastic Electron-Magnesium Scattering

Igor Bray

Particle collisions on the atomic scale are all around and even inside us. For this reason many sciences and technologies require the understanding of such collisions. Modern supercomputer resources have allowed for unprecedented breakthroughs in the field of electron-atom collisions, so much so that many feel that such problems are completely solved for relatively simple quasi one- and two-electron atoms. Here we show that contrary to popular belief the problem of elastic low-energy electron-magnesium scattering is presently an unsolved problem that shows promise of solution only with application of unexpectedly large computational resources.

**Research Objective:** Magnesium is well described as a two-electron atom where the valence electrons move in the field of the inert Ne III ionic core. As such, its structure is readily described by two-electron excitations and the convergent close-coupling (CCC) formalism of Fursa and Bray (1997) is readily applicable. The CCC method relies on taking sufficiently many Laguerre-based expansion states until convergence to the required accuracy is obtained. Typically, convergence in elastic scattering is obtained using just a few states.

For brevity of presentation we consider just the S-wave of the e-Mg system. One way of checking the convergence is to check the dependence of the results on the Laguerre exponential parameter lambda. In Figure 1, we see an extraordinary dependence of the cross section on lambda even though a very large number of states has already been included in the calculations. Clearly, even larger calculations are necessary to obtain results which are independent of lambda. These are currently underway and are showing some promise.

section on lambda even though a very large number of states has already been included in the calculations. Clearly, even larger calculations are necessary to obtain results which are independent of lambda. These are currently underway and are showing some promise.

## References:

1) D. V. Fursa and I. Bray, *Journal of Physics B* 30, 5895 (1997).

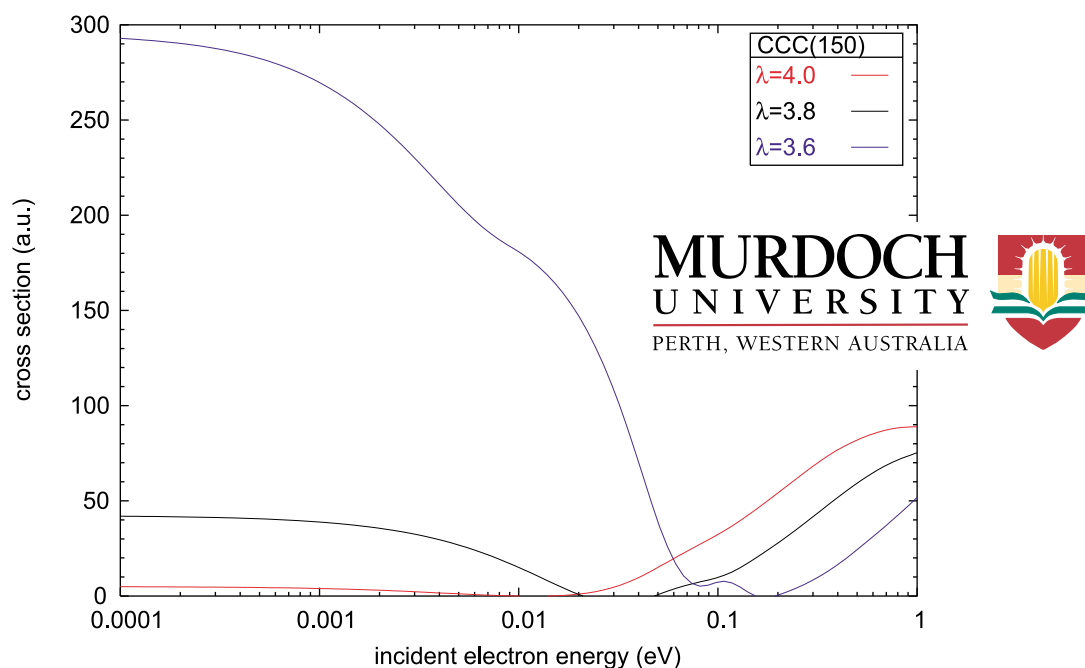


**Figure 1.** Elastic differential cross section for e-Mg S-wave scattering calculated using 150 states with the specified values of lambda in the CCC formalism.

Author and Contact: Igor Bray

Organization: Physics & Energy Studies, Murdoch University, GPO Box S1400, Perth, Western Australia, 6849

URL: <http://atom.murdoch.edu.au>

Resources: IBM SP *Tempest* at MHPCC and SUN E450 at Murdoch University

Sponsorship: Australian Research Council

# INDEX OF AUTHORS

## B

Brian Banks .....10  
Tunna Baruah .....14  
Michael Berning .....10  
Michael Bettenhausen .....12  
Robert Borchers .....10  
Lester A. Bowers .....18  
Jeffrey Bowles .....12  
Rodney Bradford .....38  
Igor Bray .....45  
Jim Brozik .....38, 40  
Paul Bundschuh .....10

## C

Keith L. Cartwright .....18  
Margaret W. Chen .....20  
Kyle Cooper .....10  
Russell M. Cummings .....22

## D

Bob Dant .....36, 42  
William DeMeo .....10  
Donald D. Drew .....16  
Bruce Duncan .....10, 30

## E

Luke Emmert .....38

## F

D. J. Fabozzi .....10, 30, 42  
Mike Fallbach .....38  
James R. Forsythe .....22

## G

Cynthia Giebink .....10  
David Gillis .....12  
Marie Greene .....36  
George Gusciora .....10

## H

Maria Hancock .....10  
Michael D. Haworth .....18  
Carl Holmberg .....10, 36, 42  
Elizabeth Hunke .....34  
Bobby Hunt .....10

## I

Detelina Ivanova .....34

## J

Stuart Jefferies .....44  
Joel T. Johnson .....1

## K

Paul Kominsky .....25  
Joseph Koning .....4  
Brian Kruse .....25

## L

Richard T. Lahey, Jr. ....16  
David Lau. ....2  
Randy J. Lefevre .....26  
Don Leo .....38  
John Luginsland .....18

## M

Angus Macnab .....32  
Mathew Maltrud .....34  
Peter J. Mardahl .....18  
Jennifer Mariana .....4  
Charles Matson .....44  
Julie McClean .....34  
Ken Meissner .....38  
Thomas Meyer .....36  
Francisco J. Moraga .....16  
Scott A. Morton .....22  
Maria Murphy .....30  
Mitch Murphy .....10  
Tony Murphy .....18

## N

D. T. Nguyen .....2

## P

Mark R. Pederson .....14

## R

Mark Radleigh .....36  
S. D. Rajan .....2  
B. R. Ratna .....6  
Joe Ritter .....38, 40  
Garry Rodrigue .....4  
Kevin Roe .....26, 28  
Frank Ruggiero .....26

## S

Kathy Schulze .....8, 44  
Jonathan V. Selinger .....6  
Mark A. Skinner .....10  
Philippe R. Spalart .....22  
Scott Splean .....42  
Kyle D. Squires .....22  
Matthew B. Steenman .....22  
Duane Stevens .....28  
James St. Ville .....2  
Bob Swanson .....30  
Brent Swartz .....25, 30

## T

Lance Terada .....36  
Prasad Thoppil .....34

## V

George Vahala .....32  
Linda Vahala .....32  
Ron Vioria .....30

## W

Michael Winter .....12  
Shawn H. Woodson .....22  
Kenneth E. Wurtzler .....22

## Y

Jeffrey Yopez .....32  
So Hui Yu .....2

# INDEX OF ORGANIZATIONS

## A

Air Force Research Laboratory ----- 18, 26, 32, 44  
Aerospace Corporation ----- 20  
Arizona State University ----- 2, 22

## B

Boeing Commercial Airlines ----- 22

## C

Cobalt Solutions, LLC ----- 22

## G

Georgetown University ----- 14

## H

Hanscom Air Force Base. ----- 26, 32  
Hawaii Institute of Geophysics and Planetology 12  
Hawthorne & York International, Ltd.----- 2

## K

Kirtland Air Force Base ----- 26, 44  
KJS Consulting ----- 8, 44  
Naval Research Laboratory----- 6

## L

Los Alamos National Laboratory ----- 34

## M

Maui High Performance Computing Center  
(MHPCC) ----- 10, 25, 26, 28, 30, 36, 42  
Maui Scientific Research Center ----- 10, 44  
Murdoch University----- 45

## N

Naval Air Systems Command ----- 22  
Naval Postgraduate School----- 34  
Naval Research Laboratory ----- 6, 12, 14

## O

Ohio State University ----- 1  
Old Dominion University ----- 2, 32

## R

Rensselaer Polytechnic Institute----- 16

## S

Science Applications International Corporation  
(SAIC) ----- 18, 38, 40

## T

Textron Systems ----- 10

## U

Unites States Air Force Academy ----- 22  
University of California at Davis ----- 4  
University of Hawaii at Manoa ----- 12, 28  
University of New Mexico ----- 38, 40

## V

Virginia Polytechnic Institute----- 38

## W

William & Mary College ----- 32



